

STUDY OF  
CONVECTION AND MAGNETIC FIELDS  
IN THE SUN

*A Thesis*  
*Submitted For The Degree of*  
*Doctor of Philosophy In The Faculty of Science*  
BANGALORE UNIVERSITY

*By*  
P. VENKATAKRISHNAN

INDIAN INSTITUTE OF ASTROPHYSICS  
BANGALORE  
INDIA

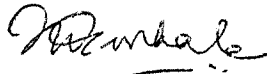
JANUARY 1984

DECLARATION

I hereby declare that the matter embodied in this thesis is the result of the investigations carried out by me in the Indian Institute of Astrophysics, Bangalore and the Department of Physics, Central College, Bangalore, under the supervision of Dr. M.H. Gokhale and Dr. B.C. Chandrasekhara and has not been submitted for the award of any degree, diploma, associateship, fellowship, etc. of any University or Institute.



(P. Venkatakrisnan)  
Candidate



M.H. Gokhale

*B. C. Chandrasekhara*  
B.C. Chandrasekhara

Supervisors

Bangalore  
Dt. 2.1.1984

DEDICATION

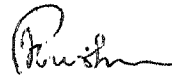
I dedicate this thesis to the memory of  
my late sister Manakam.

### ACKNOWLEDGEMENTS

It is a pleasure to acknowledge the painstaking efforts taken by my supervisors Dr. M.H. Gokhale and Dr. B.C. Chandrasekhara in seeing to the successful completion of this thesis. I also wish to thank Dr. J.C. Bhattacharyya, Director, Indian Institute of Astrophysics for his generous support with regard to computer time.

The heroic effort of Mr. A.M. Batcha in typing the entire thesis despite health restrictions should not go unacknowledged. I am similarly grateful for Mr. R. Krishnamoorthy's unstinting help in the preparation of the copies of the manuscript, right from the reproduction of the figures to the printing of the title cover and binding. In this last he was assisted by Mrs. Revathi Krishnamoorthy. Messrs. S. Muthukrishnan and R.M. Palraj drew the figures. I also thank Mrs. A. Vagiswari, Mr. H.N. Manjunath, P.N. Prabhakar and Mr. A. Elangovan for their help in the library. The consistent help rendered by all the staff members of our computer centre greatly diminished several anxieties in relation to computations.

At home, I was guarded against many routine duties of day-to-day life by my mother so that I could devote a lot of time to astronomy. In this, she was assisted by my wife, who also patiently typed the first draft from a barely legible manuscript. I must also acknowledge my son's help whose very arrival two years ago enhanced my interest in completing this work.



(P. Venkatakrisnan)

Bangalore-34  
Dt. 2.1.1984

## CONTENTS

	<u>Page</u>
ABSTRACT ... ..	1-11
Chapter 1 ... INTRODUCTION ..	1-12
1.1 Interaction of convection with magnetic fields in the sun ..	1
1.2 Some problems concerning small scale solar magnetic fields ..	4
1.3 The problems studied in this thesis ..	9
Chapter 2 ... INTERACTION OF MAGNETIC FLUX TUBES WITH THEIR ENVIRONMENT	
1. Response to imposed lateral motions ..	13-44
2.1 Introduction ..	13
2.2 The basic equations ..	14
2.3 Method of solution ..	19
2.4 Initial and Boundary conditions ..	24
2.5 The Field Geometry ..	27
2.6 Description of Results ..	31
2.7 Discussion of the results ..	38
2.8 Application to granule - flux tube interaction on the sun ..	40

## CONTENTS

			<u>Page</u>
Chapter 3	... INTERACTION OF MAGNETIC FLUX TUBES WITH THEIR ENVIRONMENT. II. Response to external pressure fluctuations ..		45-71
	3.1 A magnetic flux tube in a turbulent fluid ..		45
	3.2 The slender flux tube approximation ..		47
	3.3 The characteristic equations for a slender flux tube ..		51
	3.4 Linear response for a uniform tube to external pressure perturbations ..		54
	3.5 Nonlinear response for a polytropic tube to external pressure perturbations ..		59
Chapter 4	... NONLINEAR DEVELOPMENT OF CONVECTIVE INSTABILITY WITHIN SLENDER MAGNETIC FLUX TUBES. I. Adiabatic Flow ..		72-105
	4.1 Convection in a magnetic field ..		72
	4.2 Review of linear analyses of convective instability within slender flux tubes ..		75
	4.3 Initial and boundary conditions for the nonlinear calculations ..		84
	4.4 Results of the nonlinear calculations ..		89
	4.5 Discussion of the results ..		102

## CONTENTS

		<u>Page</u>
Chapter 5	... NONLINEAR DEVELOPMENT OF CONVECTIVE INSTABILITY WITHIN SLENDER MAGNETIC FLUX TUBES. II. The effect of radiative heat transport ..	106-119
	5.1 The effect of thermal dissipation on convective instability in a laterally unbounded vertical magnetic field ..	106
	5.2 Thermal effects in laterally bounded magnetic fields ..	110
	5.3 The energy equation for an optically thick slender flux tube exchanging heat with its surroundings ..	112
	5.4 Effect of lateral heat transport on linear convective instability in slender magnetic flux tubes ..	116
	5.5 Effect of heat transport on the nonlinear convective instability of a slender flux tube ..	122
	5.6 Discussion ..	138
Chapter 6	... SUMMARY OF CONCLUSIONS AND DISCUSSION ..	140-153
	6.1 Summary of the main results of earlier chapters ..	140
	6.2 Limitations on the applicability of the results to the solar magnetic flux tubes ..	143



## CONTENTS

	<u>Page</u>
Chapter 6	
6.3 Application to the problem of downflows within solar magnetic flux tubes	.. 148
6.4 Application to the problem of kilogauss fields of the solar magnetic flux tubes	.. 149
6.5 Future developments	.. 152
REFERENCES ...	.. 154-158

## ABSTRACT

This thesis is a study of convection in relation to solar magnetic flux tubes. The two specific problems investigated are defined in chapter 1.

The first problem concerns the interaction of magnetic flux tubes with their turbulent environment. This is dealt in two ways. First, the dynamics of gas moving along a magnetic field of imposed time-dependent geometry is considered (chapter 2). It is found that the gas is accelerated along the field in the direction of increasing lateral velocity of the field lines. When the lateral velocity has a depth-dependence similar to that of the vertical component of the photospheric granulation significant downflows are generated. Secondly, the response of slender magnetic flux tubes to external pressure fluctuations is also examined. The response is maximum when the period of the imposed pressure fluctuations matches with the time taken for 'tube waves' to traverse one scale length of these fluctuations. This maximum response is in the form of an oscillatory flow.

The second problem considered is the convective instability within slender magnetic flux tubes. First, the nonlinear evolution of velocity and magnetic field

in a tube, which is initially in a convectively unstable equilibrium, is numerically followed assuming adiabatic motions (chapter 4). The initial magnetic field is found to have a stabilizing influence on the tube. The boundary conditions are seen to exert a significant influence on the development of the instability. Next, the effect of heat transport on the instability is studied (chapter 5). When lateral exchange of heat alone is considered, the flow and the magnetic field are found to be oscillatory. The amplitudes of oscillation increase with decreasing radius of the tube. When longitudinal heat transport with constant radiative conductivity is included, the frequency of oscillations is twice that in the previous case and the amplitudes are smaller.

After discussing the limitations on the applicability of the above results they are applied to the kilogauss magnetic flux tubes in the solar photosphere (chapter 6). It is pointed out that granular buffeting of magnetic flux tubes could drive significant downflows compatible with the value of the downflow observed at higher layers of the photosphere. It is also pointed out that heat transport would make the convective collapse of flux tubes an oscillatory phenomenon.

## 1. INTRODUCTION

### 1.1 Interaction of convection with magnetic fields in the sun:

Convection is one of the modes of heat transport in a fluid. It occurs as a result of convective instability. In stars this instability arises in two different ways. In the hotter, early type, stars convective instability is created because of the concentrated nature of the energy sources in the central regions. In cooler, late type, stars it arises because of the blocking of radiative transport in their outer envelopes. The sun, being a typical late type star of spectral type G2V, possesses an outer convective envelope. This envelope influences the large scale dynamical structure of the star. The sun rotates on its axis once every 27 days. This rotation interacts with convection to produce a differential rotation viz., an angular velocity which depends on the radial distance from the centre of the sun and also on the latitude (Gilman, 1981). A combination of large scale velocity fields like differential rotation and the smaller scale velocity fields of convective turbulence are believed to maintain the global magnetic field of the sun.

The interaction of convection and magnetic fields proceeds on smaller scales as well. One such phenomenon is the magnetic network observed on the solar surface. There are two separate facets of this particular case of magneto-convective interaction. First, the supergranulation presumably pushes the magnetic flux to the boundaries of the supergranular cells to form the enhanced magnetic network (Leighton et al 1962). Secondly, the same network is seen to be coincident with enhanced chromospheric emission (Simon & Leighton 1964). This was explained as due to enhanced generation and focussing of quadropole and dipole acoustic radiation off convective turbulence in a magnetic field (Stein, 1981). Yet another example of interaction on a similar scale is the inhibition of convection in the strong magnetic fields of sunspots, as suggested by Biermann (Cowling, 1976).

On a smaller scale, we have the tiny magnetic flux tubes with kilogauss fields which interact with small scale convective eddies like the granulation, as shown by observations (Dunn & Zirker, 1973; Mehlretter, 1974). The main characteristics of these small scale photospheric magnetic fields can be summarised as follows:

- i) Most of the magnetic flux observed with arc-second resolution is concentrated into small elements (flux

tubes) of field strengths  $\approx 1000$  G to  $\approx 1700$  G and inferred sizes  $\leq 1''$  (Stenflo, 1976).

ii) The smaller elements tend to cluster into larger structures which can act cohesively so that a broad spectrum of sizes of magnetic structures is observed, in "quiet" as well as "active" regions of the sun.

iii) In "quiet" regions, magnetic flux tends to cluster in a network pattern which coincides with the boundaries of the supergranule cells. There is, however, increasing evidence for the existence of an unknown amount of flux inside the cells with fields less than 500 G in strength (Livingston and Harvey 1971) which have come to be called "inner network fields".

iv) Both network flux tubes and active region flux tubes have the same field strength with a denser population of the tubes, in active regions. The width of the  $\text{Ca}^+$  K line emission from the two types of tubes differ (Bappu & Sivaraman, 1971), indicating a difference in their internal structures.

v) The size of magnetic elements increases with increasing height and the field strength also decreases rapidly with height.

vi) Systematic downdrafts are associated with magnetic fields. These downflows have a mean value of  $\approx 0.5 \text{ kms}^{-1}$  at the height corresponding to the core of the  $6105\text{\AA}$  line (Giovannelli & Slaughter, 1978) and  $\approx 2.2 \text{ kms}^{-1}$  deeper in the photosphere where the wings of the  $15648\text{\AA}$  line (Harvey & Hall, 1975) are formed.

### 1.2 Some problems concerning small scale solar magnetic fields:

Each one of the above properties of small scale magnetic fields raises certain fundamental theoretical questions. We have first the problem of the formation and confinement of these elements with magnetic pressure approaching the external gas pressure. Once the mechanism is identified, then a further question arises as to why it does not work for the inner network fields.

Secondly, the mechanism which drives the systematic downflows in tiny magnetic elements as well as the source of mass flux to maintain the downflow are not well understood.

Finally, we have yet to fully understand the coalescence of tiny magnetic flux tubes to form larger aggregates of magnetic flux like sunspots or active regions.

Considerable theoretical effort has gone into some of these problems. Weiss and his collaborators in a series of papers (Weiss, 1966; Proctor and Galloway 1979; Galloway & Weiss 1981) have shown that circulation patterns of velocity resembling convective flow would concentrate an initially uniform magnetic field into narrow structures with mean fields a few times the equipartition value. The asymptotic structures predicted by these calculations preclude motions within these structures and this is contrary to observations. The alternative ways of concentrating field by hydraulic means e.g. by turbulent pumping, 'kneading', 'massaging' of the flux tubes (Parker, 1974a,b) yield field intensities which are in "equipartition" with the external turbulence. These, in general, are insufficient to produce kilogauss fields. Parker proposed another mechanism which is called the "superadiabatic effect" (Parker 1978a). This mechanism is based on the "frozen field" approximation that the magnetic field prevents the gas within the tube from mixing with the surroundings laterally, and hence isolates the gas. In the absence of heat exchange, any downflow would cool this isolated gas adiabatically. The reduced temperature would cause the gas to sink and enhance the downflow, until the higher visible portions of the tube are evacuated. This evacuation leads to the collapse of



the tube to a state of an intense field in equipartition with the gas pressure outside the tube. The only problem with this mechanism is the assumption of complete thermal insulation of the tube. Parker recognizes the possibility of lateral heat exchange with the surroundings by radiative diffusion but neglects it at large depths on the ground that it is small compared to convective cooling along the field. However, at the photospheric level the lateral heat exchange is indeed considerable especially for thin tubes (Spruit, 1977) and may well compensate for the adiabatic cooling.

Following a slightly different approach, Webb & Roberts (1978) showed that the slender flux tube would be subjected to a convective instability which would result in either a dispersal of the field if an initial upflowing perturbation is applied or to a collapse if the perturbation were to be a downflow. This was followed by calculations of the linear global stability of slender flux tubes embedded in a realistic model of the convection zone (Spruit & Zweibel, 1979). This analysis showed that tubes weaker than a critical field were unstable. The marginally stable fields corresponded well with observed fields in magnetic elements. From such linear analyses finite amplitude effects cannot be probed. Spruit (1979) performed a nonlinear calculation of the final collapsed

hydrostatic state of the tube corresponding to a given initial unstable state and demonstrated the collapse for the visible portions of the tube. However, one does not know whether in reality the collapsed state will be hydrostatic or hydrodynamic.

To understand the final outcome of a convective instability Hasan (1982) assumed an initial hydrostatic equilibrium of the tube embedded in a realistically stratified medium and calculated numerically the subsequent evolution of the instability. He obtained final hydrodynamic states of the tube which were independent of the initial state. The initial magnetic field had no stabilizing influence on the convective collapse.

Deinzer et al (1982) calculated static flux tube models by following the dynamical evolution of vertical slabs of magnetised gas where the amount of inhibition of convection in the magnetic field is considered as a parameter. Nordlund (1982) simulated the 3-D collapse of photospheric flux tubes and arrived at the conclusion that the superadiabaticity is an important parameter for the collapse and also that the flux concentrations are transient in character. Such studies indicate that the convective instability of magnetic flux tubes could be an important physical process aiding the formation of kilogauss fields.

The second problem of the association of downflows with magnetic elements is clouded with the uncertainties regarding the observations themselves. The most severe problem is that of the spatial resolution. The downflows always appear to be co-spatial with magnetic flux concentrations regardless of whether they occur in the quiet region network (Simon and Leighton, 1964; Tannenbaum et al 1969; Frazier, 1970) or in active region plages (Beckers & Schroter, 1968; Giovanelli & Ramsey, 1971; Sheeley, 1971; Howard, 1971, 1972). The next question is about the velocity field structure. Skumanich et al (1975) find a proportionality between the apparent velocity and apparent magnetic field. However, velocities larger than  $1 \text{ kms}^{-1}$  are ruled out by the observations of Harvey et al (1972). Indirect evidence supports the view that velocity structures are more extended than magnetic structures (Stenflo, 1976). Such being the status of the observations, one can only use them as broad guidelines for theoretical modelling.

Finally, with regard to the problem of coalescence of flux tubes, Parker (1978b) proposed an explanation in terms of the Bernoulli force between rising flux tubes. However, this might not account for continued coalescence of flux tubes after their emergence (Spruit 1981a).

### 1.3 The problems studied in this thesis:

So far, there has been no attempt to identify the driving mechanism for the systematic downflows within magnetic elements, although steady state models have been constructed (Unno & Ribes, 1978). Two possible classes of mechanisms can be thought of. The first is the class of external driving mechanisms where the flow relaxes back to hydrostatic equilibrium when the forcing terms cease to exist. The second is the class of spontaneously generated flows which come about as a result of some dynamical instability. In the case of the solar photosphere and convection zone the only horizontal forces on the vertical tubes are those due to the constant buffeting by convective turbulence. Similarly a likely mechanism capable of spontaneously generating flows in solar magnetic flux tubes is the convective instability. In this thesis, we therefore study idealised versions of these two processes. In the first case (chapters 2 and 3) we examine the response of a thin tube embedded in a stably stratified polytropic atmosphere to external perturbations which are modelled to simulate the observed behaviour of granulation.

The second problem that we study (chapters 4 and 5) is the development of convective instability in a thin tube embedded in an unstably stratified polytropic

atmosphere.

In all these calculations a numerical version of the method of characteristics was used to integrate the equations forward in time. Compared to other direct and explicit schemes like finite difference methods, the method of characteristics has the advantage of allowing the use of proper boundary conditions and does not break down near shock like discontinuities. It is, however, very slow compared to the direct schemes because of the necessity of iterations for convergence to a point of intersection of all the characteristics. For more than one space dimensions, it also becomes very arduous to programme. It must be mentioned here that only one-dimensional unsteady flows are studied in this thesis.

In chapter 2, the equations of magnetohydrodynamics for motions in a magnetic field confined to a single plane are first written using a pair of curvilinear coordinates, one along the field line and one across the field line. The equation of motion normal to the field line is replaced by a prescribed form for the velocity transverse to the field. The equations are further transformed to a frame of reference moving with the field lines. These equations are integrated by a backward marching scheme based on the method of characteristics.

In chapter 3, we utilize the slender flux tube approximation, where the thickness of the tube is assumed to be negligibly small compared to the scale length of variation of the tube diameter. The problem again reduces to that of an unsteady one-dimensional flow. We first consider the case of a uniform tube under linear approximation and obtain an analytical solution. We then numerically study the nonlinear behaviour for a stratified tube subjected to external pressure fluctuations that vary monotonically in space and oscillate in time. We also study the response of the tube to wave-like disturbances of different frequencies.

In chapter 4, we consider the convective instability of slender flux tubes embedded in an unstably stratified polytropic atmosphere for adiabatic variations. We follow the development of the instability for different initial values of  $\beta_0$ , the ratio of gas pressure to magnetic pressure. We consider the effect of two different sets of boundary conditions as well as the effect of the direction of initial velocity perturbation.

In chapter 5, we first see the effect of lateral radiative heat exchange with constant radiative conductivity on the convective flow within a thin flux

tube. Next we extend this calculation including the longitudinal heat transport. We also study a case of temperature dependent opacity. In this case, the initial stratification outside the tube cannot be polytropic in general. Hence, we first calculate the equilibrium stratification satisfying the energy equation and the equation of hydrostatic balance. We use this equilibrium state as the initial state for the time dependent calculation.

Finally, in chapter 6, we discuss the combined significance of the results of all these calculations in relation to the small scale convection and magnetic fields on the sun.

## 2. INTERACTION OF MAGNETIC FLUX TUBES WITH THEIR ENVIRONMENT

### I. Response to imposed lateral motions

#### 2.1 Introduction:

The study of the interaction of an imposed velocity field with an initially dispersed magnetic field has received much attention in the past. One of the earliest of such studies was initiated by Parker (1963). He examined the effect of an imposed velocity field with a circulatory pattern on an initially uniform magnetic field. It was seen that there would be unlimited amplification of the field at the boundaries of the velocity cell where the down-flows converge. A subsequent numerical study by Weiss (1966) showed expulsion of field from the centres of two-dimensional cells and concentration of fields at the boundaries. This study was followed by a series of investigations of increasing sophistication (e.g. Proctor & Galloway, 1979; Galloway & Weiss, 1981) with inclusion of dynamical effects in the later work. The asymptotic states of all these numerical simulations are qualitatively very much similar to that predicted by Parker (1963). Differences arise only in the factor by which the field is amplified at the boundary of the



cell, ranging from  $\approx R_m^{1/2}$  in the earlier work of Weiss (1966) to  $\approx R_m$  in the simulations of Galloway & Weiss (1981). Here  $R_m$  denotes the magnetic Reynolds number.

The results of the afore-mentioned studies could be used for a preliminary understanding of the interaction of velocity fields and magnetic fields on the sun. One could, for example, consider the magnetic network as a consequence of the interaction of supergranulation with an initially weak, uniform magnetic field. The structures predicted by the aforementioned studies preclude motions within the intense fields. In the case of the Sun, however, such structured fields are constantly buffeted by smaller scale velocity fields like waves and granulation. These in turn would set up transverse motions of the field lines. In this chapter we consider the effects of such lateral motions of field lines on the dynamics of the gas constrained to move with the field (Hasan and Venkatakrishnan, 1980). Further, we also describe an application of these results to the interaction of granules with magnetic flux tubes (Venkatakrishnan and Hasan, 1981).

## 2.2 The basic equations:

Let us consider a magnetic field that is invariant under a translation in some direction, which we can

call the x-direction without loss of generality. The magnetic field varies in the y- and z-directions. We shall assume the z-direction to be opposite to the direction of gravity. In the case of curved field lines it is convenient to transform from cartesian coordinates  $(y, z)$  to a system of curvilinear coordinates  $(s, n)$  where  $s$  is the distance measured along the field line and  $n$  denotes the distance measured along a normal curve (in the same plane). Following Kopp and Pneuman (1976) we see that the unit vectors  $\hat{s}$  and  $\hat{n}$  satisfy the following geometric relations:

$$\begin{pmatrix} \frac{\partial}{\partial t} \\ \frac{\partial}{\partial s} \\ \frac{\partial}{\partial n} \end{pmatrix} (\hat{s}, \hat{n}) = \begin{pmatrix} \frac{\partial \theta}{\partial t} \\ \frac{\partial \theta}{\partial s} \\ \frac{\partial \theta}{\partial n} \end{pmatrix} (\hat{n}, -\hat{s}), \quad (2.1)$$

where  $\theta$  is the angle the field makes with the z-axis. For inviscid and infinitely conducting gas, the equation of motion along a field line can now be expressed as

$$\begin{aligned} \frac{\partial}{\partial t} V_s + V_s \frac{\partial}{\partial s} V_s + V_n \frac{\partial}{\partial n} V_s &= -\frac{1}{\rho} \frac{\partial}{\partial s} p - g \cos \theta \\ + V_n \frac{\partial}{\partial t} \theta + V_n V_s \frac{\partial}{\partial s} \theta + V_n^2 \frac{\partial}{\partial n} \theta &, \quad (2.2) \end{aligned}$$

where  $V_s$  is the gas velocity parallel to the field,  $V_n$  the velocity normal to the field,  $p$  the gas pressure,  $\rho$  the density and  $g$  the acceleration due to gravity. Let us now consider a frame of reference fixed to the field line. Such a physical identification of a field line is possible in the infinite conductivity approximation. The space and time derivatives in such a frame will be denoted by  $\frac{D}{Ds}$  and  $\frac{D}{Dt}$  respectively. These derivatives satisfy the following operator relationships:

$$\frac{D}{Dt} \equiv \frac{\partial}{\partial t} + V_n \frac{\partial}{\partial n} \quad (2.3a)$$

and

$$\frac{D}{Ds} \equiv \frac{\partial}{\partial s} \quad (2.3b)$$

From equations (2.2) and (2.3) we have

$$\begin{aligned} \frac{D}{Dt} V_s + V_s \frac{D}{Ds} V_s &= -\frac{1}{\rho} \frac{D}{Ds} p - g \cos \theta \\ &+ V_n \frac{D}{Dt} \theta + V_n V_s \frac{D}{Ds} \theta \end{aligned} \quad (2.4)$$

In a similar manner, the equation of continuity takes the form (Kepp and Preuman 1976):

$$\frac{D}{Dt} (\rho \delta A) + \frac{D}{Ds} (\rho V_s \delta A) - \rho V_n \delta A \frac{\partial}{\partial s} \theta = 0, \quad (2.5)$$

where  $\delta A$  is the cross-sectional area of an infinitesimal flux tube surrounding the field line. It has been assumed in the above equation that  $\delta A \ll L^2$  where  $L$  is some typical scale length of variation of the physical quantities along the field. Thus all flow variables in the infinitesimal tube can be assumed to be constant in a direction normal to the field line. The evolution of the magnetic field, assuming infinite conductivity, is given by the induction equation

$$\frac{\partial}{\partial t} \underline{B} = \nabla \times (\underline{V} \times \underline{B}) , \quad (2.6)$$

which can be resolved into the components

$$\frac{\partial}{\partial t} B = - \frac{\partial}{\partial n} (V_n B) , \quad (2.7a)$$

along the field and

$$B \frac{\partial}{\partial t} \theta = \frac{\partial}{\partial s} (V_n \dot{B}) , \quad (2.7b)$$

normal to the field respectively. Using the condition for flux conservation in an infinitesimal flux tube ( $B \delta A = \text{constant}$ ) and the geometric relation for the rate of change of the angle  $\theta$  viz.

$$\frac{\mathcal{D}}{\mathcal{D}t} \theta = \frac{\partial}{\partial s} V_n , \quad (2.7c)$$

we can rewrite equations (2.7a) and (2.7b) as:

$$\frac{\mathcal{D}}{\mathcal{D}t} (\ln \delta A) = \frac{\partial}{\partial n} V_n \quad (2.7d)$$

and

$$\frac{\mathcal{D}}{\mathcal{D}s} (\ln \delta A) = \frac{\partial}{\partial n} \theta \quad (2.7e)$$

respectively. Eliminating  $\delta A$  between equations (2.7d), (2.7e) and (2.5) we have

$$\begin{aligned} \frac{\mathcal{D}}{\mathcal{D}s} V_s + \frac{\mathcal{D}}{\mathcal{D}t} (\ln \rho) + V_s \frac{\mathcal{D}}{\mathcal{D}s} (\ln \rho) + V_s \frac{\partial}{\partial n} \theta \\ - V_n \frac{\mathcal{D}}{\mathcal{D}s} \theta + \frac{\partial}{\partial n} V_n = 0 . \end{aligned} \quad (2.8)$$

We relate density and pressure by a polytropic law

$$p / \rho^\Gamma = \text{constant} , \quad (2.9)$$

where  $\Gamma$  is the polytropic index. We thus have three equations (2.4), (2.8) and (2.9) in the four dependent variables  $p$ ,  $\rho$ ,  $V_s$  and  $V_n$  respectively. The equation of motion normal to the field provides the fourth equation. In this chapter, this fourth equation

is replaced by a prescribed form of  $V_n$ , as in Kopp and Preuman (1976). The resulting flow is then studied with the aid of the rest of the equations.

### 2.3 Method of solution:

Equations (2.4), (2.8) and (2.9) form a system of hyperbolic partial differential equations and hence possess real characteristics. One can recast these equations in characteristic form using standard procedures (Sneddon, 1957). The reduced equations are as follows:

$$D \xi_+ = \Gamma (A + B/a) Dt \text{ along } \frac{D}{Dt} s = V_s + a \quad (2.10a)$$

and

$$D \xi_- = \Gamma (A - B/a) Dt \text{ along } \frac{D}{Dt} s = V_s - a, \quad (2.10b)$$

where

$$D \xi_{\pm} = D \ln p \pm \frac{\Gamma}{a} D V_s, \quad (2.10c)$$

$$A = -V_s \frac{\partial}{\partial n} \theta + V_n \frac{\partial}{\partial s} \theta - \frac{\partial}{\partial n} V_n, \quad (2.10d)$$

$$B = -g \cos \theta + V_n \frac{D}{Dt} \theta + V_n V_s \frac{\partial}{\partial s} \theta \quad (2.10e)$$

and

$$a = (\Gamma p / \rho)^{1/2}. \quad (2.10f)$$

We solved these equations as an initial value problem by prescribing the state at time  $t = 0$  and then integrating the equations forward in time.

The existence of the source terms A and B precluded any analytical solutions and hence we resorted to a numerical procedure. In this method all the flow properties were determined at pre-specified grid points using an inverse marching method (Zucrow and Hoffman, 1976). For illustration, the procedure for determining the velocity and density at a point 'd' on a later time line  $t = t_0 + \Delta t$  is described, provided one knows these quantities at three points 'a', 'b' and 'c' on a previous time-line  $t_0$  (see figure 2.1). If we draw straight lines along the characteristic directions at 'd' towards decreasing value of  $t$ , then these will intersect the previous time line at two points, say 'e' and 'f' respectively. Let us denote all flow properties along the right running characteristic (that which goes from lower values of  $\mathcal{S}$  to higher values of  $\mathcal{S}$  as  $t$  increases) by a '+' subscript. Those on the left running characteristic is likewise given a '-' subscript. A further subscript like 'a', 'b' etc. denotes the

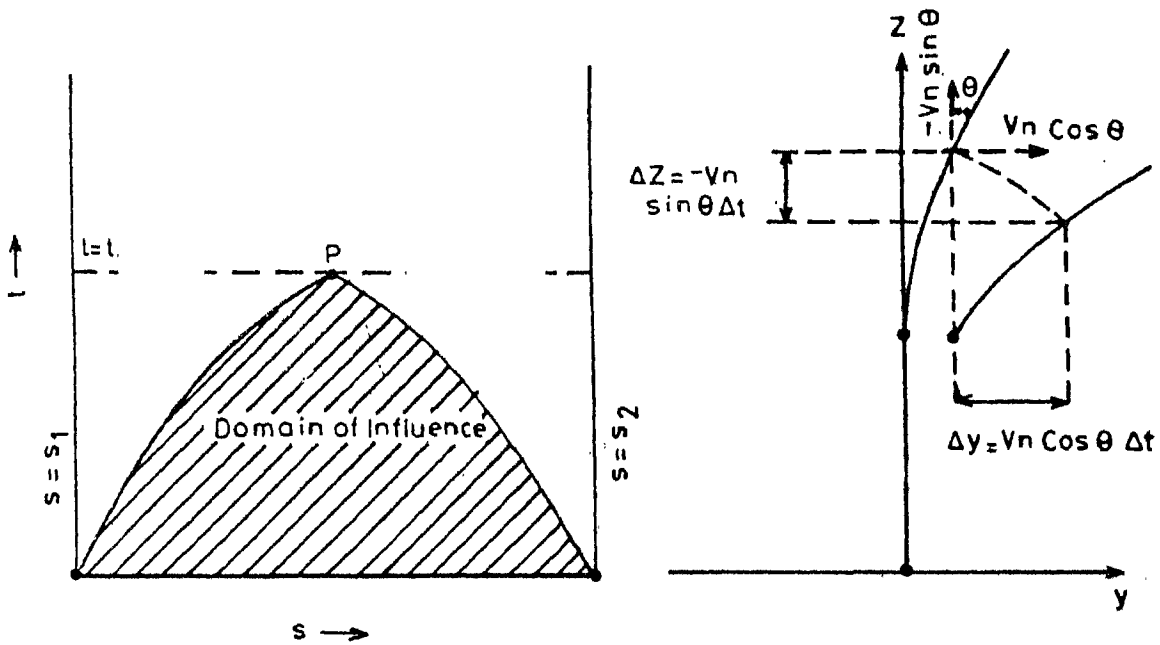
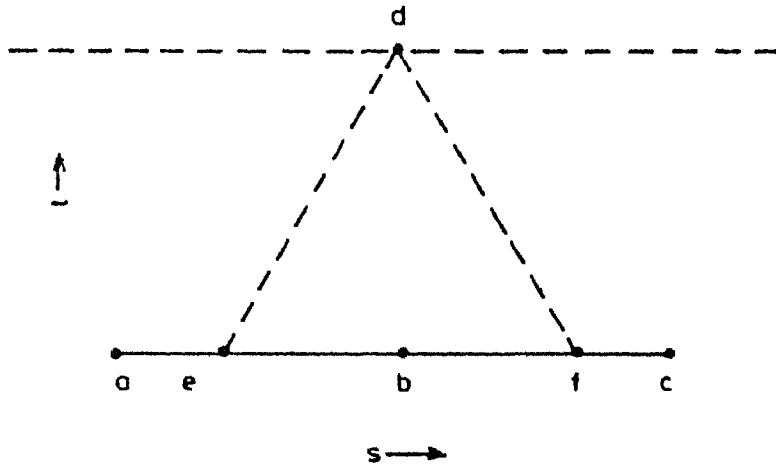


Fig.2.1 (top): The backward marching scheme for an interior point 'd' given the values at 'a', 'b' and 'c'.

Fig.2.2 (bottom left); Effect of finite boundaries on the solution of an initial value problem.

Fig.2.3 (bottom right); The motion of a point fixed on a field line moving with normal velocity  $V_n$ .



values at points 'a', 'b' etc. If we cast the equations (2.10) in finite difference form, we get

$$s_d - s_e = \Delta t (V_{s+} + a_+) , \quad (2.11a)$$

$$s_d - s_f = \Delta t (V_{s-} - a_-) , \quad (2.11b)$$

$$\ln(p_d / p_e) + \Gamma (V_{sd} - V_{se}) / a_+ = \Delta t \gamma_+ , \quad (2.11c)$$

$$\ln(p_d / p_f) - \Gamma (V_{sd} - V_{sf}) / a_- = \Delta t \gamma_- , \quad (2.11d)$$

where

$$\gamma_{\pm} = \Gamma (A_{\pm} \pm B_{\pm} / a_{\pm}) \quad (2.11e)$$

and  $\Delta t$  is the time step. We chose  $\Delta t$  so as to be within the Friedrichs - Courant - Lewy stability limit, viz.

$$\frac{\Delta t}{\Delta s} \leq \frac{1}{(|V_s| + |a|)_{\max}} . \quad (2.12)$$

Since the flow properties and the locations of points 'e' and 'f' are not known, these equations must be solved iteratively. An Euler predictor-corrector method was used for the iteration. For the predictor algorithm the following initial choice was made:

$$V_{s+}^{(0)} = V_{sa} ; \quad p_+^{(0)} = p_a ;$$

$$V_{s-}^{(0)} = V_{sc} \quad ; \quad p_{-}^{(0)} = p_c \quad ;$$

and likewise for the geometric parameters. These were used in equations (2.11a) and (2.11b) to obtain a first guess for the location of points 'e' and 'f'. The flow properties at these points were determined by interpolating between the values at points 'a', 'b' and 'c'.

For subsequent iterations in the predictor we assumed:

$$V_{s+}^{(n)} = V_{se}^{(n-1)} \quad ; \quad p_{+}^{(n)} = p_e^{(n-1)} \quad ;$$

$$V_{s-}^{(n)} = V_{sf}^{(n-1)} \quad ; \quad p_{-}^{(n)} = p_f^{(n-1)} \quad ;$$

where the superscripts denote the order of the iteration.

When the calculated value of  $\delta_e$  and  $\delta_f$  converged within a specified tolerance, the latest values of  $V_{se}$  and  $p_e$  were used to calculate the properties at point 'd' from equations (2.11c) and (2.11d). In the present study, a relative convergence within  $10^{-4}$  was found to be generally attained within five iterations.

Next, the corrector was applied to the above predicted values of  $V_{sd}$  and  $p_d$ . For the corrector, the following scheme was assumed:

$$V_{s+} = \left( \frac{V_{se} + V_{sd}}{2} \right) \quad ; \quad p_{+} = \left( \frac{p_e + p_d}{2} \right) \quad ;$$

$$V_{s-} = \left( \frac{V_{sf} + V_{sd}}{2} \right) \quad ; \quad p_{-} = \left( \frac{p_f + p_d}{2} \right) \quad .$$

Here too, an iteration is required to locate points 'e' and 'f' as well as to determine the flow properties. However, during this iteration, the values of  $V_{sd}$  and  $p_d$  (which were determined by the predictor) are not changed. After obtaining convergence for  $\delta_e$  and  $\delta_f$ ,  $V_{sd}$  and  $p_d$  are redetermined. To improve the accuracy, these corrected values of  $V_{sd}$  and  $p_d$  were substituted back into equations (2.11) and the same steps were followed. It was seen that a maximum number of 5 predictor iterations and 3 corrector iterations yielded sufficient accuracy.

#### 2.4 Initial and Boundary conditions:

In this chapter and in the next one, we present results obtained from an initial stratification which is in convectively stable hydrostatic equilibrium. A discussion of the flow that is produced as a result of convective instability is postponed to chapters 4 and 5. The initial magnetic field was chosen to have a potential configuration and hence magnetic forces did not have to be considered for the equilibrium. The energy equation was replaced by a polytropic equation of state,  $p \propto \rho^\Gamma$ . One can thus study a variety of situations ranging from the case where heat exchange is so rapid as to maintain isothermal equilibrium ( $\Gamma = 1$ ) to the case of adiabatic equilibrium ( $\Gamma = \gamma$ ) where there is no

heat exchange. One limitation of the work described in this chapter is that pressure and density were related by the same polytropic law for  $t > 0$  as well. This restriction has been relaxed to varying degrees in the subsequent chapters. Mathematically, the initial state can be represented by

$$V_{\pi}(\delta) = 0, \quad (2.13a)$$

$$V_{\delta}(\delta) = 0, \quad (2.13b)$$

$$\rho(\delta) = \rho(0) \left[ 1 - \frac{g \{ z(\delta) - z(0) \} (\Gamma - 1)}{a^2(0)} \right]^{\frac{1}{\Gamma - 1}}, \quad (2.13c)$$

$$p(\delta) = p(0) \left\{ \rho(\delta) / \rho(0) \right\}^{\Gamma}, \quad (2.13d)$$

where

$$a^2(0) = \Gamma p(0) / \rho(0). \quad (2.13e)$$

Although the initial magnetic field, being potential, does not affect the equilibrium stratification, it defines the stream geometry and will be described in the next section. At time  $t = 0$ , a non-zero  $V_{\pi}$  was introduced and the equations (2.11) were integrated as described in the previous section.

However, the scheme described in section 2.3 can be applied only to an interior point. It is well known for time-dependent initial value problems solved by the method of characteristics, that the number of boundary conditions, sufficient and necessary to solve the problem uniquely, is  $m - n$ , where  $n$  is the number of characteristics crossing the boundary from an interior point and  $m$  is the number of dependent variables. If one has fewer boundary conditions, there is no unique solution. If one imposes more than  $m - n$  boundary conditions then any incompatibility of the extra boundary conditions with the characteristic equations will lead to spurious boundary effects which can propagate into, and influence, the interior solution. The choice of physically meaningful boundary conditions becomes increasingly important as one integrates for longer time intervals. This is because beyond some critical time  $t_*$  say, all characteristics drawn backward from any interior point  $P$  (figure 2.2) will not reach the initial time-line but will terminate at either boundary. The hatched region in figure 2.2 is known as the 'domain of influence' of the initial state. Thus, at large enough times, the flow will depend more on the boundary conditions than on the initial conditions. In the present study we tried the following two different conditions for the left boundary in figure 2.1 (lower

boundary of the flow region)

$$V_{\delta}(0) = a(1 - \exp(-t/\tau)), \quad (2.14a)$$

or

$$p(0) = \text{constant}. \quad (2.14b)$$

For the right boundary in figure 2.1 (i.e. top boundary of the flow region)  $V_{\delta}$  was prescribed as the value extrapolated from the values at two preceding space points. This boundary condition assured that no kinks were produced at the end point in the spatial velocity and pressure profiles. The equation relating  $V_{\delta}$  and  $p$  along the "missing" characteristic is replaced by the boundary condition which prescribes either  $V_{\delta}$  or  $p$ . The remaining variable is then determined from the rest of the equations (2.11).

### 2.5 The Field Geometry:

At  $t = 0$ , we assumed a potential magnetic field with components

$$B_y = B_0 \exp(-kz) \sin \theta, \quad (2.15a)$$

$$B_z = B_0 \exp(-kz) \cos \theta \quad (2.15b)$$

and

$$\theta = ky, \quad (2.15c)$$

where  $k$  is a constant. At later instants of time, the field geometry is completely determined by  $V_n$ . The coordinates of a given point on the field line at different instants of time can be determined from the following equations (see figure 2.3):

$$\frac{D}{Dt} y = V_n \cos \theta, \quad (2.16a)$$

$$\frac{D}{Dt} z = -V_n \sin \theta \quad (2.16b)$$

$$\text{and } \frac{D}{Dt} \theta = \frac{\partial}{\partial s} V_n. \quad (2.16c)$$

If one chooses the velocity as

$$V_n = V_b(t) \sin ky / \sin ky_b(t), \quad (2.17)$$

where  $V_b(t)$  is the velocity of the base point  $y_b(t)$ , then the relation (2.15c) will be maintained for all times. Thus equations (2.16) are unnecessary in this case and the quantities  $\frac{\partial \theta}{\partial n}$  and  $\frac{\partial \theta}{\partial s}$  can be determined directly as:

$$\frac{\partial \theta}{\partial n} = k \sec ky \quad (2.18a)$$

and  $\frac{\partial \theta}{\partial \delta} = k \csc ky$ . (2.18b)

We did a few calculations with  $V_n$  in the form (2.17) in which  $V_b(t)$  was chosen as:

$$V_b(t) = V_0 \sin ky_b(t) \cos ky_b(t) / \sin ky_b(0), \quad (2.19a)$$

$$y_b(t) = 2 y_* \tan^{-1}(\exp -V_0(t-t_*)/y_*), \quad (2.19b)$$

$$y_* = 2 y_b(0) / \pi, \quad t_* = 0, \quad t \leq \tau, \quad (2.19c)$$

and

$$y_* = 2 y_b(\tau) / \pi, \quad t_* = \tau, \quad t > \tau. \quad (2.19d)$$

Such a behaviour of  $y_b(t)$  simulated a rapid motion for small times and a subsequent decrease of velocity asymptotically approaching zero. We chose this form to approximately represent a rapid onset of some instability and its subsequent quenching due to, for example, the enhancement of the magnetic field.

In order to keep the study sufficiently general, we also tried another form for  $V_n$  viz.

$$V_n = V_0(t) \exp \delta / H, \quad (2.20)$$



where  $H$  is a constant which can be positive or negative. Here too, we chose  $V_0(t)$  to behave with initial large rate of change and asymptotic approach to zero velocity. In one calculation  $V_0(t)$  was made to oscillate in time (see section 2.8). For the general form (2.20) the angle  $\theta$  must be calculated for each time step. We calculated this by integrating equations (2.16) from  $t_0$  to  $t_0 + \Delta t$  using an Euler predictor-corrector method, where  $\Delta t$  is the time step for the equation (2.11). Moreover since the prescribed lateral velocity stretched the field lines at every instant of time, grid distortion can occur. We compensated for this by calculating the net change in the position of a fixed point on the field line given by

$$\Delta s = \int_{z(t_0)}^{z(t_0 + \Delta t)} dz / \cos \theta . \quad (2.21a)$$

Similarly, the value of  $\frac{\partial}{\partial s} \theta$  at the new displaced point is given by

$$\frac{\partial}{\partial s} \theta = \cos \theta \frac{\partial}{\partial z} \theta . \quad (2.21b)$$

We performed the integration and differentiation in equations (2.21) using Lagrange 3-point interpolation formulae (Abramowitz and Stegun, 1965). Having obtained the coordinates  $(y, z)$  and geometric parameters at the

displaced points, we determined the corresponding quantities at the original spatial grid points again by Lagrange 3-point interpolation. In this way, the problems involved in a moving grid (like non-uniform step size) were eliminated.

## 2.6 Description of Results:

We first expressed all quantities in dimensionless units. The basic unit of length was taken as  $RT_*/g$  where  $R$  is the universal gas constant,  $T_*$  is a reference temperature and  $g$ , the acceleration due to gravity. The unit of velocity was  $(RT_*)^{1/2}$  and, therefore, time was measured in units of  $(RT_*)^{1/2}/g$ . The density was expressed in units of the density  $\rho_*$  at the base of the field line and likewise the temperature in terms of base temperature  $T_*$ . This decided the unit of pressure as  $R\rho_*T_*$  which is nothing but the pressure at the base for a perfect gas.

First we solved the equations (2.11) using the form for  $V_n$  given by (2.20). In this form the spatial dependence of the velocity is either monotonically increasing with  $\delta$  ( $H > 0$ ) or decreasing with  $\delta$  ( $H < 0$ ). Figure 2.4 shows that a positive value of  $H$  leads to an upflow whereas a negative value of  $H$  leads to a downflow. Here the value of  $V_n$  at the base is 1.0 units

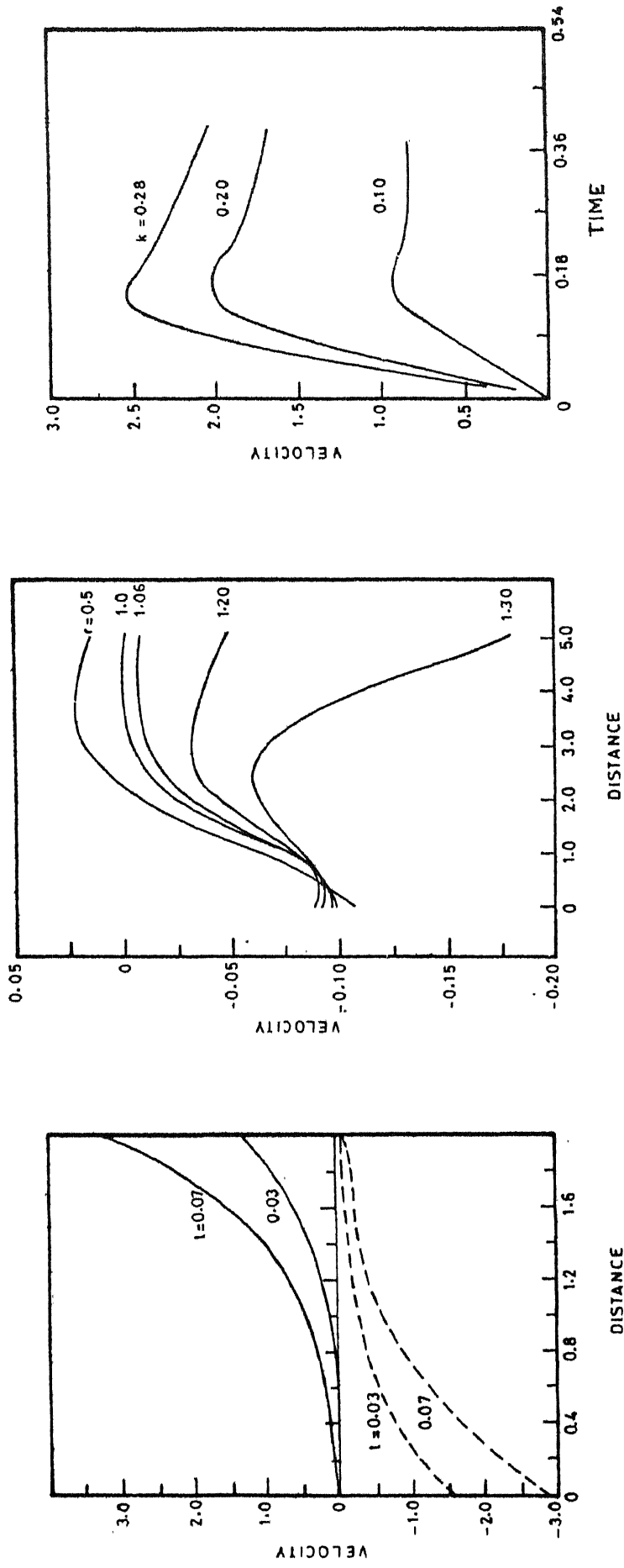


Fig. 2.4 (left): Velocity profiles resulting from the field line's lateral motion which varies exponentially with scale length  $H = +1.0$  (solid lines) and  $H = -1.0$  (dashes) at two instants of time.

Fig. 2.5 (centre): Response to lateral motion at  $t = 0.32$  for different values of the polytropic index (marked near the corresponding velocity profile).

Fig. 2.6 (right): Time dependence of velocity for different values of the curvature parameter  $k = 0.28, 0.20$  &  $0.10$ .

for  $H = -1.0$  and  $8.0$  units for  $H = +1.0$ . In the case of  $H = +1.0$ , the large value of  $V_n = 8.0$  was chosen with a view to model the flows in solar spicules (cf. Hasan & Venkatakrishnan, 1981). We notice that inspite of the great difference in the base value of  $V_n$  for the two cases, the resulting magnitudes of  $V_s$  are not much different in these two cases.

The short time behaviour of the flow for different values of the polytropic index  $\Gamma$  can be seen in figure 2.5. Here the spatial velocity profile is shown at a time  $t = 0.32$  dimensionless units. It is seen that the response of the flow to the lateral motions is stronger for larger values of  $\Gamma$  or in other words for "stiffer" equations of state.

Consider now the other form of  $V_n$  given by (2.17). The parameters quantifying the lateral motions are  $V_0$ , the amplitude of base velocity and  $k$ , a measure of the curvature of field lines. We studied the effect of each quantity separately. The effect of curvature can be seen in figure 2.6. It is seen that the peak velocity of the parallel flow increases with curvature. The decline of the flow after the rise to the peak value is simply an artifact of the imposed lateral flow which ceases after  $0.25$  time units.

The effect of magnitude of base velocity  $V_0$  can be seen by a comparison of figure 2.7 and 2.8. In figure 2.7 the spatial velocity profile is plotted at three instants of time for  $V_0 = 8.0$ . A similar plot corresponding to  $V_0 = 6.0$  is seen in figure 2.8. It can be clearly seen that even at very early epochs (e.g.  $t = 0.03$ ) the velocities of parallel flow are larger in figure 2.7 than in figure 2.8.

The choice of boundary conditions influences the transient behaviour of the flow. In figure 2.9, we see the spatial profile of pressure corresponding to the velocity profile of figure 2.7. Here, the boundary condition (2.14a) (prescribed time-dependent velocity) was imposed. A small kink can be seen propagating downstream with a velocity  $\approx 2.5$  units. At later times a second kink is also seen. The first kink represents the initial impulsive onset of the lateral motion of the field line. The second kink is created because the boundary condition (2.14a) forces  $V_\parallel$  at  $\delta = 0$  to increase even after the cessation of the lateral motion of the field line. The halt of the lateral motion reduces  $V_\parallel$  at all other points. The velocity gradient thus produced causes a compression wave to propagate upward from the base. The spatial pressure profile for a different boundary condition (2.14b) is shown in

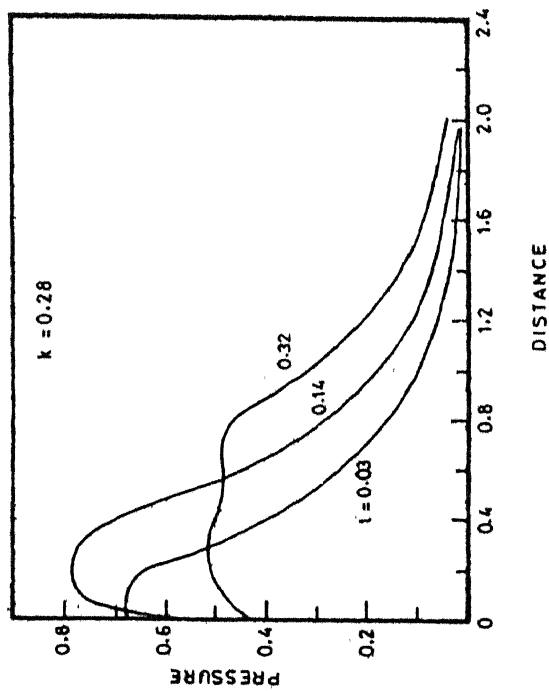
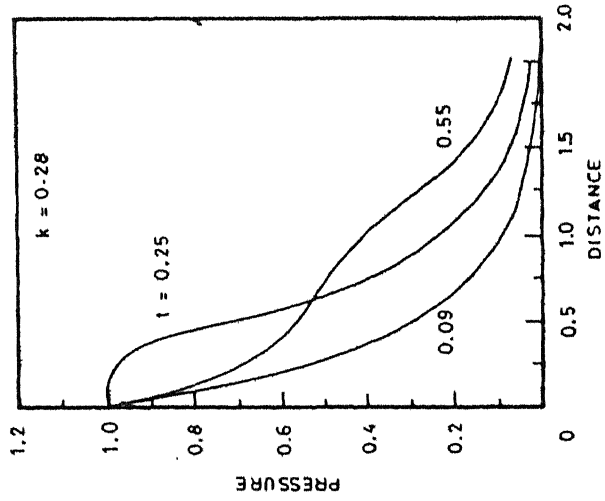
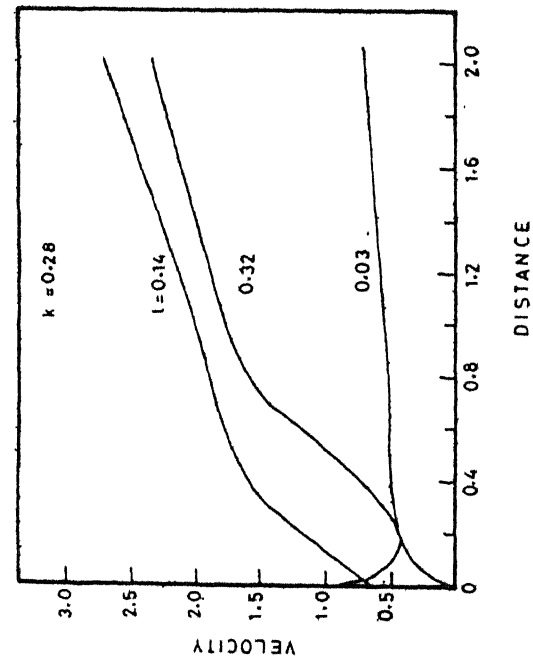
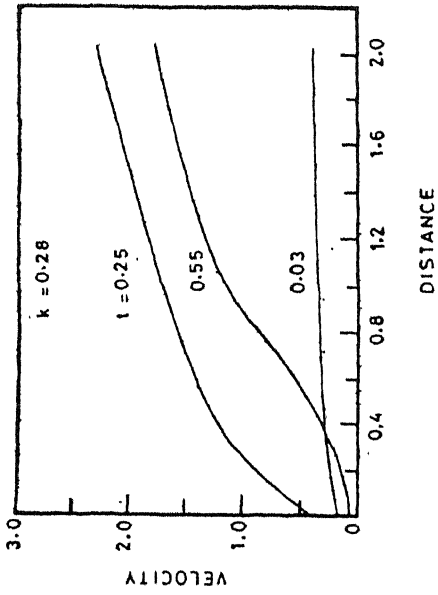


Fig. 2.7 (top left): Velocity profiles for boundary condition (2.14a) at different instants of time (marked in figure).  
 Fig. 2.8 (top right): Velocity profiles for boundary condition (2.14b) at different epochs.  
 Fig. 2.9 (bottom left): Pressure profiles corresponding to the velocity profiles of Fig. 2.7.  
 Fig. 2.10 (bottom right): Pressure profiles corresponding to the velocity profiles of Fig. 2.8.

figure 2.10. Here we see only one kink propagating upwards with a velocity of  $\approx 2.0$  units which is the initial impulse. Apparently there is no corresponding impulse travelling downwards.

Figure 2.11 and 2.12 show the temporal behaviour of the velocity and pressure at two different space points with boundary conditions (2.14a) and (2.14b) respectively. In both cases there is a rise to peak velocity followed by a decline. The peak velocities are different since the initial values for  $V_n$  at the base are different (8.0 and 6.0 respectively). We find that smaller starting values for  $V_n$  produce smaller parallel flows. It is also to be noticed that the velocity variations at two spatial points are more in phase than compared to the pressure variations at these points. The decline of the parallel flow is on a time scale comparable to the acoustic travel time over the length of the field line participating in the lateral motion. For a total length of 2.0 for the field line, the time scale of decline is approximately 0.85 units. When a larger length was assumed (4.0) the relaxation time is  $\approx 3.0$  as seen in figure 2.13 where the behaviour of the lateral flow  $V_n$  is also plotted alongside for the sake of illustration.

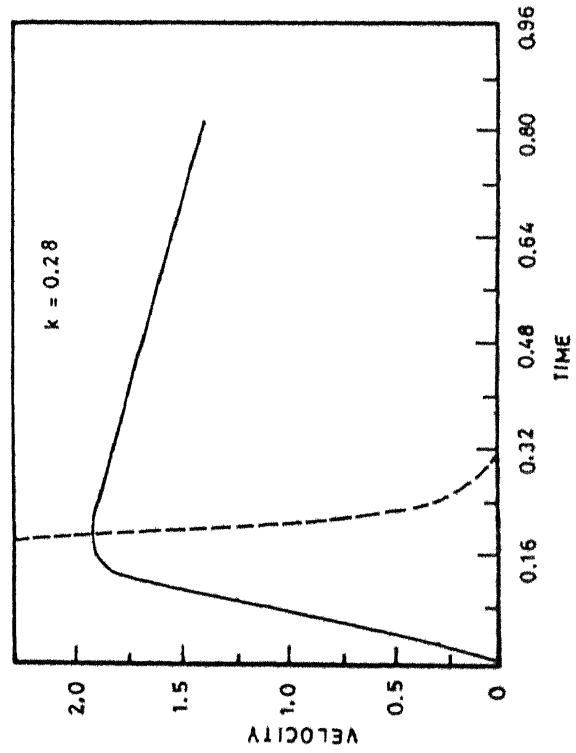
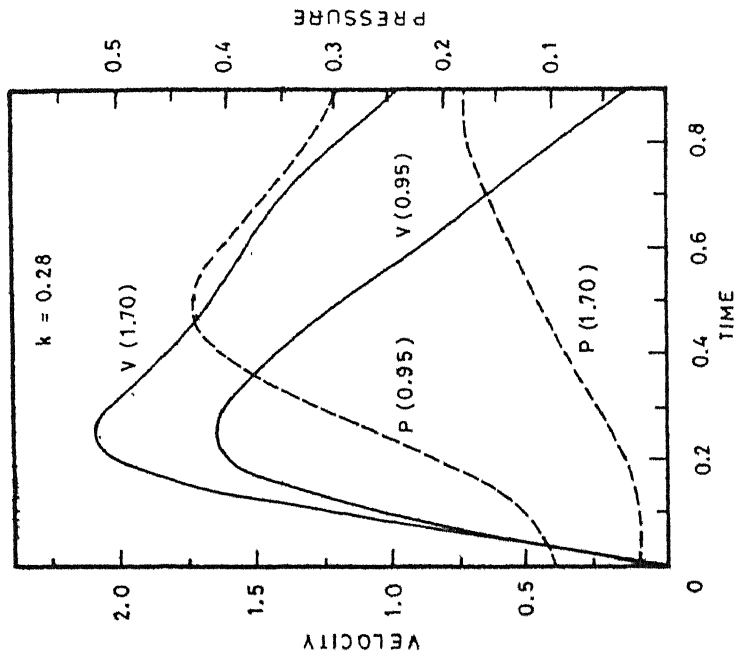
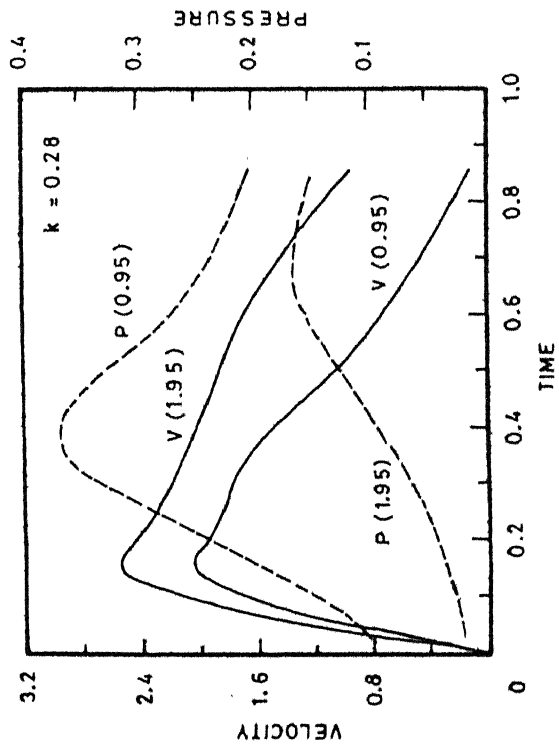


Fig. 2.11 (top left): Time dependence of velocity (solid lines) and pressure (dashes) at the two positions (value in brackets) along the field for boundary condition (2.14a).

Fig. 2.12 (top right): Variation of velocity and pressure with time at two spatial positions when boundary condition (2.14b) was applied.

Fig. 2.13: Time dependence for a longer length ( $= 4.0$ ) of the field line. The lateral velocity is also plotted (dashes).



### 2.7 Discussion of the results:

Physically one can think of two mechanisms which can accelerate the gas along the field line. The first is a "squeezing" action much as one squirts a fluid from a tube-like container. An upper limit for the acceleration can be estimated by considering an incompressible fluid. In this case the acceleration  $\frac{D}{Dt} V_s$  can be approximately written as  $-V_s \frac{D}{Dt} \ln \delta A$  where  $\delta A$  is the area of the tube. From equation (2.7d) this can be further simplified as  $-V_s \frac{\partial}{\partial n} V_n$ . This in turn, depends on the rate at which  $V_n$  changes in time. There is another mechanism for acceleration which is more effective in the present study. The non-uniform lateral motion of a line element imposes on the associated fluid element: (1) a translational motion of its centre of gravity along a curved path and (2) a rotation around the centre of gravity. The centrifugal acceleration due to the rotation of the line elements cancel out when integrated over the field line. The centrifugal acceleration due to the translational motion along the curved path, however, will remain. In the present study this is given by  $V_n \frac{D}{Dt} \theta$  which can further be simplified to  $\frac{1}{2} \frac{\partial}{\partial s} V_n^2$  using equation (2.7c). It is thus seen that this acceleration is independent of the sign of  $V_n$  but depends on the rate of change of its magnitude along

the field line. This fact explains several of the results obtained in this study. First of all, it explains why the gas is always seen to be accelerated along the direction of increasing amplitude of the lateral velocity. Since, for the case of ' $\theta = ky$ ' type of flow, the acceleration is given by  $k V_n^2 \cos\theta$ , the increase of parallel velocity with increasing curvature and with increasing amplitude of lateral base velocity for such flows can also be readily understood. A comparison of  $\frac{1}{2} \frac{\partial}{\partial s} V_n^2$  with the "squeezing" term  $-V_s \frac{\partial}{\partial n} V_n$  shows that even if one assumes  $\frac{\partial}{\partial n} V_n$  to be comparable with  $\frac{\partial}{\partial s} V_n$ , the vanishingly small value of  $V_s$  at  $t = 0$  makes the squeezing term negligible at the beginning of the squeeze. Moreover, since the sign of the "squeezing" acceleration depends on whether the lateral motion is compressive or expansive, such terms will not contribute a net acceleration in the case of oscillatory motion. This is not the case with the centrifugal term which maintains its sign irrespective of the sign of  $V_n$ . Thus such an acceleration will persist even in an oscillation of the field line provided the longitudinal gradient does not reverse its sign. This term is of great dynamical importance since even a small persistent acceleration can generate significant flows along the field after a sufficiently long period of time.

Finally, the increase of response with increase in the "stiffness" of the equation of state could be because of the faster propagation of signals in "stiffer" media leading to closer communication between the extremities of the field line. The importance of the equation of state is thus seen even in a simple change of the polytropic index. More attention will be paid to the energy equation and the equation of state in the subsequent chapters.

#### 2.8 Application to granule - flux tube interaction on the sun:

At photospheric levels, granulation forms a velocity pattern which has a typical length scale of a few thousand kilometers and a time scale of a few minutes. There are also concentrated magnetic flux elements in the photosphere which undergo "buffeting" by the granules. In fact, there exists an earlier observational study of granule-flux tube interaction (Dunn and Zirker, 1973). In that study the very fine structure of rosette centres was resolved and was named solar filigree. It was seen that filigree are jostled about by granules with lateral velocities  $\approx 1.5 \text{ kms}^{-1}$ , which is considerably larger than the rms vertical velocity of granules. The filtergram observations by Ramsey et al (1977) seem to have resolved the magnetic

elements into their filigree components. More recently, high resolution observations (Daras - Papamargaritis & Koutchmy, 1983) do show the association of filigree with strong magnetic fields. Similarly, other elements of enhanced brightness, like the calcium bright points have been identified with magnetic elements (Sivaraman and Livingston, 1982). Thus one could reasonably assume that magnetic elements are indeed laterally displaced with velocities  $\approx 1.5 \text{ kms}^{-1}$ . What is more important to the purpose of this study is a knowledge of the variation of the magnitude of the jostling with height in the solar atmosphere. In the absence of direct observational information, let us assume a form for the lateral motion of the field lines which is related to the observed form of the granular velocity field. Observations of the granular velocity variation with height in the solar atmosphere (Durrant et al, 1979) indicate a decrease of the rms vertical velocity with height. The scale height of the variation is  $\approx 500 \text{ km}$ . The life time of the granule varies between 2 to 15 minutes. The time variation of a single granulation flow can, therefore, be approximated by a sine function with a half period equal to the granule life-time. More specifically, one can represent the granular velocity  $V_g$  as

$$V_g = V_0 \exp(-z/H) \sin(\pi t/T). \quad (2.22)$$

In the present calculation the form (2.22) was assumed for  $V_n$  with  $V_0 = 0.7$ ,  $H = 2.0$  and  $T = 3.5$  in dimensionless units corresponding to  $0.5 \text{ kms}^{-1}$ ,  $500 \text{ km}$  and  $120 \text{ s}$  respectively for a reference temperature  $T_* = 6000 \text{ K}$ . The initial magnetic field was chosen to be purely vertical and the gas was assumed to be initially stratified with a polytropic index of  $\Gamma = 1.064$ . This value of  $\Gamma$  was chosen to fit the Harvard-Smithsonian Reference Atmosphere (Gingerich et al 1971) for a height of  $500 \text{ km}$  above the photosphere which also corresponds to the height range in which downflows have been observed in tubes (Giovanelli & Slaughter, 1978).

The results are shown in figure 2.14 where the variation of the fluid velocity component along the magnetic field is plotted as a function of the distance along the field at different instants of time. The flow begins as a downflow and remains as such throughout the life time of the lateral velocity field. The magnitude of the velocity along the field initially decreases with height, but at later instants of time, it increases with height. The observations of Giovanelli & Slaughter (1978) actually show a decrease of velocity with height. However, the present

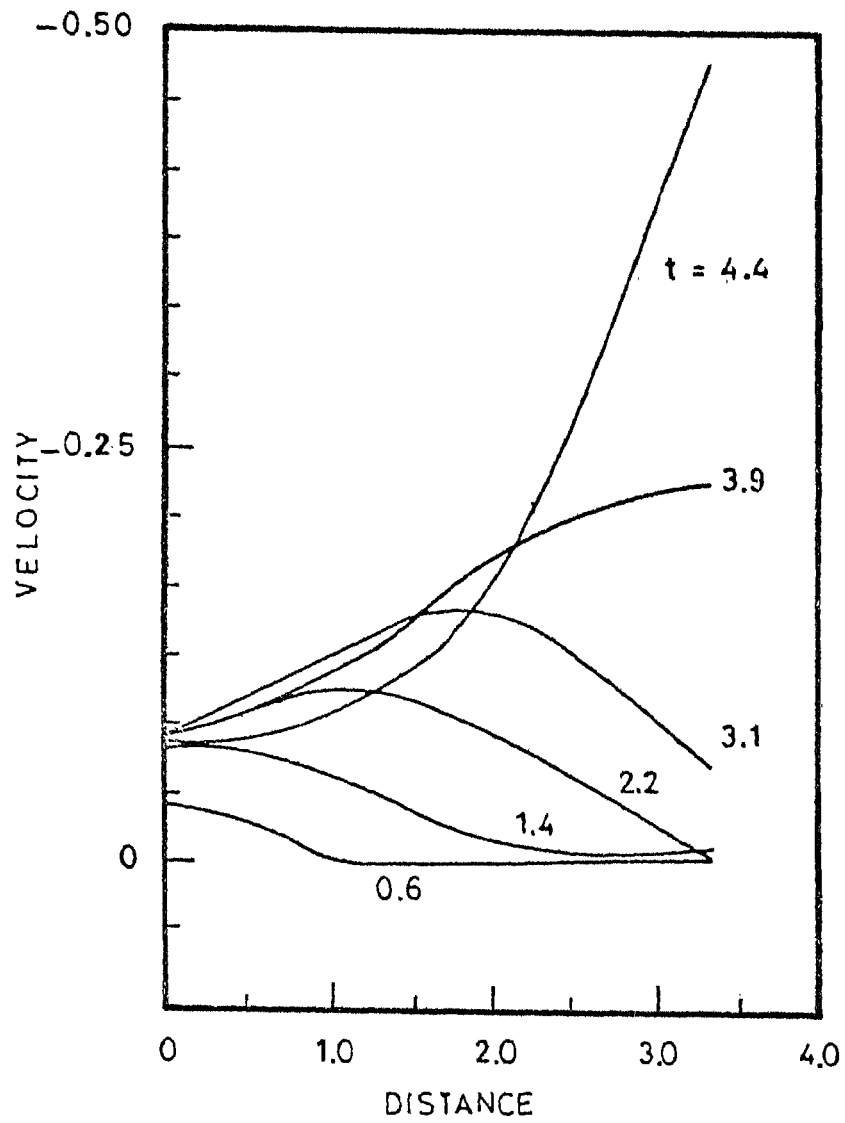


Fig. 2.14: The velocity profile at different instants of time is plotted for the simulation of granular buffeting.

calculations do not include the back-reaction of the field on the flow and assume that the lateral motions are directly proportional to the granular velocity field. One cannot, therefore, make detailed comparisons with observations especially for durations of time larger than the Alfvén travel time over the length of the field. For a field of strength  $\approx 1000$  G and length  $\approx 500$  km, this works out to approximately 60 s.

A more detailed discussion of these points is postponed to chapter 6. It is sufficient to note here that one can expect significant downflows to be generated within flux tubes as a result of the jostling of these tubes by granulation. If the jostling decreases monotonically with height, then the flows would be downflows at all times.

### 3. INTERACTION OF MAGNETIC FLUX TUBES WITH THEIR ENVIRONMENT

#### II. Response to external pressure fluctuations

##### 3.1 A magnetic flux tube in a turbulent fluid:

The previous chapter dealt with the result of bending motions produced in the tube by external turbulence. It is easier to excite such kink modes than the sausage or squeezing modes in a tube (Spruit, 1981b). In the case of a compressible fluid one does not know a priori what fraction of the energy from the "squeezing" agency goes into the increase of the internal energy of the fluid and what fraction is actually used for driving fluid motions. On the other hand, if one squeezes a tube containing an incompressible fluid, the entire energy of the squeeze will be converted into the kinetic energy of the fluid flow along the tube.

The response of thin tubes containing incompressible fluids to external turbulence has been studied by Parker (1974b). He considers two aspects of this problem. In the first case the tube walls are assumed to move in a prescribed manner. This results in a change in the magnetic field due to flux conservation. The fluid velocity is also affected due to mass conservation. The changes in the magnetic and velocity



fields influence the gas pressure inside the tube due to momentum conservation. The time average of the solutions of the equations of continuity, motion and flux conservation yields an expression for the mean magnetic pressure enhancement which is equivalent to the dynamical pressure  $\rho V_e^2$  caused by external turbulence. By assuming  $V_e \approx 3 \text{ kms}^{-1}$  and  $\rho \approx 10^{-7} \text{ g cm}^{-3}$ , Parker obtains fields of the order of 600 G.

Parker also considered the case of the massaging of a flux tube by external turbulence (Parker 1974a). He idealises the effect of eddies advected downward along the tube walls in terms of a moving constriction travelling downwards with the speed of the intergranular downflow. Even in this case he obtains fields of the order of the "equipartition" value of about 600 G.

The response of a flux tube containing a compressible fluid to external pressure variations was studied by Roberts (1979). He obtained a resonance when the time scale of the external pressure fluctuations matched with the time taken for a "tube" wave to travel across one wavelength of the fluctuation. Roberts concluded that the tube could absorb energy at the resonant frequency from the wide spectrum of frequencies incident on the tube. He suggested that this could be the driving mechanism for spicules. It should be noted that

the motions produced by this mechanism are oscillatory. Furthermore, it is not known whether nonlinear effects would smother the resonance. The response of a flux tube to external pressure perturbations has also been suggested as a diagnostic for estimating the thickness of the tube (Venkatakrisnan, 1979). The analysis of the interaction of a flux tube with its environment can be simplified by considering the slender flux tube approximation which shall be described in the following section.

### 3.2 The slender flux tube approximation:

The slender flux tube approximation rests on the assumption that the radius of the tube varies on a length scale much larger than the radius itself. This approximation enables one to study dynamical phenomena within tubes which are stratified by gravity. Such studies have been reviewed by Venkatakrisnan (1981) and more recently by Spruit & Roberts (1983). The rigorous derivation of the equations of a slender flux tube is given in an appendix by Roberts & Webb (1978). It is based on a perturbation expansion of all variables in powers of  $(r/\Lambda)$  where  $r$  is the radial distance from the axis of the tube and  $\Lambda$  is some measure of the length scale of variation of the tube radius. By formally equating the terms independent of  $r/\Lambda$ ,

Roberts and Webb (1978) obtained the following equations of zero order in  $r/\Lambda$

$$\frac{\partial}{\partial t} (\rho/B) + \frac{\partial}{\partial z} (\rho v/B) = 0, \quad (3.1)$$

$$\frac{\partial}{\partial t} v + v \frac{\partial}{\partial z} v + \frac{1}{\rho} \frac{\partial}{\partial z} p + g = 0, \quad (3.2)$$

$$\left\{ \frac{\partial}{\partial t} p - \left( \frac{\gamma p}{\rho} \right) \frac{\partial}{\partial t} \rho \right\} + v \left\{ \frac{\partial}{\partial z} p - \left( \frac{\gamma p}{\rho} \right) \frac{\partial}{\partial z} \rho \right\} \\ = -(\gamma-1)(\nabla \cdot \underline{F}), \quad (3.3)$$

$$B^2 = 8\pi (p_e - p), \quad (3.4)$$

where  $p$ ,  $\rho$ ,  $v$  and  $B$  are the pressure, the density, the fluid velocity along the tube axis, and the magnetic field inside the tube, respectively;  $p_e$  is the gas pressure outside the tube, and  $\underline{F}$  is the energy flux.

The static equilibrium solution of this system of equations was actually first obtained by Parker (1955) in a different context. One can construct a family of static solutions in terms of two functions  $\theta(z)$  (the ratio of the temperature at a depth  $z$  outside and inside the tube) and  $\beta(z)$  (the ratio of gas pressure to magnetic pressure inside the tube). The equilibrium solution is then written as

$$T_{oi} = T_{oe} / \theta , \quad (3.5)$$

$$B^2 = 8 \pi p_{oe} / (1 + \beta) , \quad (3.6)$$

$$p_{oi} = p_{oe} \beta / (1 + \beta) , \quad (3.7)$$

$$\rho_{oi} = \theta \rho_{oe} \beta / (1 + \beta) . \quad (3.8)$$

In addition,  $p_{oe}$  and  $p_{oi}$  must satisfy the equation of hydrostatic balance. Inside the tube this equation is

$$\frac{d}{dz} p_{oi} = - \rho_{oi} g . \quad (3.9)$$

Substituting for  $p_{oi}$  and  $\rho_{oi}$  in equation (3.9) we have the following identity,

$$\frac{d}{dz} \left( \frac{\beta}{1 + \beta} \right) = - (\theta - 1) \left( \frac{\beta}{1 + \beta} \right) \frac{\rho_{oe} g}{p_{oe}} .$$

Hence there exists an extremum for  $\beta / (1 + \beta)$  at  $\theta = 1$ .

Furthermore if  $\theta = 1$  at all  $z$ , then  $\beta$  is also

independent of  $z$ . Let us now perturb any dynamical variable by a small amount  $q$  which is of the form

$q = q_0(z) \exp i \omega t$ . Then the linearised form of the equations (3.1) through (3.4) reduce to a single

second order ordinary differential equation in one variable (Roberts & Webbs, 1978), viz.

$$a_2 \frac{d^2}{dz^2} V + a_1 \frac{d}{dz} V + a_0 = 0, \quad (3.10)$$

where  $a_2$ ,  $a_1$ , and  $a_0$  are, in general, functions of  $z$ . By means of suitable transformations, this equation can be written in the canonical form

$$\frac{d^2}{dx^2} y + f(\omega^2; x) y = 0. \quad (3.11)$$

The curve  $f(\omega^2; x) = 0$  separates the "propagating" and "evanescent" regimes in  $x$  for a given  $\omega^2$ . Conversely it represents a "local" dispersion relation for  $\omega^2$  separating "propagating" and "evanescent" frequencies at some  $x$ . Alternatively, it represents a sufficient condition on  $\omega^2$  for the existence of bounded solutions.

If one solves equation (3.11) subject to boundary conditions on  $y$  at two points  $x_1$  and  $x_2$ , we obtain an eigenvalue problem for  $\omega^2$ . For adiabatic variations  $\omega^2$  is real, leading to oscillations when it is positive and instability when it is negative.

The case of instability will be discussed in chapter 4. In the case of oscillations, it is seen

that only one mode exists as opposed to two in the case of an unbounded medium. This "suppression of modes" has been noted and discussed by Cram and Wilson (1975) and will occur only if  $T_{oi} = T_{oe}$  (Roberts, 1981a,b). The phase velocity of the "allowed" mode is smaller than the minimum of either the Alfvén velocity or the sound velocity. It is called the "tube" velocity in the literature and is given by

$$C_T = \left( \frac{A^2 S^2}{A^2 + S^2} \right)^{1/2}, \quad (3.12)$$

where  $A$  and  $S$  are the Alfvén and sound speeds respectively. "Tube" waves in thin tubes are essentially the counterparts of "slow" waves of finite tubes. The properties of tube waves have been well studied (Roberts & Webb, 1978; Spruit, 1981a,b; Rae & Roberts, 1982). In the next section, we reduce the nonlinear equations to the characteristic form with a view to use them in our computations.

### 3.3 The characteristic equations for a slender flux tube:

If one neglects the heat source terms in equation (3.3) then the system of equations (3.1) through (3.4) is a hyperbolic system of partial differential equations and will, therefore, possess real characteristics. Equations (3.1) through (3.3) can be rewritten as

$$\left( \mathbf{I} \frac{\partial}{\partial t} + \mathbf{A} \frac{\partial}{\partial z} \right) \mathbf{Y} = \mathbf{b} \quad (3.13)$$

where

$$\mathbf{I} = \begin{pmatrix} 1 & 0 & 0 \\ 0 & 1 & 0 \\ 0 & 0 & 1 \end{pmatrix} ; \quad \mathbf{A} = \begin{pmatrix} v & 0 & c_T^2 \rho \\ 0 & v & \rho c_T^2 / s^2 \\ 1/\rho & 0 & v \end{pmatrix} ;$$

$$\mathbf{Y} = \begin{pmatrix} p \\ \rho \\ v \end{pmatrix} ; \quad \mathbf{b} = \begin{pmatrix} Q \\ \rho/s^2 \\ -g \end{pmatrix} \text{ and } Q = c_T^2 \left( \frac{\partial}{\partial t} p_e + v \frac{\partial}{\partial z} p_e \right) / A^2.$$

Multiplying equation (3.13) by  $\sigma^T$ , the transpose of  $\sigma$ , where  $\sigma = \begin{pmatrix} \sigma_1 \\ \sigma_2 \\ \sigma_3 \end{pmatrix}$  is any arbitrary constant vector, we have:

$$\left( \sigma^T \frac{\partial}{\partial t} + \sigma^T \mathbf{A} \frac{\partial}{\partial z} \right) \mathbf{Y} = \sigma^T \mathbf{b}. \quad (3.14)$$

Let  $\lambda_n$  be the  $n$ th eigenvalue of the equation

$$\mathbf{A}^T \sigma_n = \lambda_n \sigma_n \quad (3.15)$$

where  $\sigma_n$  is the corresponding eigenvector. Then

(3.14) transforms to

$$\sigma_n^T \left( \frac{\partial}{\partial t} + \lambda_n \frac{\partial}{\partial z} \right) \mathbf{Y} = \sigma_n^T \mathbf{b}. \quad (3.16)$$

If  $\lambda_n$  is such that

$$\lambda_n = - \left( \frac{\partial}{\partial z} \xi_n / \frac{\partial}{\partial t} \xi_n \right)^{-1}$$

where  $\xi_n(x, t) = \text{constant}$  is some curve in the  $t-x$  plane, then equation (3.16) reduces to

$$\sigma_n^\top \frac{d}{dt} \mathbf{Y} = \sigma_n^\top \mathbf{b}, \quad (3.17)$$

along the curve  $\xi_n = \text{constant}$ . If the original system of equations were fully hyperbolic, then there would be  $m$  real eigenvalues where  $m$  is the number of elements in  $\mathbf{Y}$ . In the present case, the  $\lambda_n$ 's are given by

$$\lambda_1 = v + c_T; \quad \lambda_2 = v - c_T; \quad \lambda_3 = v$$

where  $c_T = SA / (G^2 + A^2)^{1/2}$  is the velocity of "tube waves, with

$$\sigma_1 = \sigma \begin{pmatrix} 1 \\ 0 \\ \rho c_T \end{pmatrix}; \quad \sigma_2 = \sigma \begin{pmatrix} 1 \\ 0 \\ -\rho c_T \end{pmatrix}; \quad \sigma_3 = \sigma \begin{pmatrix} 1 \\ -S^2 \\ 0 \end{pmatrix},$$

where  $\sigma$  is an arbitrary constant. The compatibility equations are, therefore,

$$dp + \rho c_T dv = (\alpha + \beta) dt \quad \text{along } \lambda = v + c_T, \quad (3.18)$$

$$dp - \rho c_T dv = (\alpha - \beta) dt \quad \text{along } \lambda = v - c_T, \quad (3.19)$$

and

$$dp - \left(\frac{r\beta}{\rho}\right) d\rho = 0 \quad \text{along } \lambda = v, \quad (3.20)$$



where

$$\alpha = Q \quad \text{and} \quad \beta = -\rho C_T g.$$

It is interesting to note that there are normally 4 characteristics for one-dimensional unsteady flow in an unbounded magnetic field (Pai, 1962). The fact that the number in the present case is 3 is again reminiscent of the "suppression of modes" referred to in the previous section. Equation (3.18) through (3.20) cannot be solved analytically in general and we will resort to the numerical method described in chapter 2. Before proceeding we present an analytical solution representing the linear response of a uniform tube to external pressure perturbations.

#### 3.4 Linear response for a uniform tube to external pressure perturbations:

The linearised version of equation (3.18) through (3.20) can be written as

$$\frac{1}{A^2} \frac{\partial}{\partial t} p_1 + \frac{\partial}{\partial t} p_1 + \rho_0 \frac{\partial}{\partial z} v_1 = \frac{1}{A^2} \frac{\partial}{\partial t} p_{e1} - \int_0^1 v_1 \frac{\partial}{\partial z} \ln(\rho_0 / B_0), \quad (3.21)$$

$$\rho_0 \frac{\partial}{\partial t} v_1 + \frac{\partial}{\partial z} p_1 = -\rho_1 g, \quad (3.22)$$

$$\frac{\partial}{\partial t} p_1 - \left( \frac{r p_0}{\rho_0} \right) \frac{\partial}{\partial t} \rho_1 = -v_1 \left( \frac{\partial}{\partial z} p_0 - \frac{r p_0}{\rho_0} \frac{\partial}{\partial z} \rho_0 \right), \quad (3.23)$$

where the subscript '1' denotes perturbed quantities and '0' denotes unperturbed quantities. For a uniform tube these simplify to

$$\frac{1}{A^2} \frac{\partial}{\partial t} p_1 + \frac{\partial}{\partial t} \rho_1 + \rho_0 \frac{\partial v_1}{\partial z} = \frac{1}{A^2} \frac{\partial}{\partial t} p_{e1}, \quad (3.24)$$

$$\rho_0 \frac{\partial v_1}{\partial t} + \frac{\partial}{\partial z} p_1 = 0, \quad (3.25)$$

with  $p_1 = s^2 \rho_1$ . The characteristic directions in the (t-z) plane are given by

$$\lambda \equiv \frac{dz}{dt} = \pm c_T.$$

Let us now transform to the characteristic curves given by

$$\xi(z, t) = z - c_T t \quad \text{and} \quad \eta(z, t) = z + c_T t.$$

The equations (3.24) and (3.25) now become

$$\frac{\partial}{\partial \xi} (p_1 - \rho_0 c_T v_1) = - \frac{c_T}{2A^2} \frac{\partial}{\partial t} p_{e1} \quad (3.26)$$

$$\text{and } \frac{\partial}{\partial \eta} (p_1 + \rho_0 c_T v_1) = \frac{c_T}{2A^2} \frac{\partial}{\partial t} p_{e1} \quad (3.27)$$

Thus

$$p_1 + \rho_0 c_T v_1 = f_1(\xi) + \frac{c_T}{2A^2} \int \frac{\partial}{\partial t} p_{e1} d\eta \quad (3.28)$$

and

$$p_1 - \rho_0 c_T v_1 = f_2(\eta) - \frac{c_T}{2A^2} \int \frac{\partial}{\partial t} p_{e1} d\xi, \quad (3.29)$$

where  $f_1$  and  $f_2$  are arbitrary functions.

Hence

$$p_1 = \frac{f_1(\xi) + f_2(\eta)}{2} + \frac{c_T}{4A^2} \int \frac{\partial}{\partial t} p_{e1} (d\eta - d\xi) \quad (3.30)$$

and

$$v_1 = \frac{f_1(\xi) - f_2(\eta)}{2\rho_0 c_T} + \frac{1}{4\rho_0 A^2} \int \frac{\partial}{\partial t} p_{e1} (d\eta + d\xi). \quad (3.31)$$

However,

$$d\eta + d\xi = 2dz \quad \text{and} \quad d\eta - d\xi = 2c_T dt.$$

Thus equations (3.30) and (3.31) reduce to

$$p_1 = \frac{f_1(z - c_T t) + f_2(z + c_T t)}{2} + \frac{c_T^2}{2A^2} \int \frac{\partial}{\partial t} p_{e1} dt \quad (3.32)$$

and

$$v_1 = \frac{f_1(z - c_T t) - f_2(z + c_T t)}{2 \rho_0 c_T} + \frac{1}{2 \rho_0 A^2} \int \frac{\partial}{\partial t} p_{e1} dz. \quad (3.33)$$

Let us assume the following form for  $p_{e1}$  :

$$p_{e1} = p_{e0} \exp - \frac{z}{H} \sin \omega t.$$

Then equations (3.32) and (3.33) further reduce to

$$p_1 = \frac{f_1(z - c_T t) + f_2(z + c_T t)}{2} + \frac{c_T^2}{2A^2} p_{e1} \quad (3.34)$$

and

$$v_1 = \left\{ f_1(z - c_T t) - f_2(z + c_T t) \right\} / 2 \rho_0 c_T - \frac{H \omega}{2 \rho_0 A^2} p_{e0} \cos \omega t \exp - \frac{z}{H}. \quad (3.35)$$

Applying initial conditions  $p_1(0) = p_{10}(z)$  and

$v_1(0) = v_{10}(z)$ , we have

$$p_{10}(z) = \frac{f_1(z) + f_2(z)}{2} \quad (3.36)$$

and

$$v_{10}(z) = \left\{ f_1(z) - f_2(z) \right\} / 2 \rho_0 c_T - \frac{\omega H}{2 \rho_0 A^2} p_{e0} \exp - \frac{z}{H}. \quad (3.37)$$

Hence

$$f_1(z) = p_{10}(z) + \rho_0 c_T \left\{ v_{10}(z) \right.$$

$$\left. + \frac{\omega H}{2\rho_0 A^2} p_{e0} \exp\left(-\frac{z}{H}\right) \right\} \quad (3.38)$$

and

$$f_2(z) = p_{10}(z) - \rho_0 c_T \left\{ v_{10}(z) + \frac{\omega H}{2\rho_0 A^2} p_{e0} \exp\left(-\frac{z}{H}\right) \right\}. \quad (3.39)$$

Let

$$p_{10}(z) = 0 \quad \text{and} \quad v_{10}(z) = 0.$$

Then

$$f_1(z) = \frac{c_T \omega H}{2A^2} p_{e0} \exp\left(-\frac{z}{H}\right) \quad (3.40)$$

and

$$f_2(z) = -\frac{c_T \omega H}{2A^2} p_{e0} \exp\left(-\frac{z}{H}\right). \quad (3.41)$$

Thus

$$\begin{aligned} & \left\{ f_1(z - c_T t) + f_2(z + c_T t) \right\} / 2 \\ & = \frac{c_T \omega H}{2A^2} p_{e0} e^{-\frac{z}{H}} \sinh\left(\frac{c_T t}{H}\right) \end{aligned}$$

and

$$\begin{aligned} & \left\{ f_1(z - c_T t) - f_2(z + c_T t) \right\} / 2\rho_0 c_T \\ & = \frac{\omega H}{2\rho_0 A^2} p_{e0} e^{-\frac{z}{H}} \cosh\left(\frac{c_T t}{H}\right). \end{aligned}$$

Finally,

$$p_1(z, t) = \frac{c_T^2}{2A^2} p_{e0} e^{-\frac{z}{H}} \left( \sin \omega t + \frac{\omega H}{c_T} \sinh \frac{c_T t}{H} \right) \quad (3.42)$$

and

$$v_1(z, t) = \frac{H\omega}{2\rho_0 A^2} p_{e0} e^{-\frac{z}{H}} \left( \cosh \frac{c_T t}{H} - \cos \omega t \right). \quad (3.43)$$

It is thus seen that both  $p_1$  and  $v_1$  have an oscillatory component as well as a monotonically increasing component which grows on a time scale of approximately  $H/c_T$ . Since the above analysis is valid only for small amplitudes, one cannot say whether the growing component persists in the presence of nonlinear terms. The next section deals with a numerical study of the nonlinear problem with the additional feature of a stratified tube.

### 3.5 Nonlinear response for a polytropic tube to external pressure perturbations:

We now present the results of numerical solutions of the nonlinear equations (3.18) through (3.20). We assumed an initial hydrostatic equilibrium with a polytropic stratification and space independent  $\beta_0$ . The time dependent calculations were performed only for a single value of  $\beta_0 = 2.0$ . In the solar photosphere, this value of  $\beta_0$  corresponds to  $\approx 1800$  G which is

approximately the value of the field within intense magnetic flux tubes. Since the magnetic field imparts a kind of "rigidity" to the associated fluid, weaker fields would imply a "softer" equation of state for the tube and, therefore, one would expect smaller values for the resulting longitudinal flow as compared to the response for a tube with stronger fields.

We chose the value of the polytropic index  $\Gamma = 1.1$  for matching with the Harvard-Smithsonian Reference Atmosphere as has been mentioned in section 2.8.

The choice of the form of the external pressure perturbation needs some consideration. There are in general three possible classes of forms. There are the propagating disturbances produced by progressive waves. A second class is the standing wave pattern and finally we have an evanescent wave pattern. In the solar atmosphere large power has been observed to exist in the five minute oscillation and in the granulation. The former can be considered as an example of a standing oscillations (Leibacher & Stein 1981) while the latter has been observed to have an rms velocity distribution that decreases with height (Durrant et al 1979). The amount of power existing in progressive waves is not well known but the meagre information that is available

(Deubner 1976) indicates that this power is not very significant. It is, therefore, adequate to consider only the second and the third forms of the external pressure perturbation. We, therefore, studied the response of the tube to the following two forms of the external pressure perturbation:

$$p_{e1} = p_{e0} \cdot \exp -\frac{z}{H} \cdot \sin \frac{\pi}{T} t \quad (3.44)$$

and

$$p_{e1} = p_{e0} \cos k_z z \sin \omega t \quad (3.45)$$

where  $p_{e0}$  is the amplitude of pressure fluctuation,  $H$  is the scale height,  $T$  is the period,  $k$  is the wave number and  $\omega$  is the angular frequency.

Observations can yield only the approximate scale height of the variation of vertical rms velocity. To convert velocity fluctuations to pressure fluctuations one can use the equation of motion to write approximately

$$\frac{p_1}{p_0} \approx \frac{\omega}{(k_z + g/s^2)} \frac{v_z}{g},$$

where  $k_z$  is some measure of the vertical velocity variation. If  $k_z \ll g/s^2$  (as is the case for



granulation) then

$$p_1 / p_0 \approx \frac{\omega}{g} v_z \approx \frac{2\pi}{Tg} v_z .$$

Using typical values for  $T \approx 300 \text{ s}$ ,  $g \approx 2 \times 10^4 \text{ cm s}^{-2}$  and  $v_z \approx 10^5 \text{ cm s}^{-1}$  corresponding to granulation, we have

$$p_1 / p_0 \approx 0.1 .$$

This estimate is an overestimate since it assumes axially symmetric perturbations to act coherently at all depths on a single flux tube. In reality the buffeting of the flux tube would proceed in an incoherent manner thereby reducing the efficiency of conversion of velocity fluctuations into pressure fluctuations.

We treated this efficiency factor as a "fudge" factor. In particular, we assigned a modest value of 0.1 to this factor in the present calculations, thus taking  $p_1 / p_0 = 0.01$  which in dimensionless units implied  $p_{e0} = 0.01$ .

We first present the results corresponding to the pressure perturbations given by equation (3.44). In the calculation,  $T = 3.0$  in dimensionless units and three values of  $H = 1.0, 0.1$  and  $0.01$  were tried. For a temperature of  $\approx 6000 \text{ K}$ , the unit of length is

$\approx 250$  km and the unit of time is  $\approx 30$  s.

The time dependence of the longitudinal velocity near the midpoint of the tube ( $z = 0.48$ ) is shown in figure 3.1 for the three values of  $H$  mentioned above. It is evident from the figure that the response is more vigorous for the case of  $H = 1.0$ , than for the other two cases. The reason is that  $H = 1.0$  corresponds to the slowest decline of the pressure fluctuations with height. For the other two cases the pressure fluctuations become vanishingly small at  $z = 0.48$ . The fact that the response for  $H = 0.1$  is not very different from that for  $H = 0.01$  is again a reflection of the fact that at  $z = .48$ , the direct effect of pressure perturbations is so small that numerically it is difficult to distinguish between the two small quantities.

An interesting point to note is that the velocity fluctuations for  $H = 0.1$  and  $H = 0.01$  vary on a time-scale larger than the period of the external pressure fluctuations. There is an increase of downflow till a time  $\approx 2.5$  and then one sees a very gradual decrease of the downflow. The maximum of the pressure fluctuation occurs at the base of the tube and hence the delayed response at  $z = 0.48$  can be understood in terms of the time taken by tube wave to propagate over half the length

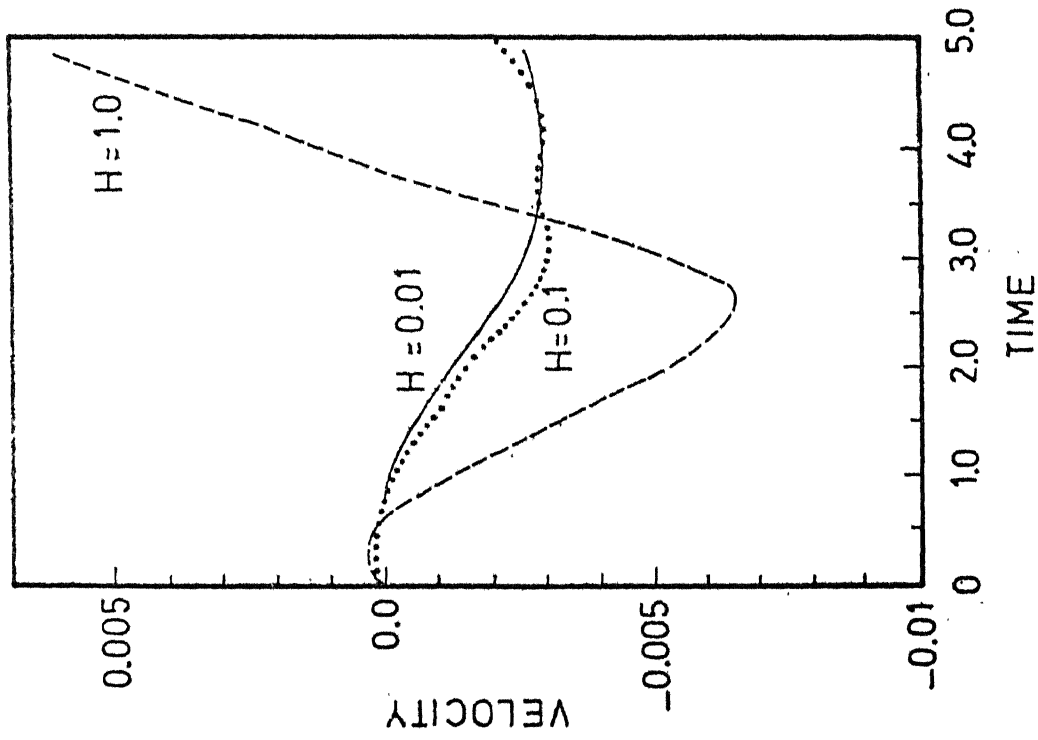
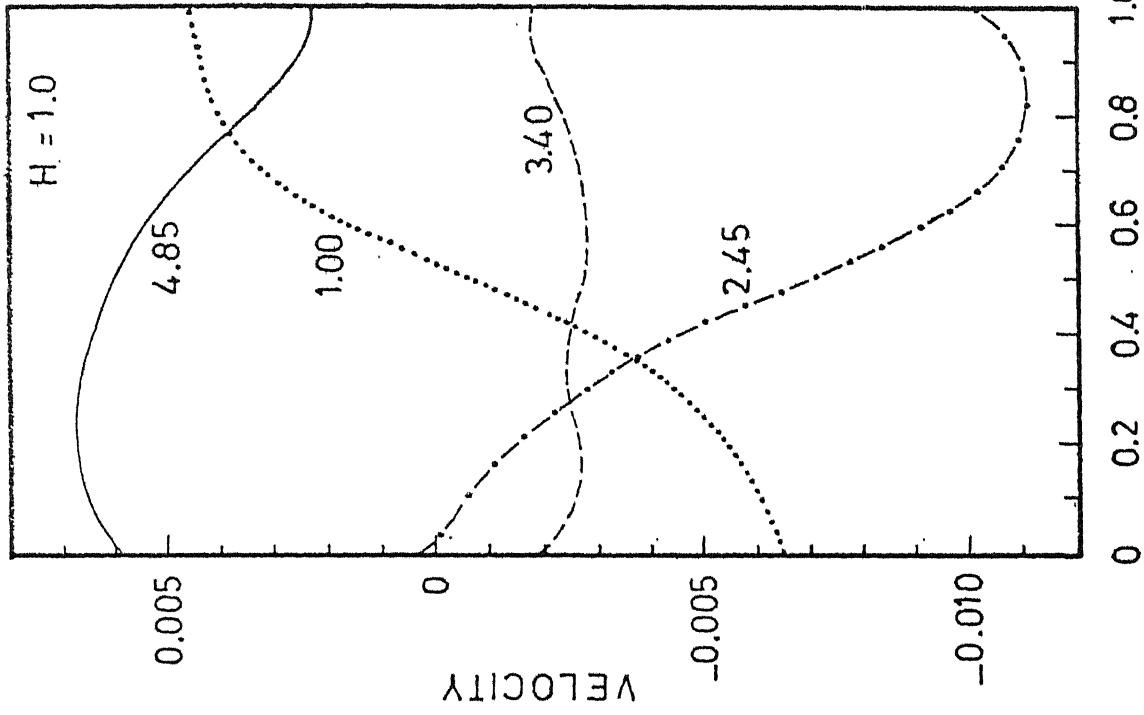


Fig.3.1 (left): Response to external pressure fluctuations decreasing with height with scale length  $H = 1.0$  (dashes),  $0.1$  (dots) &  $0.01$  (solid line).

Fig.3.2 (right): Velocity profiles at different epochs (marked in figure) resulting from evanescent pressure fluctuations with  $H = 1.0$ .

of the tube. The magnitude of this propagated compression would be larger than the in situ compression owing to the small values of  $H$ . We can, therefore, understand the change of slope in the response curve in figure 3.1 at  $t \approx 2.5$ . The effect of the dilatation would also be delayed in a similar manner but the computations were not followed to such times.

One can contrast such a behaviour with that for  $H = 1.0$ . Here we see that the velocity is in step with the external pressure fluctuation. The slower spatial variation of the external pressure fluctuation in this case maintains the in situ pressure fluctuation at a larger magnitude than the advected component and hence the latter component does not show up. Figures 3.2, 3.3 and 3.4 show the spatial profiles of the velocity at different times for the cases  $H = 1.0$ ,  $0.1$  and  $0.01$  respectively. In all these figures one sees that the velocity profile consists of both a downflow and an upflow with a node at the centre for  $t \approx 1.0$ . In the case of  $H = 1.0$ , the node disappears and we see downflow at all  $z$  when  $t = 2.45$ . This profile changes to one of almost uniform velocity at  $t = 3.40$ . Finally, at  $t = 4.85$  we see upflow at all points. In the other two cases of  $H = 0.1$  and  $H = 0.01$ , the phase of upflow at all  $z$  is not seen to be attained after a similar lapse

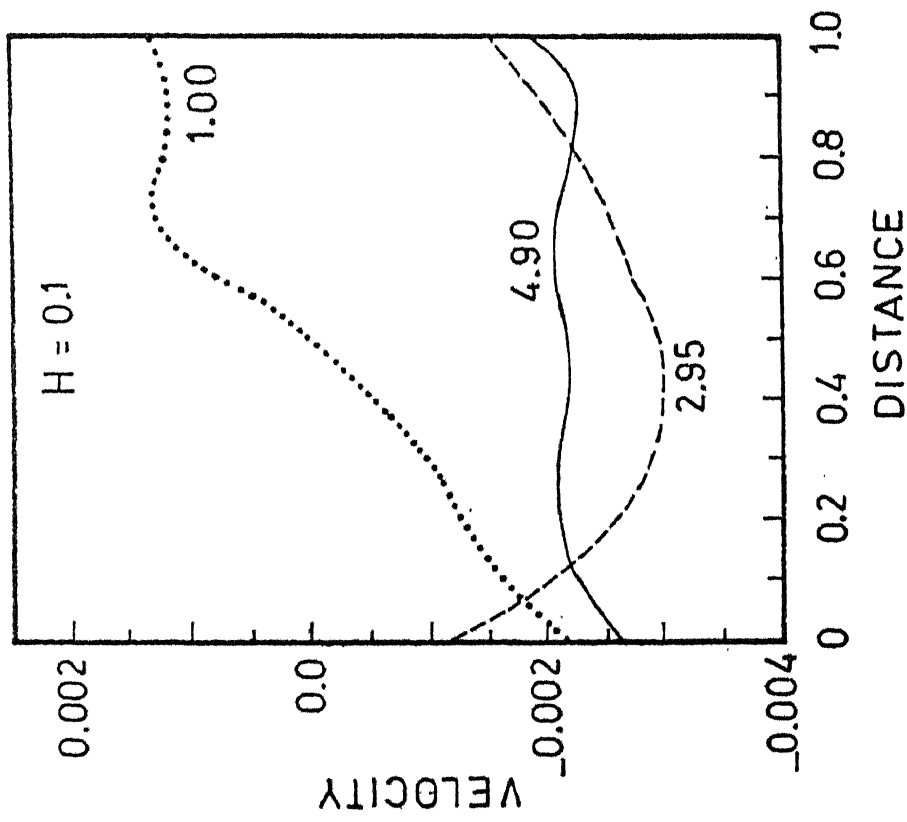


Fig.3.3 : Spatial velocity profiles at different instants of time (marked in figure) for  $H = 0.1$

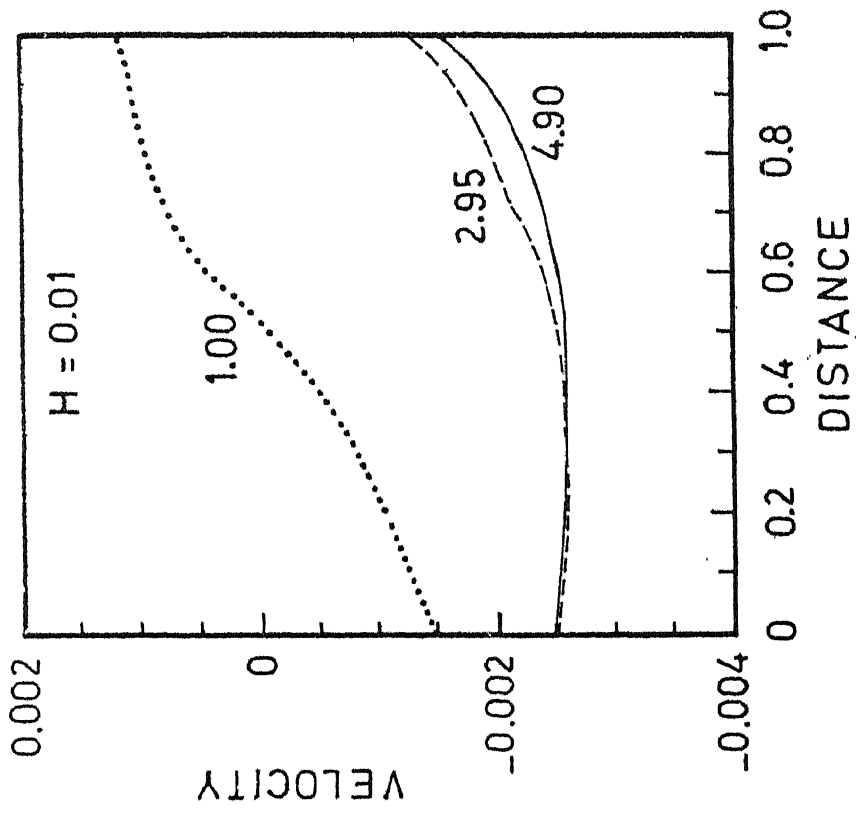


Fig.3.4 : Same as in figure 3.3, but with  $H = 0.01$

of time. This is entirely due to the predominance of the advected component of the response as mentioned earlier. One is, therefore, led to believe that if the external pressure perturbation is confined to the base regions of the tube and if the time period of the perturbation is small compared to the tube travel time, then unidirectional flows can be maintained for longer times. For the case of granulation, however, the vertical scale height of variation of velocity field is  $\approx 500$  km and the time scale of variation  $T \approx 300\delta$ . On the other hand, the tube travel time for a tube 500 km long is  $\approx 100\delta$ . Thus one would expect the response to be more like the case of  $H = 1.0$  in figure 3.1, i.e. the resulting longitudinal flow would be oscillatory rather than steady. The maximum magnitude of this velocity turns out to be  $\approx 0.01$  in dimensionless units which corresponds to  $\approx 100 \text{ ms}^{-1}$  at a height where the sound speed is  $\approx 10 \text{ kms}^{-1}$ . If the efficiency of conversion from velocity to pressure fluctuation is increased one would expect the magnitude of the longitudinal velocity fluctuation to increase correspondingly.

Let us next consider the results for pressure fluctuations given by equation (3.45). The time behaviour is given in figures 3.5 for various values of  $\lambda$ , where

$$\lambda = \omega / k C_T$$

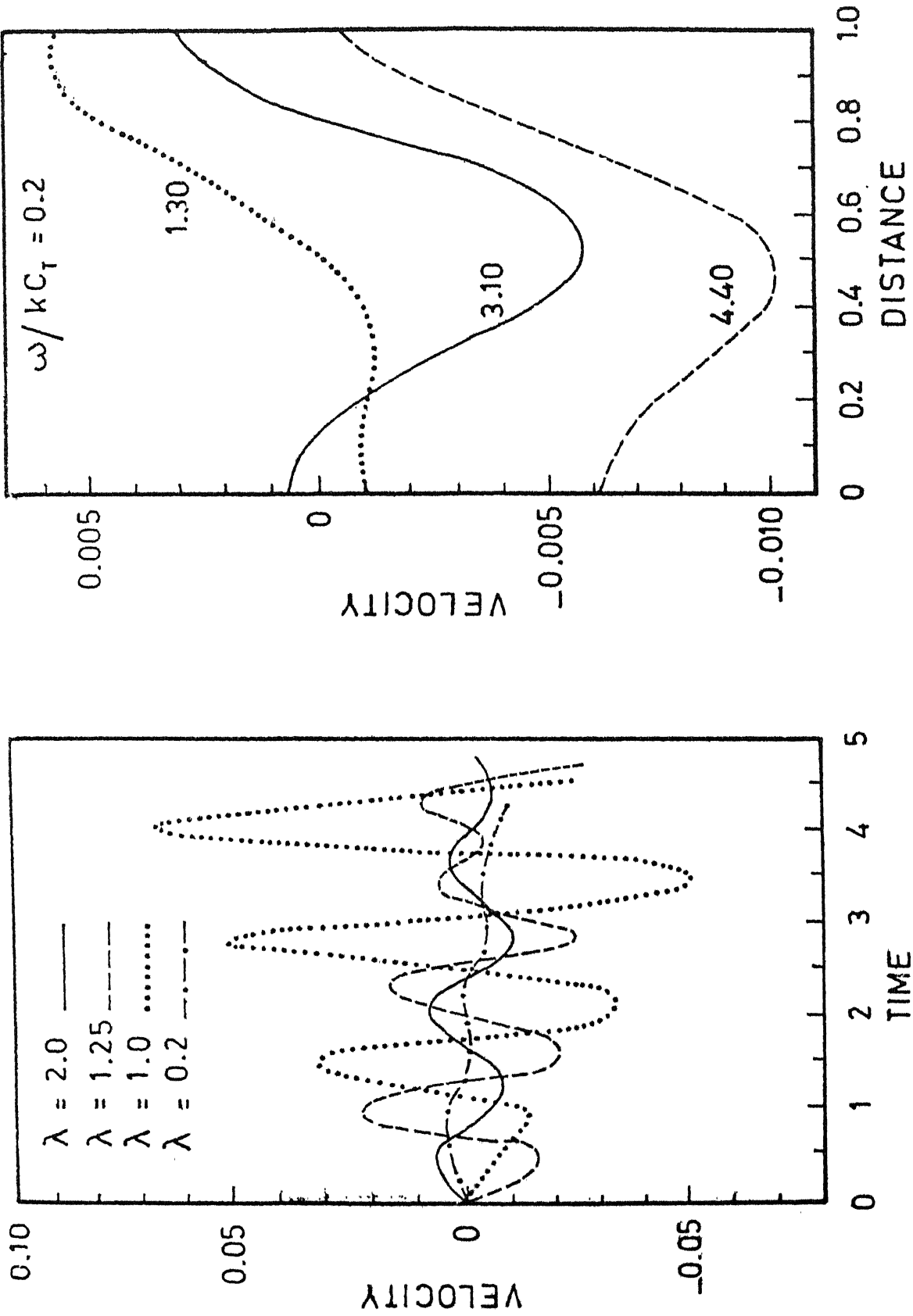


Fig.3.5 (left): Response to wave-like pressure fluctuations with unit wavelength and different values of  $\omega / kC_T$ .

Fig.3.6 (right): Velocity profiles at different epochs for  $\omega / kC_T = 0.2$ .

Here the wave number  $k$  was kept constant at  $\pi$ . This corresponded to two antinodes of the pressure fluctuation at the ends of the tube. The frequency was then chosen as different multiples of  $k C_T$ . As can be seen in figure 3.5, there is a distinct 'resonant' behaviour at  $\lambda = 1$ , i.e.  $\omega = k C_T$ . This confirms Robert's (1979) prediction of a resonance from a linear analysis. Unfortunately the calculations were not followed long enough in time to see whether the amplitude saturates or continues to build up until shocks are produced.

The mean velocity in the 'non-resonant' cases shows a tendency to drift to negative values although the computations are not extensive enough to confirm this. This tendency for drifting to negative velocities is also seen in the spatial velocity profiles as given by figures 3.6 to 3.10. The only exception is figure 3.7 which corresponds to the 'resonant' case. The skewness of the profiles is also less for this case.

The magnitude of longitudinal velocity for the resonant case is also interesting. The maximum value reached is  $\approx 0.1$  which corresponds to  $\approx 1 \text{ kms}^{-1}$  when sound speed is  $\approx 10 \text{ kms}^{-1}$ . This is only a lower limit since the saturation value was not reached in the



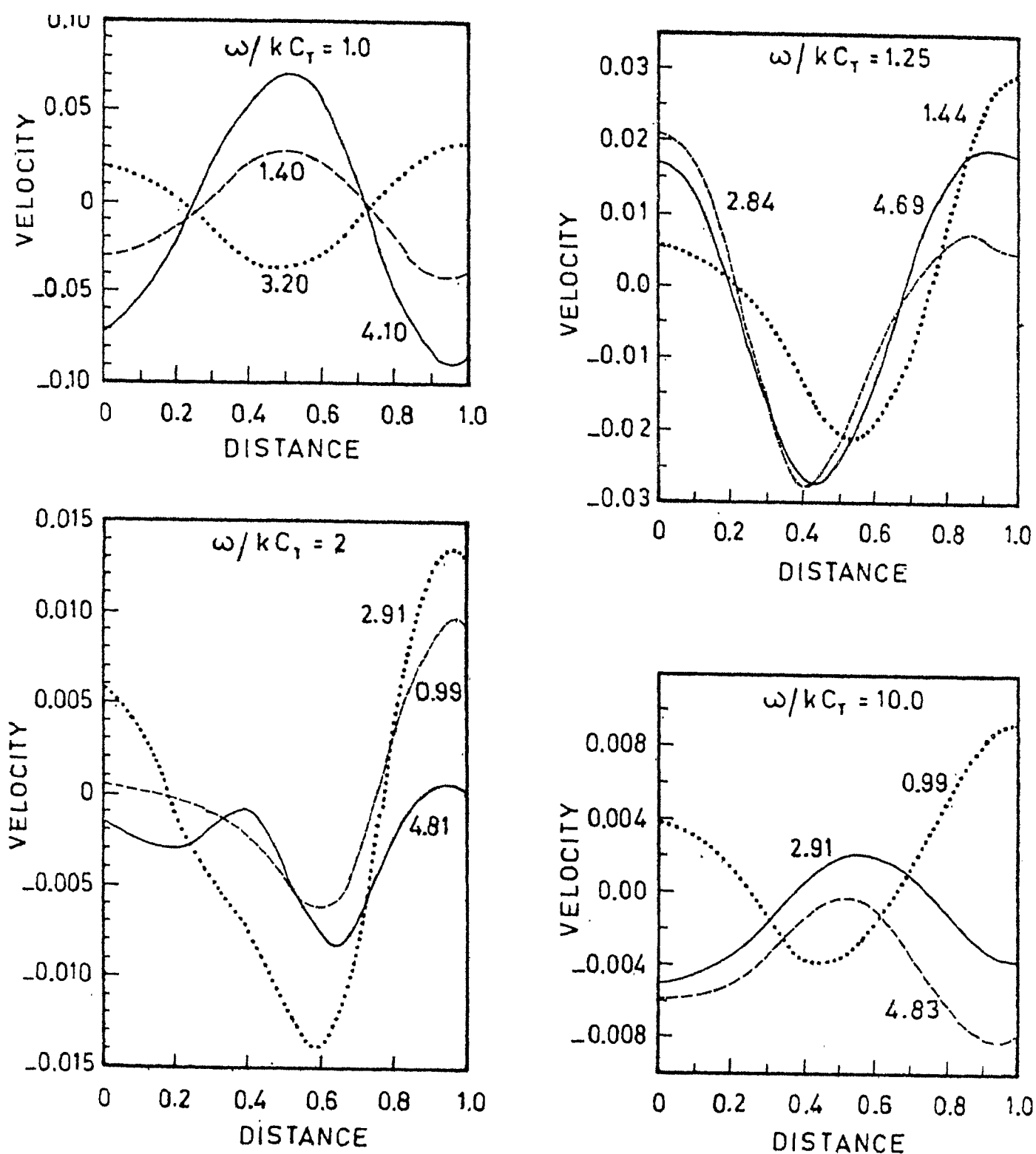


Fig.3.7 to 3.10: Spatial velocity profiles at different instants of time for  $\omega / k C_T = 1.0$  (top left), 1.25 (top right), 2.0 (bottom left) & 10.0 (bottom right) respectively.

calculation. Moreover, one does not know whether this value will be further increased consequent to an increase in the amplitude of the external pressure fluctuation.

On the whole, it seems that the resonance would lead to observable effects in real flux tubes on the sun. The flow would, however, be oscillatory with a time scale corresponding to the tube travel time.

In summary, one sees that the maximum response to external pressure fluctuations of both standing and evanescent forms occurs when the tube travel time is of the order of time scale of the fluctuations and in either case this maximum response is oscillatory rather than steady. In relation to observations of the solar magnetic flux tubes, this would mean that the observed systematic downflows are unlikely to be due to the external pressure fluctuations.

#### 4. NONLINEAR DEVELOPMENT OF CONVECTIVE INSTABILITY WITHIN SLENDER FLUX TUBES

##### I. Adiabatic Flow

##### 4.1 Convection in a magnetic field:

The influence of magnetic fields on convection and vice versa depends on several parameters. The destabilizing effects depend on the superadiabatic temperature gradient. Countering this are the stabilizing effects of the magnetic field and the various dissipative processes arising from the thermal conductivity, viscosity and electrical resistivity of the fluid. Consequently various dimensionless numbers exist in the literature which are ratios of some of these properties of the fluid.

According to Cowling (1976a), it was Walen (1949) who first suggested that convective instability may be strongly affected by a magnetic field unless the dimensions of the convective elements in the direction of the magnetic field are sufficiently large. Walen assumed the fluid to be ideally conducting and neglected other dissipative effects as well. By equating the force produced by the bending of field lines into a

curve of radius  $\lambda$ , to the buoyancy force produced by heating of the liquid from below, he obtained the minimum  $\lambda_m$  below which convection cannot exist as

$$\lambda_m = \left( \pi B^2 / 2 \rho g \alpha \beta \right)^{1/2}$$

Here  $B$  is the field strength,  $\rho$  is the density of the liquid,  $\alpha$  is the coefficient of volume expansion,  $\beta$  is the temperature gradient and  $g$  is the acceleration due to gravity. The onset of instability in a Boussinesq fluid with finite thermal conductivity, electrical resistivity and viscosity has been studied in great detail (Thompson, 1951; Chandrasekhar, 1952, 1961; Danielson, 1961; Weiss, 1964; Gibson, 1966). For a plane layer of depth  $d$ , the stabilising effect of a uniform magnetic field is represented by the dimensionless Chandrasekhar number

$$Q = B^2 d^2 / 8 \pi \rho \eta \nu$$

where  $\eta$  is the electrical resistivity and  $\nu$  is the kinematic viscosity. The other dimensionless numbers which describe the configuration are the Rayleigh number  $R = \alpha \beta g d^4 / \kappa \nu$ , where  $\kappa$  is the thermometric conductivity; the Prandtl number  $\sigma = \nu / \kappa$  and the magnetic Schmidt number  $\tau = \nu / \eta$ . If  $\kappa \leq \eta$ , linear instability sets in as in ordinary

Rayleigh-Benard convection when the Rayleigh number exceeds a critical value  $R^{(e)}$ . This value of  $R^{(e)}$  increases with  $Q$  showing the stabilizing influence of the magnetic field. However, when  $\chi > \eta$  the instability can also set in as a growing oscillation which is variously called overstability or oscillatory convection. For  $Q$  sufficiently large the overstability can set in at a Rayleigh number  $R^{(o)}$  which can be smaller than  $R^{(e)}$ .

In the case of a compressible fluid without dissipation, a local condition for stability was obtained by Gough & Tayler (1966). The fluid is convectively stable if

$$\left( \frac{d \ln T}{d \ln p} \right) - \left( \frac{d \ln T}{d \ln p} \right)_{ad} < \frac{B^2}{B^2 + 8\pi\tau\beta}$$

It can be seen that strong magnetic fields can inhibit the onset of convection, though such conditions do not commonly occur in stars (Tayler 1971) except in small scales like in sunspots. Some efforts have been made to combine the effects of compressibility and dissipation (Kato, 1966; Syrovatsky & Zhugzhda, 1968a,b; Antia, 1979). If the Alfvén speed is small compared with the sound speed, the slow magnetosonic oscillations become overstable; if the Alfvén speed is large, the fast magnetosonic mode can be destabilized (Cowling, 1976b).

Considerable efforts have gone into the understanding of large amplitude evolution of the instability (see the review by Proctor & Weiss, 1982). Developments in bifurcation theory have aided the description of finite-amplitude behaviour in the neighbourhood of critical points of the onset of instabilities. A few cases of subcritical convection have been discovered (Busse 1975). Quasi-hydrodynamical calculations using truncated model expansions (Knobloch et al 1981) as well as numerical solution of the full set of non-linear partial differential equations on a computer (Weiss, 1981a,b,c) have revealed interesting behaviours like the formation of structured magnetic fields. Little is known about nonlinear compressible magnetoconvection when the Mach number becomes finite. For instance, one does not know what limits the field strength in isolated flux tubes, especially when these are stratified by gravity. However, certain approximations have rendered tractable the problem of the stability of thin tubes. An account of the current understanding of convective instability within slender magnetic flux tubes will be given in the following section.

#### 4.2 Review of linear analyses of convective instability within slender flux tubes:

In the preceding section we briefly reviewed the theoretical effort in understanding the onset of convective instability in a fluid permeated by a uniform magnetic field and the evolution of this instability to a finite amplitude. In this connection, a class of solutions obtained by Weiss and his collaborators (Weiss 1966; Galloway and Weiss, 1981) for an incompressible fluid leads to a common feature of narrow intense magnetic structures. There also occurs a mutual exclusion of magnetic fields and velocity fields. It is natural to ask the question whether such concentrated magnetostatic structures can result even in compressible fluids stratified by gravity and heat transport. A direct way of answering this question would be to assume an equilibrium model for the structured field and then examine its stability. However, stability analysis of two dimensional structures is fraught with the impossibility of the separation of linear perturbations into their normal modes. It is here that the slender flux tube approximation, described in chapter 3, becomes invaluable, by reducing the equations to those of a single dimension. As mentioned there, it was Roberts & Webb (1978) who rigorously derived the basic equations in this approximation. Here we rewrite their equilibrium solution for convenience of further discussion.

Such a solution can be constructed from any given arbitrary stratification of the pressure  $p_e(z)$ , the density  $\rho_e(z)$  and the temperature  $T_e(z)$  outside the tube along with an arbitrary magnetic field  $B_o(z)$ . The equations then become

$$p_o(z) = p_e(z) - B_o^2 / 8\pi, \quad (4.1)$$

$$\rho_o(z) = \rho_e(z) + \frac{1}{g} \frac{d}{dz} \frac{B_o^2}{8\pi} \quad (4.2)$$

$$\text{and } T_o(z) = \frac{\mu(p_o, T_o)}{\mathcal{R}} p_o(z) / \rho_o(z), \quad (4.3)$$

where the subscript 'o' denotes the quantities within the tube,  $\mathcal{R}$  is the gas constant and  $\mu(p_o, T_o)$  is the mean molecular weight. If one further assumes

$T_o / \mu(p_o, T_o) = T_e / \mu(p_e, T_e)$  at all heights then one obtains a simple relation between  $p_o$  and  $B_o$  viz.,

$$p_o / 8\pi B_o^2 = \beta_o, \quad (4.4)$$

where  $\beta_o$  is independent of  $z$ . With the further assumption that  $\mu = \text{constant}$ , the linearised equations reduce to (Webb & Roberts, 1978),

$$\frac{d}{dz} \left\{ \sigma(z) \frac{d}{dz} \hat{v} \right\} + \left\{ \omega^2 r(z) - q(z) \right\} \hat{v} = 0, \quad (4.5)$$



where

$$\sigma(z) = \rho_0 c_T^2 / B_0, \quad \gamma(z) = \rho_0 / B_0,$$

$$q(z) = \frac{\rho_0 c_T^2}{B_0} \left[ \frac{N_0^2}{c_T^2} + \frac{d}{dz} \left( \frac{B_0'}{B_0} + \frac{g}{c_0^2} \right) + \left( \frac{B_0'}{B_0} + \frac{g}{c_0^2} \right) \left( \frac{c_T^2}{c_0^2} - \frac{N_0^2}{g} \right) \right],$$

$$c_0^2(z) = \gamma g \Lambda_0, \quad c_T^2(z) = c_T^2(0) \Lambda_0(z) / \Lambda_0(0),$$

$$N_0^2(z) = \left( \frac{g}{\Lambda_0} \right) \left( \frac{\gamma-1}{\gamma} + \Lambda_0' \right), \quad c_T^2(0) = \frac{V_A^2(0) c_0^2(0)}{c_0^2(0) + V_A^2(0)},$$

$$V_A^2(0) = B_0^2(0) / 4\pi\rho_0(0), \quad \Lambda_0(z) = \mu T_0(z) / Rg,$$

and  $\hat{v} = v(z) \exp -i\omega t$  is the amplitude of the velocity perturbation  $v(z)$ . This equation (4.5) together with one boundary condition each at  $z = 0$  and  $z = -d$  constitutes the standard form of the Sturm-Liouville boundary-value problem. For boundary conditions such that  $[\sigma(z) \hat{v}^* \hat{v}']_{-d}^0 \leq 0$ , Webb and Roberts (1978) obtain a sufficient condition for stability as

$$N_0^2 / c_T^2 + \frac{d}{dz} \left( \frac{B_0'}{B_0} + \frac{g}{c_0^2} \right) + \left( \frac{B_0'}{B_0} + \frac{g}{c_0^2} \right) \left( \frac{c_T^2}{c_0^2} - \frac{N_0^2}{g} \right) > 0, \quad (4.6)$$

for  $-d < z \leq 0$ .

For the special case of  $T_e = T_0$ , this reduces to

$$0 > -\Lambda_0' - \left(\frac{\gamma-1}{\gamma}\right),$$

which is the usual condition for convective stability in the absence of a magnetic field. For the case of constant  $B_0$  in the tube, equation (4.6) reduces to

$$B_0^2 / (B_0^2 + 8\pi\gamma\beta_0) > -\Lambda_0' - \left(\frac{\gamma-1}{\gamma}\right),$$

throughout  $-d \leq z \leq 0$ , which is the same as the condition obtained by Gough & Tayler (1966) for an uniform laterally unbounded magnetic field. When the equilibrium stratification is in the form of a polytrope with  $p_e \propto \rho_e^\Gamma$  and  $T_e = T_0$  then it is possible to obtain the necessary and sufficient condition for stability as (Webb & Roberts, 1978)

$$\frac{4}{\gamma\Lambda_0'^2} \cdot \left(\frac{\gamma-1}{\gamma} + \Lambda_0'\right) \left(\frac{\gamma}{2} + \frac{C_0^2}{V_A^2}\right) + \left(1 + \frac{1}{2}\Lambda_0'\right)^2 > 0. \quad (4.7)$$

This last result was for the boundary conditions  $\hat{v} = 0$  at  $z=0$  and  $z \rightarrow -\infty$ . For  $-\left(\frac{\gamma-1}{\gamma}\right) > \Lambda_0' > -\frac{3}{2} + \left(\frac{2}{\gamma}\right)^{1/2}$  there is a critical value of  $C_0^2 / V_A^2$  given by

$$\left(\frac{C_0^2}{V_A^2}\right)_{\text{crit}} = \frac{-\gamma}{4(\Lambda_0' + \frac{\gamma-1}{\gamma})} \cdot \left\{ \left(\Lambda_0' + \frac{3}{2}\right)^2 - \frac{2}{\gamma} \right\}, \quad (4.8)$$

below which the solution is stable. Thus, a sufficiently strong field can render the tube stable. On the other hand, if  $\Lambda_0' < -\frac{3}{2} + \left(\frac{d}{\gamma}\right)^{1/2}$  then the tube cannot be stabilized by any finite value of the magnetic field, however large.

For a different boundary condition at the bottom of the tube viz.,  $\hat{v} = 0$  at  $z = -d$ , Webb & Roberts find that with a given value of  $\beta_0$  and  $\Lambda_0'$ , there exists a critical depth  $d_*$ , such that for  $d < d_*$  the perturbation is always stable. They finally suggest that a photospheric flux tube of moderate field strength (a few hundred gauss) is convectively unstable. The result of this instability is either the dissolution of the tube with the field being dispersed; or an increase in the field strength until a stable equilibrium is once again possible. They also suggested that the instability would generate a downflow though not necessarily a steady one. Spruit & Zweibel (1979) assumed a realistic stratification of the medium surrounding the tube based on the convection zone model of Spruit (1977) with  $T_0 / \mu(p_0, T_0) = T_e / \mu(p_e, T_e)$ . In this case, we have seen that the ratio  $\beta_0$  of the gas pressure to magnetic pressure is independent of height. Their treatment includes the effect of ionization on the thermodynamics of the gas. The linearised equations used were the same as in

Webb & Roberts (1978). However, the coefficients of the final second order differential equation for the velocity perturbation in this case depend on the variable thermodynamic properties of the gas. Thus this equation becomes

$$\frac{d^2}{dz^2} \hat{v} + \frac{1}{2} a (1+2\epsilon) \frac{d\hat{v}}{dz} + \frac{1}{2} a^2 \left[ \frac{\omega^2}{ga} \left( \frac{z}{r} + \beta_0 \right) + (Q\delta - \epsilon)(1+\beta_0) \right] = 0, \quad (4.9)$$

where

$$a = p_0' / p_0 ; \quad \epsilon = \left( \frac{\gamma'}{a\gamma} \right) \left( \frac{1}{1 + \beta_0 r/2} \right) ;$$

$$\delta = (d \ln T / d \ln p) - (d \ln T / d \ln p)_{ad} ;$$

$$Q = 1 - (\partial \ln \mu / \partial \ln T)_p ; \quad R = 1 + (\partial \ln \mu / \partial \ln p)_T$$

and

$$\gamma = c_{p0} / (c_{v0} R) .$$

Spruit & Zweibel (1979) solved the equation (4.9) numerically subject to the boundary condition

$$\hat{v}(z_0) = \hat{v}(z_1) = 0 , \quad (4.10)$$

at depths  $z_0$  and  $z_1$ . This is an eigenvalue

problem for  $\omega^2$ . Since no dissipative processes were included,  $\omega^2$  was real. For instability,  $\omega = i\eta$  where  $\eta$  is the growth rate. That value of  $\eta$  for which  $\eta = 0$  then represents the state of marginal stability. They found that the tube is unstable for  $\beta_0 > 1.83$  with the corresponding eigen mode having no nodes in the middle of the tube. When  $z_1$  was changed from 5000 km to 195000 km, the marginal value of  $\beta_0$  corresponding to the fundamental mode changed to 1.51 showing that the deeper layers of the convection zone contribute very little to the instability. These values of  $\beta_0$  correspond to a magnetic field  $B \approx 1000$  G. Thus this detailed study confirms the earlier work of Webb & Roberts (1978) that convective instability sets a limit on the minimum field strength for a stable tube. However, these results of Spruit & Zweibel (1979) differ from those of Unno & Ando (1979) who find only one unstable mode with marginal stability at  $\beta_0 = 0.026$ . Spruit & Zweibel (1979) attribute this difference to Unno & Ando's inappropriate choice of boundary condition at the top. Spruit (1979) calculated the new equilibrium states corresponding to initially unstable states for different values of the initial  $\beta_0$ . The final states showed maximum collapse in the region of maximum superadiabaticity, thus confirming the role of convective instability in the collapse.

There are several questions to be answered before one fully understands the process of convective collapse. The first question is whether the magnetic field does inhibit convective instability when nonlinearities are taken into account. The second is whether the final state of the unstable tube depends crucially on the direction of the initial perturbing flow. A third question is about the dynamical status of the final state. These questions can be answered only by studying the time dependent evolution of the instability to large amplitudes from an initial unstable state. Hasan (1982) performed such a calculation for a tube with an initial equilibrium similar to the zero order state assumed by Spruit & Zweibel (1979). He found that the tubes evolved to a final steady hydrodynamical state. Moreover, these final states were all independent of the initial state and the instability occurred no matter how large the initial magnetic field was. This result would imply very large fields for the collapsed tubes, as also extremely high flow velocities for the gas within the tubes. Such large velocities are not observed and it is unlikely that such high fields exist either. In this chapter we present results of similar time dependent nonlinear calculations (Venkatakrisnan, 1983), however, with an initial polytropic stratification. This

stratification strictly satisfies the equations of motion, continuity and energy. Thus any flow resulting from these calculations can be unambiguously attributed to convective instability. A limitation of our calculations is the assumption of a short length ( $\approx 1$  pressure scale height) for the tube. However, as seen in Spruit & Zweibel (1979), it is only a very short height range in the convection zone that contributes to the instability. Thus the secular behaviour of 'short' tubes can be expected to be not much different from that of longer tubes with realistic stratification. Moreover the slender flux tube approximation is likely to fail in the solar convection zone for lengths larger than the height of a convective eddy. This can be seen by visualising the 3-D juxtaposition of different eddies. If field lines are concentrated at the junctions of converging flows and dispersed at centres of the convective cells, then the area of cross-section of a tube would increase abruptly between different layers of the eddies.

#### 4.3 Initial and boundary conditions for the nonlinear calculations:

The derivation of the nonlinear equations for a slender flux tube by Roberts & Webb (1978) was given in

chapter 3. The characteristic form of those equations was also derived there. We now describe the initial and boundary conditions used in the numerical integration of the resulting characteristic equations for the present case of convective instability. It is convenient to work with dimensionless quantities. For the calculations presented in this chapter, we chose the unit of length as the pressure scale height at the bottom of the tube. The unit of velocity was chosen as the isothermal sound speed at the bottom. This fixed the unit of time as the ratio of these two quantities. The temperature, pressure and density were measured in units of the temperature, pressure and density at the bottom of the tube. The unit of magnetic field was chosen such that the corresponding magnetic pressure equalled the gas pressure at the base of the tube. For a depth of  $\approx 200$  km below the photosphere in Spruit's (1977) model, these units become  $\approx 300$  km for length,  $\approx 9 \text{ kms}^{-1}$  for velocity,  $\approx 30\text{s}$  for time,  $\approx 10^4$  K for temperature,  $3 \times 10^5 \text{ dynes cm}^{-2}$  for pressure and  $\approx 4.5 \times 10^{-7} \text{ g cm}^{-3}$  for density respectively. The depth of  $\approx 200$  km corresponds to the place where it is also approximately equal to the pressure scale height.

We chose the configuration of the tube at  $t = 0$ , to be polytropic with equal temperatures inside and



outside the tube. In this case it is known that the magnetic field also varies with a scale height that is twice that of the pressure scale height. The ratio of the gas pressure to the magnetic pressure is thus a constant denoted by  $\beta_0$ . In terms of the units mentioned above, the initial values of temperature  $T_0$ , density  $\rho_0$ , pressure  $p_0$  and magnetic field  $B_0$  are given by

$$\begin{aligned} T_0 &= 1 - \frac{\Gamma-1}{\Gamma} z, \\ \rho_0 &= T_0^{\frac{1}{\Gamma-1}}, \\ p_0 &= \rho_0^\Gamma, \\ B_0 &= (p_0 / \beta_0)^{1/2}, \end{aligned}$$

where  $\Gamma$  is the value of polytropic index. As was mentioned in chapter 2, the boundary conditions exert significant influence on the flow especially for large times. The choice of boundary conditions in the calculations of this chapter was dictated partly by considerations of ease in programming and partly by relevance to physical situations. For instance, a boundary condition like constancy of mass flux ( $= \rho v/B$ ) and the condition of compatibility with the interior solution together lead to the solution of a quadratic equation in one variable given the other two variables. This would in general necessitate a choice of the proper root lending a certain amount of ambiguity to the global solution. In the present study we chose two alternative

sets of boundary conditions at the top and base of the tube. In one set, called "closed-closed" boundary conditions, the Eulerian pressure was kept invariant in time at both ends of the tube. In the other set the Eulerian pressure was constant at the base while the Lagrangian pressure was maintained constant at the top. This latter set was called "closed-open" boundary conditions.

In the case of "closed-closed" boundary conditions, the horizontal pressure balance implied that the local field intensity was constant in time. In the slender tube approximation, this meant that the flux tube was constrained to maintain a time-independent area of cross-section at both ends. Such a constraint could perhaps be valid at <sup>the</sup> base of the tube if the external flows are strong enough to maintain a constant radius for the tube. Furthermore, the calculations of Spruit (1979) show negligible change in field strength at deeper layers after the collapse. However, it is difficult to imagine a similar confinement at the top of vertical tubes. For a tube that bends back to the photosphere at low heights, the rigidity of the tube as well as the pressure of the ambient atmosphere will tend to prevent changes in its cross section at its top. Thus, the "closed-closed" boundary condition could be

considered as simulating conditions within such bent tubes.

The boundary condition at the apex of the tube for "closed-open" set is equivalent to covering the mouth of the tube with a movable piston on which is placed a constant weight. Such a condition implies that gas moves up and down without leaking out horizontally from the top of the tube. It is hoped that this boundary condition simulates the condition in vertical "open" flux tubes on the solar surface. As mentioned in chapter 3, the time dependent equations (3.18) through (3.20) were integrated in time using a backward marching scheme by the method of characteristics. In the present calculation external pressure is constant in time and therefore,  $\alpha = (C_T^2/A^2)(v \, d p_e/dz)$  in equations (3.18) and (3.19) respectively. Since the scheme is essentially an explicit one, the time step was chosen to be small enough to satisfy the Courant-Friedrichs-Lewy stability criterion. The spatial step length was chosen to be 0.02 times the total length of the tube (assumed to be of unit length) which is supposed to yield a numerical accuracy of  $\approx 0.04\%$ . One particular case was recalculated with step sizes of 0.01 and 0.005 respectively. The solutions at large times differed only by 10% and 15% respectively from the solution for

step size = 0.02. Hence all further calculations were performed with the same step size of 0.02.

#### 4.4 Results of the nonlinear calculations:

The various parameters of the calculations are the superadiabaticity  $\delta$ , the ratio of gas pressure to magnetic pressure  $\beta_0$ , the length of the tube, the magnitude and direction of the initial perturbing flow and the two sets of boundary conditions. Our calculations largely concentrated on the effect of different values of  $\beta_0$ . A few calculations were performed for different values of  $\gamma$  keeping  $\Gamma$  and  $\beta_0$  fixed. The effect of the direction of the perturbing flow was also studied, as well as the effect of boundary conditions. For the purpose of understanding the evolution of the instability, the time profiles of the various fluid dynamical variables are of interest. The spatial profile must also be constantly monitored to check on the validity of the slender flux tube (SFT) approximation. If  $R_0$  is the observed radius of the collapsed tube and  $B_0$  is the observed field strength, then flux conservation implies that the initial radius at  $t = 0$  be given by

$$R_i = R_0 (B_0 / B_e)^{1/2}.$$

Here  $B_e$  is the equipartition field which is taken as the initial field before collapse. For  $B_e \approx 700 \text{ G}$ ,  $B_0 \approx 1400 \text{ G}$ ,  $R_0 \approx 100 \text{ km}$ , the initial radius  $R_i$  is  $\approx 170 \text{ km}$  at the top of the tube. The scale length of variation of the tube radius is 4 times the pressure scale height for the initial equilibrium. If the temperature at the base of the tube is  $\approx 10^4 \text{ K}$  and if  $\Gamma = 3$  then the pressure scale height at the top is  $\approx 100 \text{ km}$  and hence the scale length of variation of the tube radius is  $\approx 400 \text{ km}$ . Thus, at  $t = 0$ , the SFT approximation is satisfactory at the top and quite good at greater depths. However, for  $t > 0$ , the behaviour subsequent to the development of large curvatures in the field lines should be accepted only after verifying the validity of the SFT approximation.

We now present the results of our calculations. First we will briefly describe some general features of the behaviour of velocity and magnetic fields in the tube. We see that the variation of flow velocity and magnetic field are related. The field attains a maximum value when the magnitude of the velocity attains a maximum. Hence, a description of the time profile of either quantity serves to describe that of the other. In general the development of the instability occurs in two stages. Initially the flow velocity increases

approximately linearly with time. When it attains a value  $e$ -times that of the initial perturbation, there is a rapid change of slope in the velocity versus time diagram. We shall call the initial slow rise of velocity as the linear phase and the subsequent fast increase as the nonlinear phase. Let us now look into the linear phase.

Figure 4.1 shows the variation of velocity with time at  $\alpha = 0.5880$ . The different curves are for different values of  $\beta_0$  and common values of  $\Gamma = 3.0$  and  $\gamma = 1.95$ . The boundary conditions are "closed-closed" boundary conditions. For brevity we call such tubes as closed tubes. The growth to the  $e$ -folded velocity is generally oscillatory with a period of one tube travel time, which is the time taken by tube waves to travel over the length of the tube. It is seen that these oscillations are more prominent for smaller values of  $\beta_0$  and are more or less absent for larger values of  $\beta_0$ . These oscillations arise purely because of the initial perturbations at  $t = 0$ . Since we neglect viscosity and heat exchange, one would expect the oscillations to be undamped for all  $t > 0$ , unless the mean state changes so fast that it swamps the oscillations. Another interesting trend seen in figure 4.1 is that the time of onset of the nonlinear phase increases

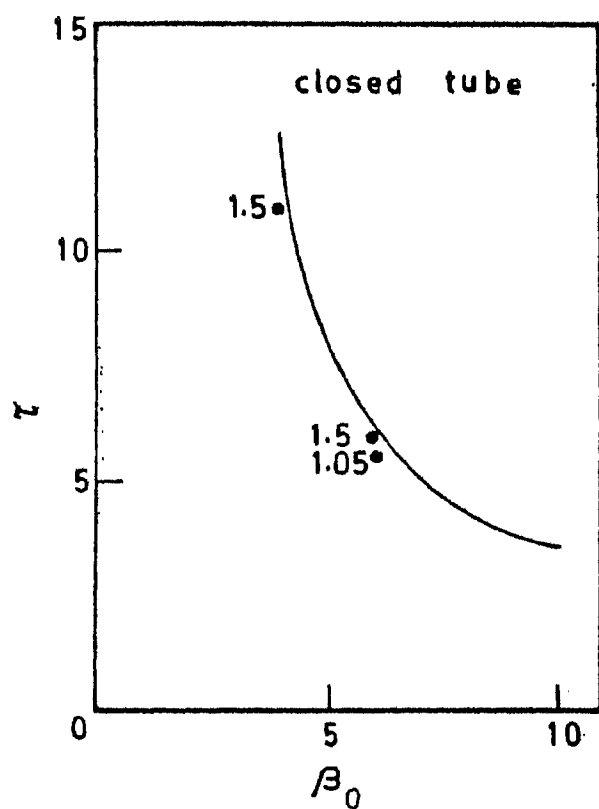
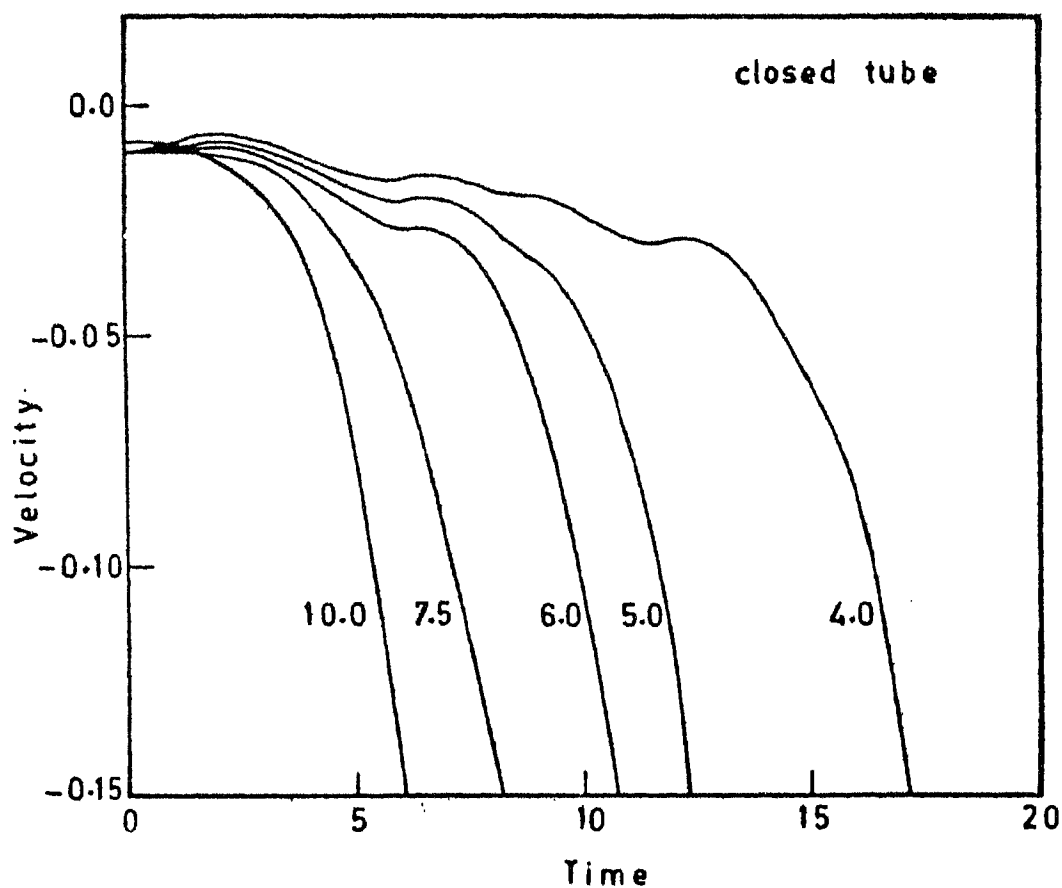


Fig.4.1 (top): Linear phase of instability with  $\Gamma = 3.0$ ,  $\gamma = 1.95$  and different values of  $\beta_0$  (marked in figure) for a "closed" tube.

Fig.4.2 (bottom): Variation of the time  $\tau$  of onset of nonlinear phase with  $\beta_0$ .

with decrease of  $\beta_0$ . This is due to the stabilizing influence of the magnetic field.

This stabilizing influence of the magnetic field can be seen more clearly in figure 4.2. Here, the time  $\tau$  of the onset of nonlinear behaviour is plotted against  $\beta_0$ . The curve changes slope and bends towards larger values of  $\tau$  for smaller values of  $\beta_0$ . Thus  $\tau$  approaches infinity as  $\beta_0$  approaches a finite value. From a practical view point one can then assume that tubes with smaller values of  $\beta_0$  are stable. The solid curve of figure 4.2 represents the values of  $\tau$  for  $\Gamma = 3$  and  $\gamma = 1.95$ . A few calculations were also made for different values of  $\gamma$ . Such points are represented by filled circles. It is clearly seen that tubes with smaller values of  $\gamma$  show greater in stability, as expected.

Figures 4.3 and 4.4 show the evolution of velocity and magnetic field respectively in the nonlinear phase. The initial development in the nonlinear phase consists of a rapid increase of downflow and magnetic field followed by a less rapid change. The nonlinear phase could not be calculated for the case  $\beta_0 = 7.5$  and  $\beta_0 = 10.0$ . In these cases, transient pressure enhancements occurred at the base of tube at early stages of the evolution. These made the gas pressure inside the



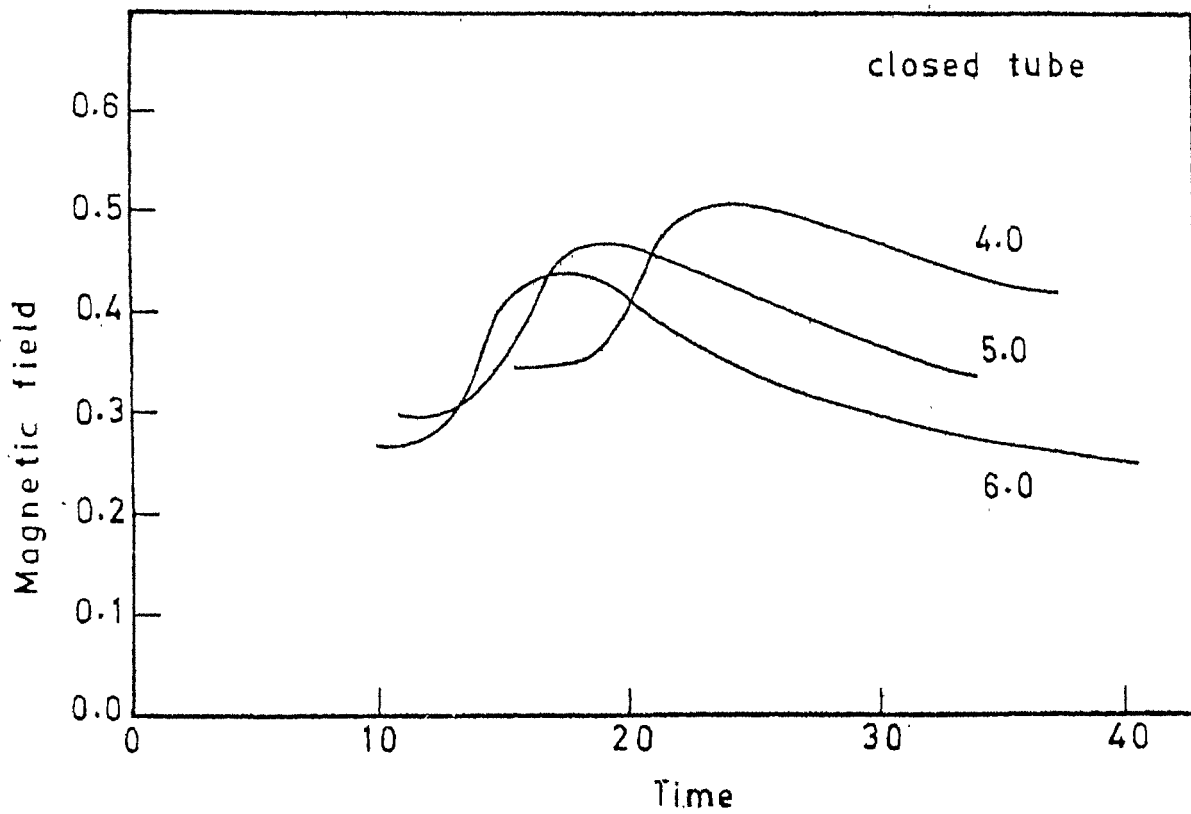
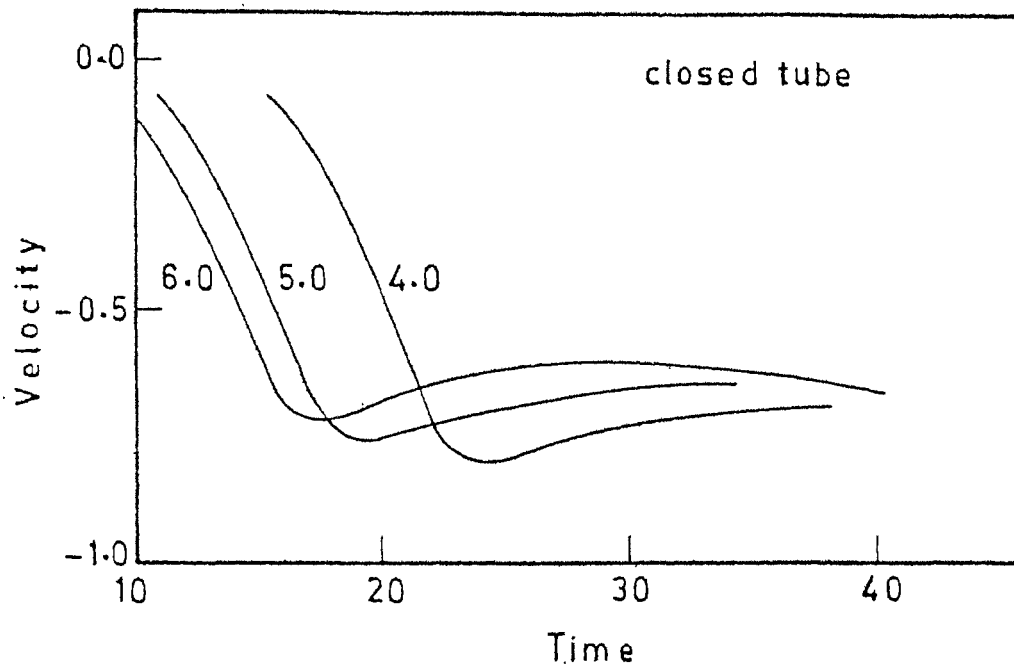


Fig.4.3 (top): Time dependence of velocity in nonlinear phase for  $z = 0.588$  and three values of  $\beta_0$ .

Fig.4.4 (bottom): Variation of magnetic field with time at  $z = 0.588$  in the nonlinear phase for three values of  $\beta_0$ .

tube locally exceed the external gas pressure invalidating the SFT approximation. In reality such a pressure enhancement will be contained either by the tension forces set up by the local dilatation of the tube, or by the damping of the pressure enhancement due to acoustic radiation from the tube. For smaller values of  $\beta_0$  e.g.  $\beta_0 = 6.0, 5.0$  and  $4.0$  no steady state was seen even after several tens of time units. This, however, does not rule out the possibility of a steady state at a very large time. To confirm the destabilization by superradiability, we next used a smaller value of  $\gamma$ . Figures 4.5 and 4.6 show the time behaviour of velocity and magnetic field for  $\gamma = 1.5$  and  $\beta_0 = 4.0$ . As compared with the behaviour for  $\gamma = 1.95$  (with  $\beta_0 = 4.0$ ) the motions are more violent and the onset of nonlinear phase occurs earlier.

To study the role of the direction of initial perturbation we calculated the evolution of an initial updraft for  $\beta_0 = 6.0$  and two values of  $\gamma$  (1.5 and 1.95) Figure 4.7 shows the linear regime while figure 4.8 shows the nonlinear behaviour. The onset of nonlinear phase occurs earlier for smaller value of  $\gamma$  showing the increased instability for larger superradiability. The nonlinear phase, as shown in figure 4.8, is interesting in that a steady hydrodynamic state with large upflows

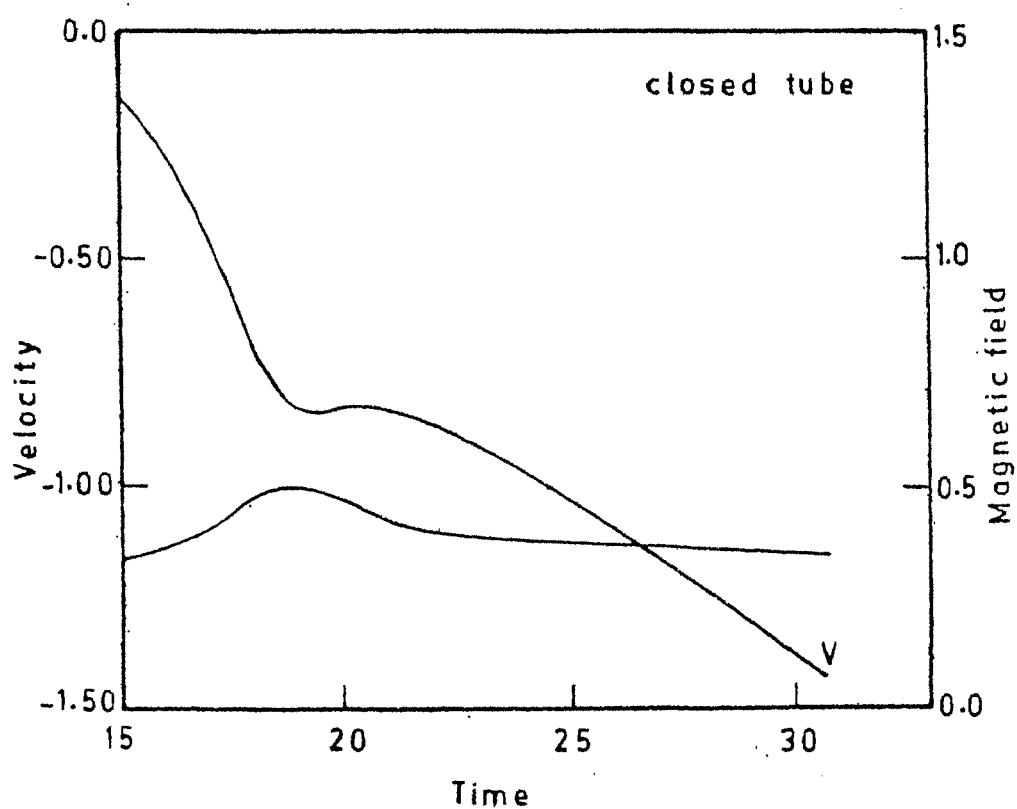
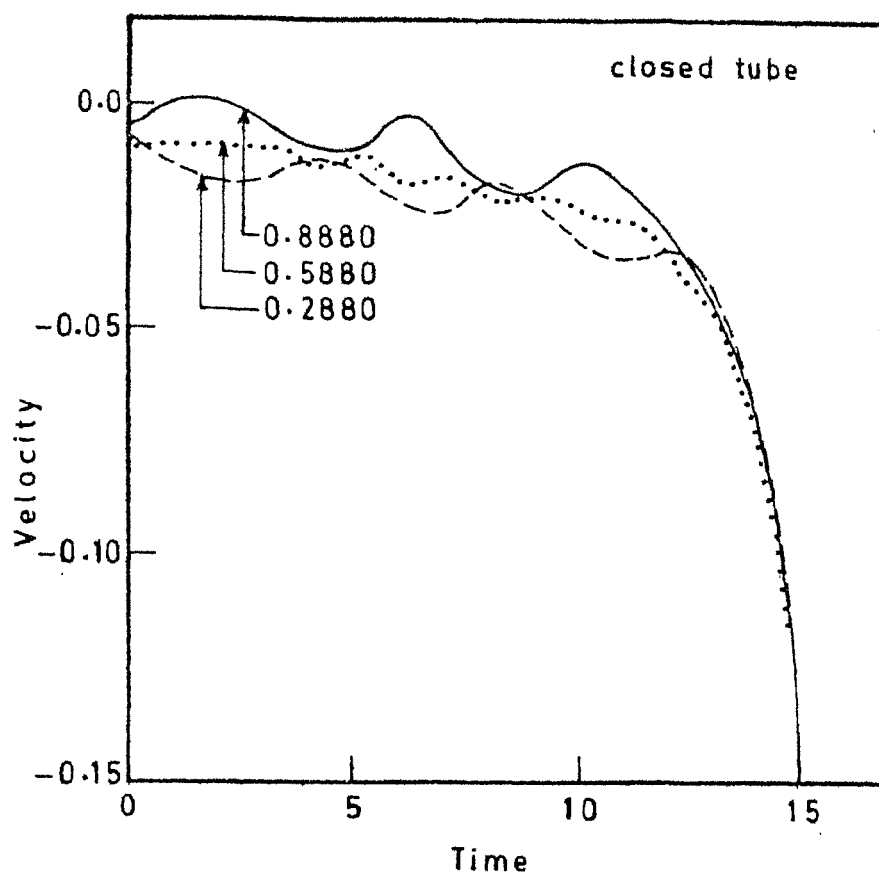


Fig.4.5 (top): Changes of velocity with time during linear phase of instability with  $\beta_0 = 4.0$  &  $\gamma = 1.5$  at  $z = 0.888, 0.588$  &  $0.288$ .

Fig.4.6 (bottom): Variation of magnetic field and velocity (marked with V) in the nonlinear phase for  $\beta_0 = 4.0$  &  $\gamma = 1.5$  at  $z = 0.588$ .

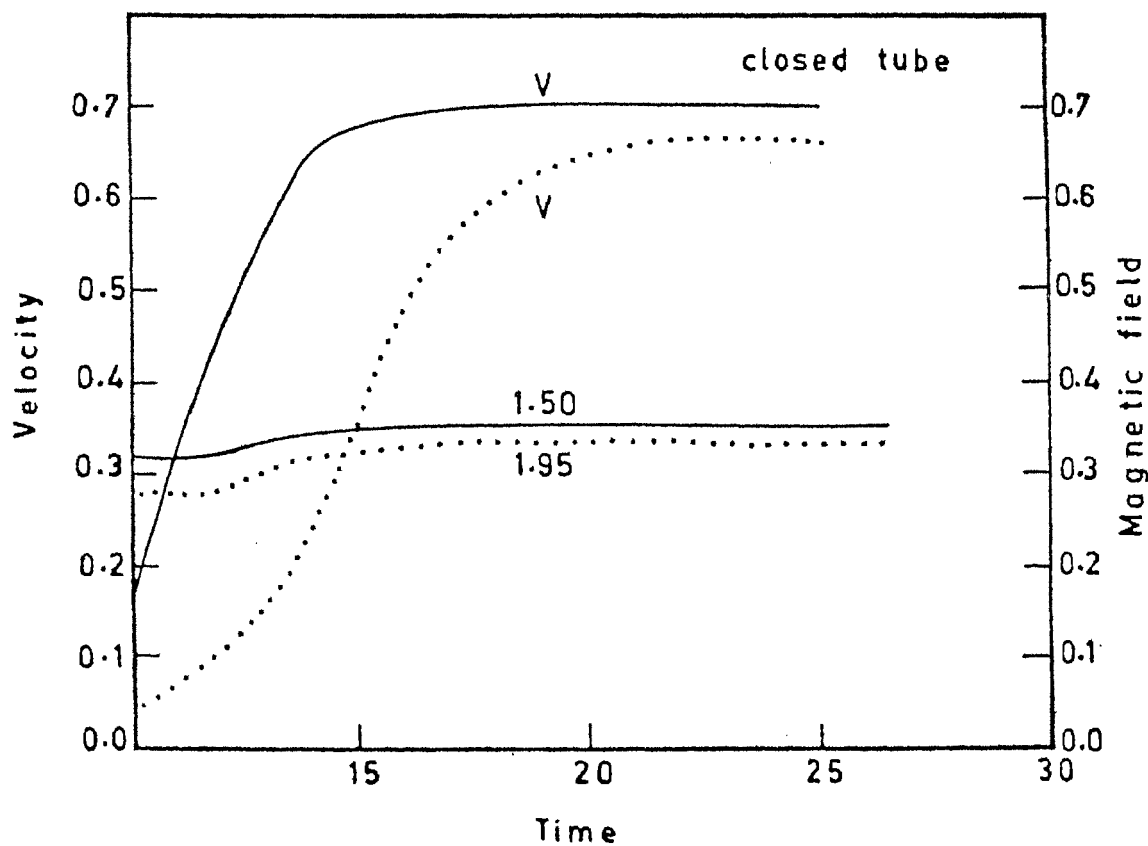
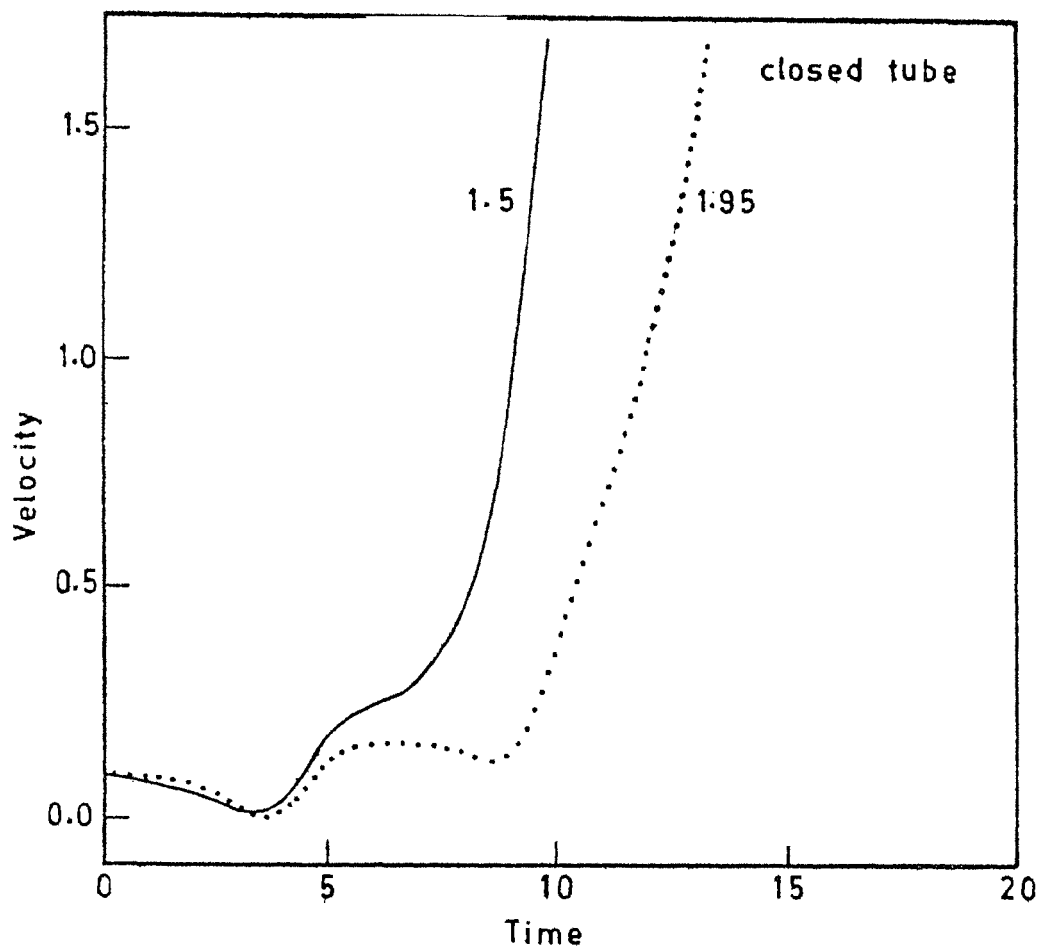


Fig.4.7 (top): Linear phase of velocity response to initial upflowing perturbation for  $\beta_0 = 6.0$  and  $\gamma = 1.5$  &  $1.95$  at  $z = 0.588$ .

Fig.4.8 (bottom): The nonlinear development of magnetic field and flow velocity (marked with  $V$ ) for  $\beta_0 = 6.0$ ,  $\gamma = 1.5$  &  $1.95$ .

and no dispersal of the field is seen in both cases.

We now go on to the case of the "closed-open" boundary conditions. Figure 4.9 shows the time dependence of flow velocity for  $\beta_o = 2.0$  and  $\gamma = 1.95$ . Here we see an interesting manifestation of overstability. The violet phase does not set in even after 40 time units. We see no significant change of phase in the oscillations at different values of  $z$ . Hence, these seem to be standing oscillations with a greater amplitude of the oscillation at  $z = 0.5880$  than at  $z = 0.2880$ .

When a larger value of  $\beta_o$  was chosen ( $\beta_o = 4.0$ ), the resulting velocities were smaller than in the corresponding case of "closed-closed" boundary condition. Figure 4.10 shows the linear phase. In figure 4.11 which depicts the nonlinear phase we see the saturation of flow and field to steady values. There is amplification of the field with greater enhancements at larger heights.

Figures 4.12 and 4.13 show the result of starting with an initial updraft for  $\beta_o = 6.0$ . We see that instead of any monotonic increase, there are time dependant fluctuations. The updraft turns into a downflow, then reverts to an upflow of larger amplitude

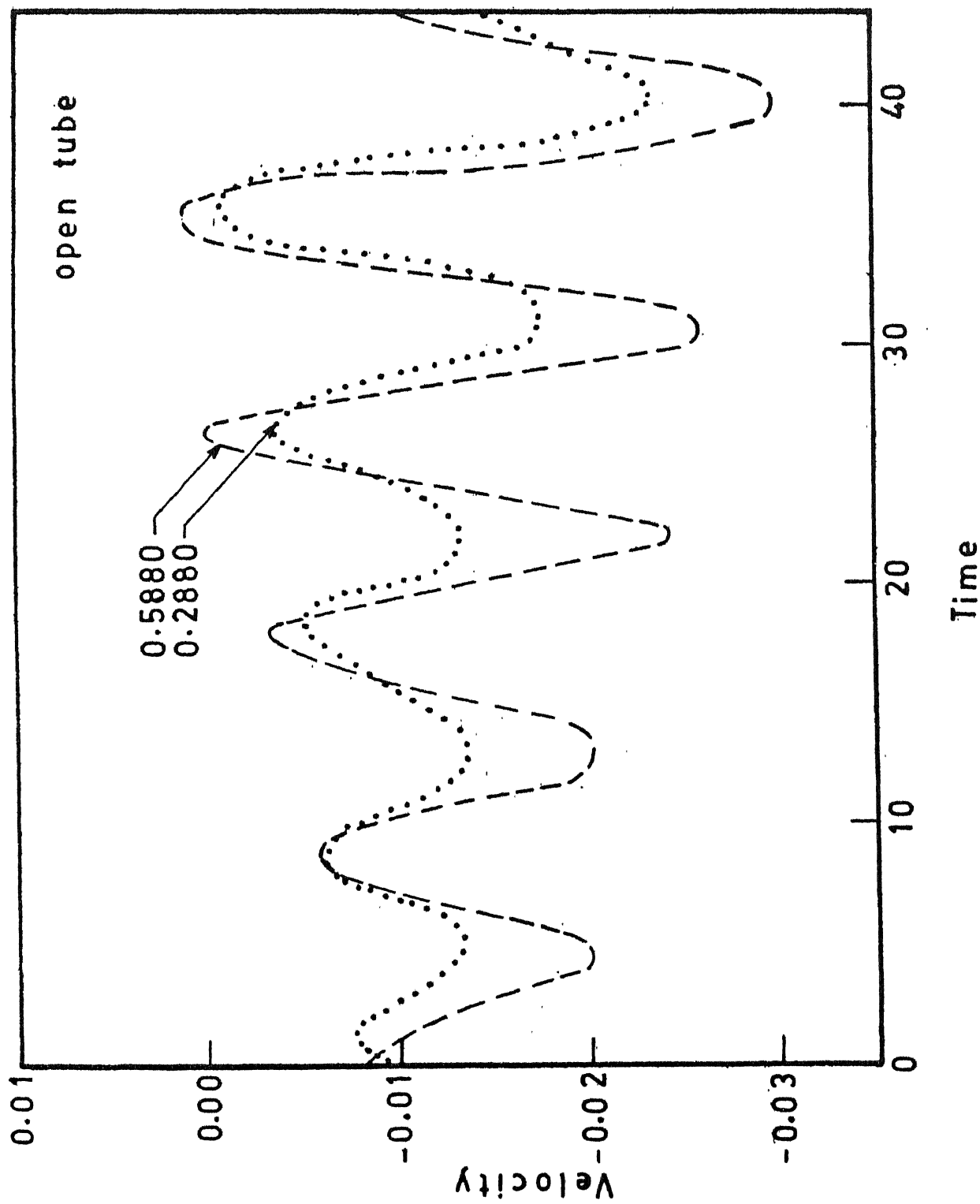


Fig.4.9: Time dependence of velocity in an "open" tube with  $\Gamma = 3$ ,  $\gamma = 1.95$  &  $\beta_0 = 2.0$  at  $z = 0.588$  &  $0.288$ .

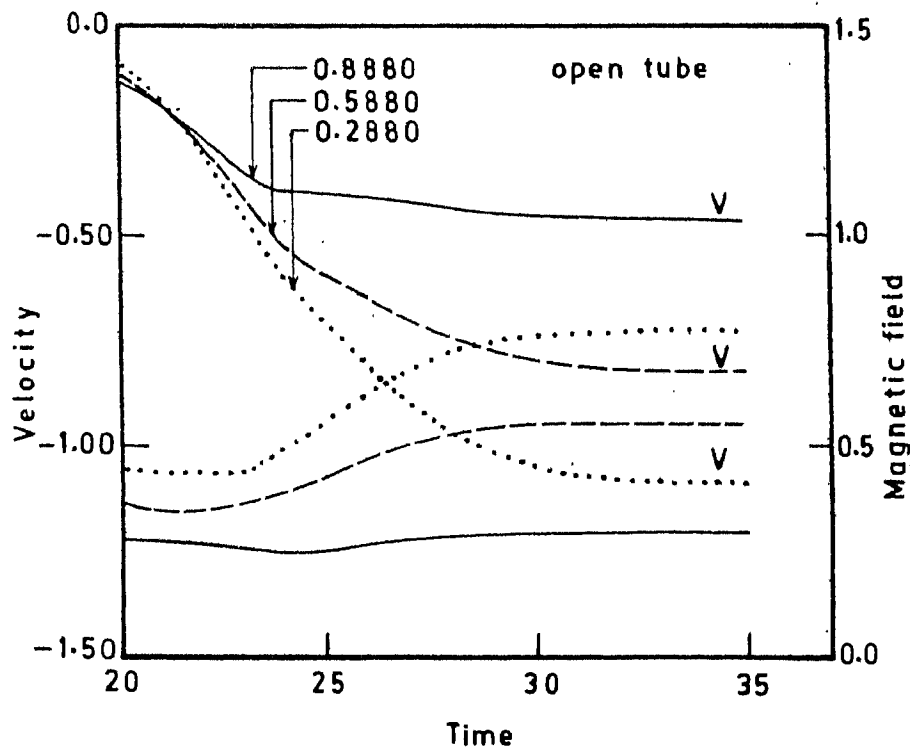
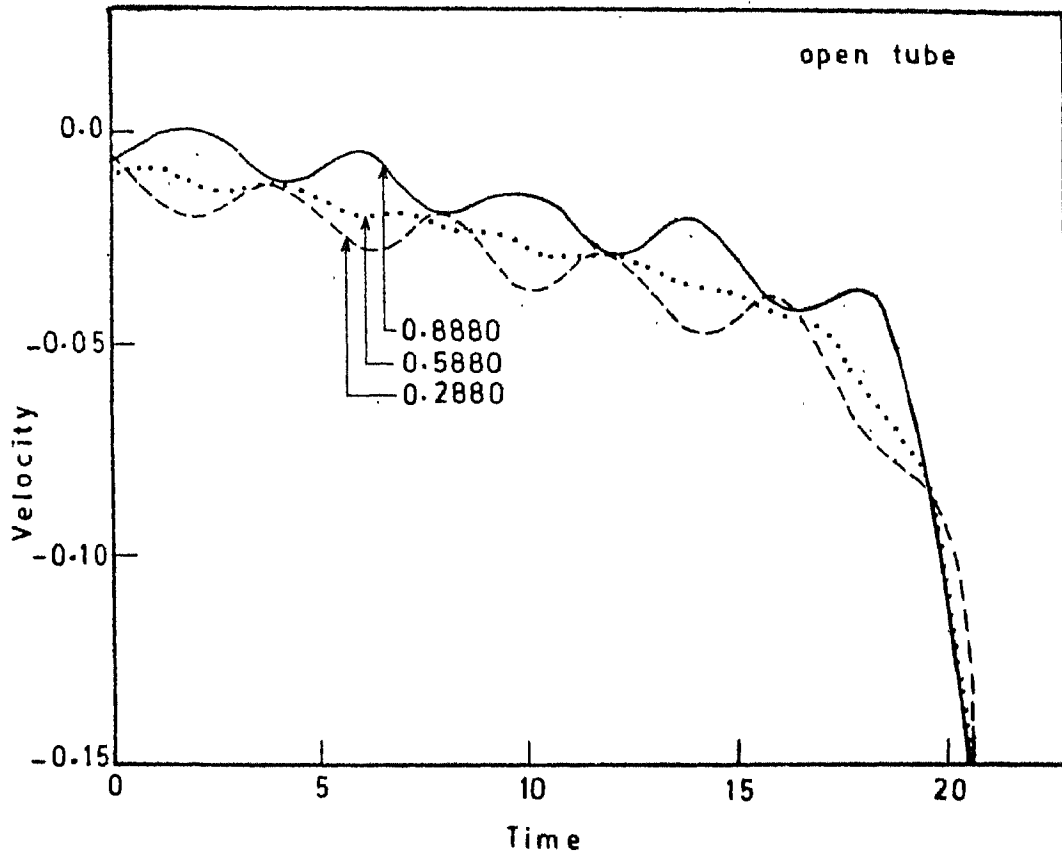


Fig.4.10 (top): Linear phase of velocity variation at three positions in the tube (marked in figure) with  $\beta_0 = 4.0$  &  $\gamma = 1.95$ .

Fig.4.11 (bottom): Nonlinear development of magnetic field and velocity (marked with V) at three positions in a tube with  $\beta_0 = 4.0$  &  $\gamma = 1.95$ .

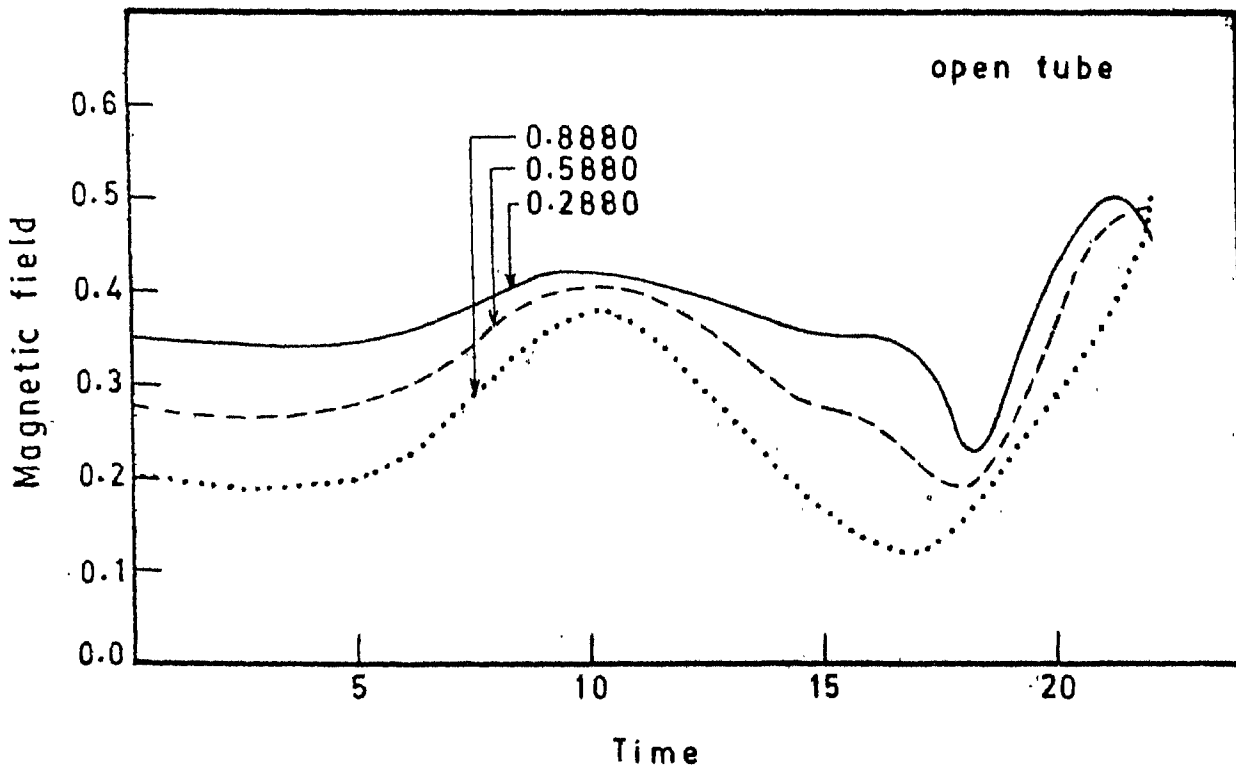
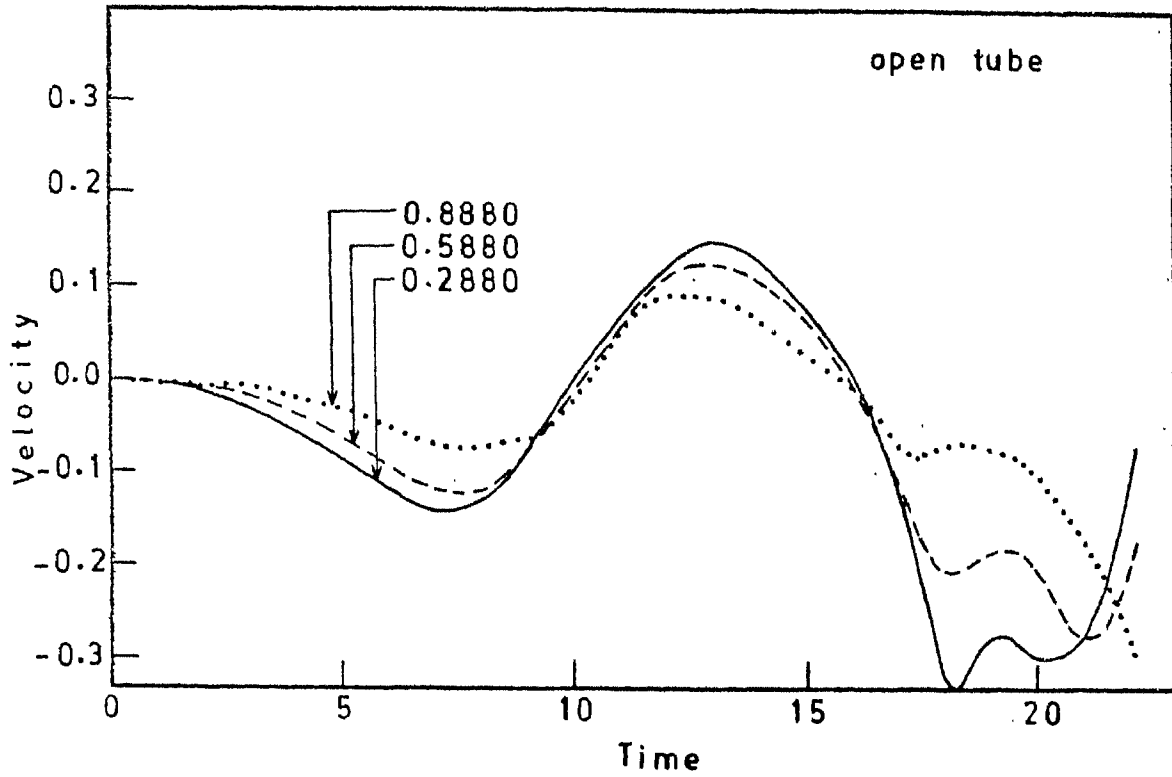


Fig.4.12 (top): Velocity response to initial upflow at  $z = 0.888$ ,  $0.588$  &  $0.288$  with  $\beta_0 = 6.0$  &  $\gamma = 1.95$ .

Fig.4.13 (bottom): Time dependence of magnetic field corresponding to the velocity response in figure 4.12.



than the initial perturbation. It then reverses sign and goes over once again as a downflow. We have noted in our computer outputs that during this excursion into the domain of negative velocities, the gas pressure at the top of the tube decreases until it vanishes. This is purely a numerical artifact caused by the boundary condition at the top of the tube. A similar behaviour is seen when an initial downflow is introduced at  $t = 0$ . In this case, however, (not shown in figure) the downflow reverses sign into an upflow and then becomes a downflow once again. For this reason, numerical breakdown (i.e. vanishing of pressure at the top) occurs at an earlier epoch than for the case with the initial updraft.

#### 4.5 Discussion of the results:

These calculations were not fully comprehensive on two counts. First each case was followed for only limited lengths of time. Secondly a finely spaced grid of  $\beta_0$  was not explored. In spite of these two limitations, one can draw some general conclusions regarding the development of convective instability within slender flux tubes.

Two quantities influence the course of the instability. One is the initial value of magnetic field

represented by  $\beta_0$ . The other is the set of boundary conditions.

Let us first discuss the case of "closed-open" boundary conditions. We see a range of behaviour, like overstability at  $\beta_0 = 2.0$ , the evolution to a steady flow at  $\beta_0 = 4.0$  and a large amplitude unsteady behaviour at  $\beta_0 = 6.0$ . This shows that the magnetic field exerts considerable stabilizing influence on the convective instability. A little more of discussion of the overstability at  $\beta_0 = 2.0$  is in order. Linear theory generally does not provide for any overstability in the absence of dissipation. An exception to this rule is the effect of rotation on convection in a slowly rotating star (Ledoux and Walraven 1958). There one obtains oscillatory convection with frequencies of the order of the rotational frequency and growth rates corresponding to convective growth rates. An explanation to the present overstability perhaps lies in the nonlinear terms. These nonlinear terms might not be very large because of the strong stabilizing influence of the magnetic field. However, they could lead to secular behaviour on time scales larger than the dynamical time scale. Hence, we conjecture that these secular terms feed energy into the oscillations leading to overstability.

The boundary condition of constant Lagrangian pressure at the top allows for the sharing of a portion of the kinetic energy of axial flow ~~with energy of~~ dilatation of the tube. Such a sharing of energy is prohibited for the tube with constant Eulerian pressure at the top. Thus one might expect less violent behaviour for tubes with "closed-open" boundary condition because of the damping of the axial flow by additional oscillations of the tube's radius than for those with "closed-closed" boundary conditions. We do see smaller axial velocities for "open" tubes in our calculations. In the case of  $\beta_0 = 4.0$  for example, the "open" tube attains a steady state, while the "closed" tube has already moved into the regime of large-amplitude unsteady behaviour.

An interesting feature is the response to an initial upflow. Whereas the flow reverses sign in the open tube it monotonically increases to a steady value in the case of a closed tube. This indicates the greater instability of the closed tube. The fact that for  $\beta_0 = 6.0$  in a closed tube, an upflow attains steady value while downflow leads to an unsteady behaviour, suggests that upflows are less destabilizing than downflows. There is no reason to expect this on the basis of linear theory and hence seems to be an essential result of nonlinearity. A second point is the absence

of dispersal of the tube following an upflow. This could perhaps be due to the fact that the boundary conditions do not prevent mass flux at either end of the tube. Thus any downflow does not lead to an evacuation of the tube, while an updraft does not inundate the tube. Hence, the question of dispersal of tube does not arise in the case of an upflow with continuing mass flux.

In summary, one sees that the magnetic field and boundary conditions determine the various kinds of instability. The stronger fields prevent direct instability but overstability sets in at some  $\beta_0$ . For smaller fields the instability evolves into a steady state, while for still smaller fields, unsteady states are seen at later times.

The flow velocities which arise as a result of the instability are quite significant. If these velocities really exist in the thin solar magnetic flux tubes then they would cause an immense drain of the photospheric material into the sun. However, radiative leak into the tubes might not be insignificant at the top of the convection zone. Such radiative exchange of heat with the surroundings may help in reducing the flow velocity. In the next chapter we study the problem of heat leak in some detail.

5. NONLINEAR DEVELOPMENT OF CONVECTIVE INSTABILITY  
WITHIN SLENDER MAGNETIC FLUX TUBES

II. The effect of radiative heat transport

5.1 Effect of thermal dissipation on convective  
instability in a laterally unbounded vertical  
magnetic field.

The famous Schwarzschild criterion for convective instability is based on the fact that the dynamical timescale is much smaller than the time scale of thermal relaxation. A convective bubble rises buoyantly on the dynamical time scale and hence its heat exchange with the surroundings is generally negligible. Therefore, it expands adiabatically. If the ambient fluid has a temperature gradient which is greater than the adiabatic gradient, the density inside the rising bubble continues to be smaller than the surroundings. This leads to a runaway process viz. the convective instability. The thermal diffusion time-scale is proportional to the square of the eddy length whereas the dynamical timescale is determined by the Brünt-Väisala frequency which is independent of the eddy size. One can, therefore, imagine the existence of a critical eddy size below which convective instability will not exist for a given value of thermal diffusivity.

The presence of a vertical magnetic field has a stabilizing influence on a stratified medium. The early investigations of magneto-convection with heat diffusion did not take compressibility into account, (e.g. Chandrasekhar 1961). Instead, the effects of viscosity and electrical resistivity were included. It was seen that whenever the resistivity  $\eta$  was greater than the heat diffusivity  $\chi$ , convective instability sets in as a monotonically growing instability at a critical value of the Rayleigh number  $R^{(e)}$ . This value of  $R^{(e)}$  increased with increasing Chandrasekhar number  $Q$ , thereby demonstrating the stabilizing influence of the magnetic field. In stellar interiors the radiative heat diffusivity is generally much larger than the electrical resistivity of the fluid. In such a situation, Chandrasekhar (1961) proved that for a viscous Boussinesq fluid permeated by a sufficiently weak vertical magnetic field, overstability would set in at a Rayleigh number  $R^{(o)}$  which is less than  $R^{(e)}$ , the critical Rayleigh number for onset of the overturning convection.

Kato (1966) gave a mathematical treatment of convective instability in the presence of a magnetic field in a thermally conducting inviscid, fluid of zero electrical resistivity. The main thrust of his

work was to demonstrate the effect of compressibility. A compressible fluid can support more modes of waves than a Boussinesq fluid. The pure wave modes possible in a uniform compressible magneto-fluid are the Alfvén mode, the fast mode and the slow mode. For a superadiabatically stratified fluid, the Alfvén mode and fast mode are not affected by the superadiabatic temperature gradient, but the slow mode is considerably modified. Kato (1966) calls the modified mode as the convective-slow mode which is oscillatory when the magnetic restoring force is stronger than the destabilizing buoyancy force and which turns into a non-oscillatory convective mode for small values of the magnetic field. In the case of an inviscid Boussinesq fluid, any adverse temperature gradient was shown to lead to overstability irrespective of the value of the magnetic field. When compressibility is included, a regime of damped oscillations exists for  $Q > Q^{(d)}$  where  $Q^{(d)}$  depends on the Rayleigh number. Thus for sufficiently weak magnetic fields in the absence of finite electrical resistivity or fluid viscosity, the instability always sets in as an overstability. The effect of compressibility was to admit the possibility of the damping of these oscillations at sufficiently large values of the magnetic field.

The above analysis of Kato was a local analysis which did not take into account the effect of boundary conditions. The classification and behaviour of the linear modes of a polytropic fluid with vertical magnetic field and imposed boundary conditions have been explored in detail by Antia and Chitre (1979). With increasing magnetic field they find that the convective-slow modes tend to be stabilized. For higher values of thermal diffusivity, the fast modes are destabilized and their growth rates are seen to increase with magnetic field. Thus for low magnetic field the slow modes would dominate over the fast mode while at moderate values of the magnetic field, the fast modes would begin to dominate. The growth rate of both the series of modes showed a maximum with respect to the horizontal wave number, which gave a preferred horizontal length scale for overstable modes.

The investigations described so far were based on linear theory. Moore & Spiegel (1966) have presented results for a nonlinear oscillator which is jointly operated by a destabilizing force and a restoring force and which loses heat in accordance with Newton's law of cooling. The main parameters of the oscillator were  $R$ , the square of the ratio of the heat loss timescale to the timescale defined by the destabilizing



force and  $T$ , which is the square of the ratio of heat loss timescale to the timescale defined by the restoring force. Relaxation oscillations were analytically demonstrated for weak restoring forces and small heat loss. Moore and Spiegel also explored numerically several regimes in  $R$ - $T$  space and a wide variety of behaviour was shown. They concluded that even a single destabilizing mechanism would lead to a variety of phenomena in the nonlinear domain. However, their results afford only a general picture of the various possibilities and specific cases will have to be treated in greater detail. The effect of lateral boundaries would be the next logical factor to consider especially because of the structured nature of solar magnetic fields. The investigations of the effect of lateral boundaries will be reviewed in the next section.

## 5.2 Thermal effects in laterally bounded magnetic fields:

The presence of lateral boundaries has important thermodynamical consequences especially for magnetic flux tubes in the solar convection zone. The strong magnetic fields of the tubes inhibit overturning convection and thereby reduce the efficiency of convective transport of heat along the tube axis.

The high electrical conductivity of the fluid precludes exchange of gas with the surroundings preventing also the lateral heat transport by convection. Therefore, the only process by which the tube exchanges heat with its surroundings is by radiation. In particular, tubes of small radius are significantly influenced by lateral heat exchange as demonstrated in the flux tube models of Spruit (1977). From an observational point of view the most important effect of the lateral heat exchange in these models is the angle dependent radiation emanating from the tube. Spruit used this feature to make certain predictions for the centre to limb variation of the continuum contrast. From comparison with observations he could also estimate the magnetic field and size distribution of the tubes.

If we sacrifice the details resulting from the finite tube thickness, we can make progress in estimating the effects of thermal dissipation on the stability of magnetic structures by using the slender flux tube approximation. Webb & Roberts (1980) studied the effect of thermal dissipation on tube wave propagation. In the limit of both large dissipation (isothermal limit) and small dissipation (adiabatic limit) these authors showed that the waves are temporarily damped. For waves of given frequency it was shown that evanescent waves

become propagating in the presence of thermal dissipation. Similarly progressive waves are spatially damped when heat exchange is considered. These conclusions were obtained assuming optically thin disturbances. In the next section we formulate the energy equation for an optically thick slender flux tube exchanging heat with the surroundings.

5.3 The energy equation for an optically thick slender flux tube exchanging heat with its surroundings:

The complete energy equation for a slender flux tube is (Roberts & Webb, 1978),

$$\left( \frac{\partial}{\partial t} p + v \frac{\partial}{\partial z} p \right) - \left( \frac{\tau p}{\rho} \right) \left( \frac{\partial}{\partial t} p + v \frac{\partial}{\partial z} p \right) = - \nabla \cdot \underline{F} . \quad (5.1)$$

If heat transport is by radiation, we have in the optically thick case,

$$F = - K \nabla T , \quad (5.2)$$

where  $K = 16\sigma T^3 / 3\chi\rho$  is the radiative conductivity with  $\chi$  as the opacity per unit gram and  $\sigma$  as the Stefan-Boltzmann constant. Such a "diffusion" approximation may not be strictly valid for very thin tubes

at the photosphere (Unno & Kibes, 1979) but we will assume in what follows that the tube has sufficient optical thickness. In the computations reported in the earlier chapters, we have neglected the radial dependence of the dynamical variables in the slender flux tube approximation. Such an omission is not correct when radial heat transport is to be studied. In section 5.2, we saw that radial heat transport is indeed important. It would also exert a significant influence on the convective instability of thin tubes in particular. For example, a downflow initiated by convective instability tends to cool the tube. This would be offset by heat entering the tube from outside. This heating would inhibit the further sinking of the displaced gas and thereby inhibit the downflow. In order to understand such effects in a more quantitative way let us assume the following profile for the radial temperature distribution, viz.,

$$T = T_0(z) + T_1(z) \left( \frac{r}{\Lambda} \right) + T_2(z) \left( \frac{r}{\Lambda} \right)^2 + \dots, \quad (5.3)$$

where  $\Lambda$  is the scale length of the longitudinal variation of the tube radius. After substituting equation (5.3) in (5.2) with

$$\underline{F} = -K \left( \frac{\partial}{\partial r}, 0, \frac{\partial}{\partial z} \right) T(r, z) \quad (5.4)$$

and multiplying the resulting equation by  $(r/\Lambda)$ , we have, upto first order in  $r/\Lambda$ :

$$\begin{aligned} \frac{KT_1}{\Lambda^2} + \left(\frac{r}{\Lambda}\right) \left[ \left\{ \left(\frac{T_1}{\Lambda}\right)^2 + \left(\frac{\partial T_0}{\partial z}\right)^2 \right\} \left(\frac{\partial}{\partial T} + \frac{\partial p}{\partial T} \frac{\partial}{\partial p}\right) K \right. \\ \left. + K \left( \frac{4T_2}{\Lambda^2} + \frac{\partial^2 T_0}{\partial z^2} \right) - \frac{1}{(r-1)} \left( \frac{\partial}{\partial t} + v \frac{\partial}{\partial z} \right) p \right. \\ \left. + \left(\frac{r}{r-1}\right) \left(\frac{p}{\rho}\right) \left(\frac{\partial}{\partial t} + v \frac{\partial}{\partial z}\right) \rho \right] = 0. \end{aligned} \quad (5.5)$$

Equating the coefficients of each power of  $\frac{r}{\Lambda}$  to zero, we have

$$KT_1 / \Lambda^2 = 0 \quad (5.6a)$$

and

$$\begin{aligned} \left\{ \left(\frac{T_1}{\Lambda}\right)^2 + \left(\frac{\partial T_0}{\partial z}\right)^2 \right\} \left(\frac{\partial}{\partial T} + \frac{\partial p}{\partial T} \frac{\partial}{\partial p}\right) K \\ + K \left( \frac{4T_2}{\Lambda^2} + \frac{\partial^2 T_0}{\partial z^2} \right) - \frac{1}{(r-1)} \left(\frac{\partial}{\partial t} + v \frac{\partial}{\partial z}\right) p \\ + \left(\frac{r}{r-1}\right) \left(\frac{p}{\rho}\right) \left(\frac{\partial}{\partial t} + v \frac{\partial}{\partial z}\right) \rho = 0. \end{aligned} \quad (5.6b)$$

The equation (5.6a) yields

$$T_1 = 0. \quad (5.6c)$$

Substituting equation (5.6c) in (5.6b) gives

$$\left(\frac{\partial T_0}{\partial z}\right)^2 \left(\frac{\partial}{\partial T} + \frac{\partial p}{\partial T} \frac{\partial}{\partial p}\right) K + \left(4\frac{T_0}{\Lambda^2} + \frac{\partial^2 T_0}{\partial z^2}\right) K$$

$$-\left(\frac{1}{r-1}\right) \left(\frac{\partial}{\partial t} + v \frac{\partial}{\partial z}\right) p + \left(\frac{r}{r-1}\right) \left(\frac{p}{f}\right) \left(\frac{\partial}{\partial t} + v \frac{\partial}{\partial z}\right) p = 0. \quad (5.6d)$$

Finally by setting  $T = T_i$  at  $r = 0$  we obtain  $T_0 = T_i$

and by setting  $T = T_e$  at  $r = r_0$  we have

$$T_0 = (T_e - T_i) \Lambda^2 / r_0^2, \quad (5.6e)$$

where  $r_0$  is the radius of the tube. Substituting equation (5.6e) in (5.6d) we have the final energy equation:

$$\begin{aligned} & \left(\frac{\partial}{\partial t} + v \frac{\partial}{\partial z}\right) p - \left(\frac{r p}{f}\right) \left(\frac{\partial}{\partial t} + v \frac{\partial}{\partial z}\right) p \\ & = (r-1) \left[ K \left\{ 4 \frac{(T_e - T_i)}{r_0^2} + \frac{\partial^2 T_i}{\partial z^2} \right\} + \left(\frac{\partial T_i}{\partial z}\right)^2 \left(\frac{\partial}{\partial T} + \frac{\partial p}{\partial T} \frac{\partial}{\partial p}\right) K \right]. \quad (5.7) \end{aligned}$$

In what follows, we study the effect of heat transport given by equation (5.7) on the instability of a slender flux tube.

First, in section 5.4 we will study the linear convective instability in the presence of the first

term of the R.H.S of equation (5.7). In section 5.5.1 we will study the nonlinear development of convective instability with only the first term of the R.H.S of equation (5.7) and using equations (3.18) and (3.19) with  $\alpha = (C_T^2 / A^2)(v dp_e/dz)$ . The influence of the second term in the R.H.S of equation (5.7) will be included in section 5.5.2 while all the terms would be jointly considered in section 5.5.3.

5.4 Effect of lateral heat transport on linear convective instability in slender magnetic flux tubes:

The linearised form of the nonadiabatic slender flux tube equations are

$$\frac{1}{B_0} \left( \frac{\partial p_1}{\partial t} + \frac{\partial p_0 v_1}{\partial z} \right) - \frac{\rho_0}{B_0^2} \left( \frac{\partial B_1}{\partial t} + v_1 \frac{\partial B_0}{\partial z} \right) = 0, \quad (5.8)$$

$$\rho_0 \frac{\partial v_1}{\partial t} + \frac{\partial p_1}{\partial z} + \rho_1 g = 0, \quad (5.9)$$

$$\begin{aligned} & \left( \frac{\partial p_1}{\partial t} - \frac{\gamma p_0}{\rho_0} \frac{\partial p_1}{\partial t} \right) + v_1 \left( \frac{d p_0}{dz} - \frac{\gamma p_0}{\rho_0} \frac{d \rho_0}{dz} \right) \\ & = (\gamma - 1) \left\{ K \left( \frac{\partial^2 \theta_1}{\partial z^2} - \frac{4 \theta_1}{\tau_0^2} \right) + \left( \frac{dT_0}{dz} \right)^2 \left( \frac{\partial K}{\partial p} p_1 + \frac{\partial K}{\partial T} \theta_1 \right) \right\}, \end{aligned} \quad (5.10)$$

$$\theta_1 = T_0 \left( p_1 / p_0 - \rho_1 / \rho_0 \right) \quad (5.11)$$

and

$$B_1 = -p_1 / 4\pi B_0 \quad (5.12)$$

where  $\rho_1$ ,  $p_1$ ,  $\theta_1$  and  $B_1$  are the perturbations of the zero order quantities viz. density  $\rho_0$ , pressure  $p_0$ , temperature  $T_0$  and magnetic field  $B_0$  respectively. In the presence of lateral heat transport alone, the equation is

$$\begin{aligned} \left( \frac{\partial p_1}{\partial t} - \frac{\gamma p_0}{\rho_0} \frac{\partial \rho_1}{\partial t} \right) + v_1 \left( \frac{d p_0}{dz} - \frac{\gamma p_0}{\rho_0} \frac{d \rho_0}{dz} \right) \\ = -4(\gamma - 1) K \theta_1 / r_0^2. \end{aligned} \quad (5.13)$$

We further write  $K = \rho_0 C_v \chi$ ,

where  $\chi$  is the radiative diffusivity and assume that  $\chi$  is constant. Then the final energy equation is

$$\begin{aligned} \left( \frac{\partial}{\partial t} + \frac{1}{\tau} \right) p_1 - \left( \frac{\gamma p_0}{\rho_0} \right) \left( \frac{\partial}{\partial t} + \frac{1}{\gamma \tau} \right) \rho_1 \\ + v_1 \left( \frac{d p_0}{dz} - \frac{\gamma p_0}{\rho_0} \frac{d \rho_0}{dz} \right) = 0, \end{aligned} \quad (5.14)$$

where

$$\tau = r_0^2 / 4 \chi.$$

We choose the perturbations to be of the form

$$q = \hat{q}(z) \exp \sigma t.$$

Substituting this form of the perturbation in equations (5.8), (5.9) and (5.14) and eliminating  $\hat{\rho}_1$  and  $\hat{B}_1$



between the resulting equations we have

$$\Lambda \frac{d}{dz} (\rho_0 \hat{v}_1) = - \left( \frac{1}{2} - \frac{\delta \sigma}{\sigma + 1/\tau} \right) (\rho_0 \hat{v}_1) - \frac{\sigma}{\tau g} \left( \frac{\tau \beta}{2} + \frac{\sigma + 1/\tau}{\sigma + 1/\tau} \right) \hat{p}_1 \quad (5.15)$$

and

$$\Lambda \frac{d}{dz} \hat{p}_1 = - \left( \frac{\sigma + 1/\tau}{2/\tau + \sigma} \right) \hat{p}_1 - \left( \sigma \Lambda - \frac{g \delta}{\sigma + 1/\tau} \right) (\rho_0 \hat{v}_1), \quad (5.16)$$

where

$$\delta = (\Gamma - \gamma) / \Gamma \gamma.$$

Transforming to a variable  $x$  given by

$$dx = - dz / \Lambda,$$

We have

$$\frac{d}{dx} (\rho_0 \hat{v}_1) = \mu (\rho_0 \hat{v}_1) + f_1 \hat{p}_1 \quad (5.17)$$

and

$$\frac{d}{dx} \hat{p}_1 = \eta \hat{p}_1 + f_2 (\rho_0 \hat{v}_1), \quad (5.18)$$

where

$$\mu = \frac{1}{2} - \frac{\delta \sigma}{\sigma + 1/\tau}; \quad \eta = \frac{\sigma + 1/\tau}{2/\tau + \sigma};$$

$$f_1 = \frac{\sigma}{\tau g} \cdot \left( \frac{\tau \beta}{2} + \frac{\sigma + 1/\tau}{\sigma + 1/\tau} \right); \quad f_2 = \sigma \Lambda - \frac{g \delta}{\sigma + 1/\tau}.$$

Eliminating  $p_1$  from equations (5.17) and (5.18) we have

$$\begin{aligned} \frac{d^2}{dx^2} (\rho_0 \hat{v}_1) - (\mu + \eta) \frac{d}{dx} (\rho_0 \hat{v}_1) \\ - (f_1 f_2 - \mu \eta) (\rho_0 \hat{v}_1) = 0. \end{aligned} \quad (5.19)$$

A further transformation

$$y = (\rho_0 \hat{v}_1) \exp\left(\frac{\mu + \eta}{2} x\right)$$

yields

$$\frac{d^2}{dx^2} y - \left\{ \frac{(\mu - \eta)^2}{4} + f_1 f_2 \right\} y = 0. \quad (5.20)$$

If we impose a boundary condition of vanishing  $y$  at two points  $x=0$  and  $x=x_1$ , then solutions of equation (5.20) must be of the form

$$y \propto \exp i k x \quad (5.21)$$

where  $k = 2\pi/x_1$  is the "wave number".

Substitution of equation (5.21) in equation (5.20) gives the following "local dispersion relation"

$$k^2 + (\mu - \eta)^2/4 + f_1 f_2 = 0. \quad (5.22)$$

We rewrite this equation in dimensionless form in terms of

$$\tilde{\sigma} = \sigma (\Lambda/g)^{1/2} \quad \text{and} \quad \epsilon = \tau (g/\Lambda)^{1/2}.$$

The dispersion relation now reads as

$$\begin{aligned} \tilde{\sigma}^2 (a_4 \tilde{\sigma}^2 + b_4) + \epsilon \tilde{\sigma} (a_3 \tilde{\sigma}^2 + b_3) \\ + \epsilon^2 (a_2 \tilde{\sigma}^2 + b_2) = 0, \end{aligned} \quad (5.23)$$

where

$$a_4 = 4(1 + \tau \beta_0/2)/\tau; \quad b_4 = 4k^2 + \lambda^2 - 4(1 + \tau \beta_0/2)\delta/\tau;$$

$$a_3 = 4\left(\frac{\tau+1}{\tau} + \beta_0\right)/\tau; \quad b_3 = \{8k^2 - \lambda - 4(1 + \beta_0/2)\delta\}/\tau;$$

$$a_2 = 4(1 + \beta/2)/\tau^2; \quad b_2 = 4k^2 + 1/4$$

and

$$\lambda = 1/2 - 2/\tau + 1/\Gamma.$$

Thus there exist four modes in this case. For small values of  $\epsilon$  one can see that two roots of equation (5.23) would be of order  $\epsilon$  and two would be of order unity. In the limit of vanishing  $\epsilon$ , the larger roots <sup>are</sup> given by

$$\tilde{\sigma}^2 = -b_4/a_4. \quad (5.24)$$

These are nothing but the convective modes of an

adiabatic slender flux tube. It is worth mentioning here that Webb & Roberts (1980) obtained only 3 modes for the uniform zero order case. For the zero order polytropic state they did obtain a fourth degree equation in  $\sigma$ , but they have not commented on the extra mode for the stratified case. An inspection of equations (5.15) and (5.16) clearly shows that the extra mode appears because of non-zero  $g$ . Following the nomenclature of Defouw (1970) we shall call this fourth mode as the thermal-convective mode. It is interesting to note that Defouw's dispersion relation for a Boussinesq fluid in a uniform vertical magnetic field also had four roots.

For small  $\epsilon$ , a perturbation expansion of  $\sigma$  as

$$\sigma = \sigma_0 + \epsilon \sigma_1 + \epsilon^2 \sigma_2 + \dots$$

yields

$$\sigma = \sigma_0 - \epsilon (a_3 \sigma_0^2 + b_3) / 2a_4 \sigma_0^2, \quad (5.25)$$

for the convective modes and

$$\sigma = \epsilon [ \{-b_3 \pm (b_3^2 - 4b_2b_4)^{1/2}\} / 2b_4 ], \quad (5.26)$$

for the thermal modes,

where  $\sigma_0^2 = -b_4/a_4$

We thus see that when  $\sigma_0^2 < 0$ , the overstability is possible provided

$$(a_3 \sigma_0^2 + b_3) / 2a_4 > 0. \quad (5.27)$$

We can also see that when  $\sigma_0^2 > 0$ , the effect of thermal dissipation is merely to alter the growth rates of the instability.

However, such a straightforward classification of the modes into convective modes and thermal modes will no longer be possible when  $\sigma_0 \rightarrow 0$ . In this case all the four roots of equation (5.23) will be small and a complete solution of the equation becomes unavoidable. However,  $\sigma_0 \rightarrow 0$  implies an almost neutral stratification which occurs only in the very deep layers of the solar convection zone. We shall not consider this problem in this thesis but move on to the nonlinear development of convective instability in the presence of heat dissipation.

### 5.5 Effect of heat transport on the nonlinear convective instability of a slender flux tube:

We are mainly interested in the first few hundred kilometers below the photosphere where the superadiabaticity is large. In this region the radiative

diffusivity ranges from a value of  $2.33 \times 10^{10} \text{ cm}^2 \text{ s}^{-1}$  at a temperature of  $1.003 \times 10^4$  to  $3.504 \times 10^{12} \text{ cm}^2 \text{ s}^{-1}$  at the photosphere (Spruit 1977). Such a gradient in the diffusivity cannot support a hydrostatic polytropic model in general. We, therefore, consider first the case of constant radiative conductivity in an unstably stratified polytropic tube in order to understand the general effect of radiative conductivity on the instability. Even here we proceed in two steps. We first study the case of lateral heat exchange alone and then include the axial heat transport as well, in a few subsequent calculations.

#### 5.5.1 Lateral heat exchange:

We saw in Section 5.3 that the energy equation for an optically thick slender flux tube with lateral heat exchange resembles that for the case of an unbounded fluid losing heat according to Newton's law of cooling. When the tube cools due to a convective downflow, the heat enters laterally to equalise the temperature thereby inhibiting the downflow. Similarly when a parcel of fluid rises in the tube, the excess heat is radiated away laterally, thereby reducing the forces of buoyancy. The time scale for temperature equalisation depends both on the radiative conductivity and on the lateral dimensions of the tube.

We computed the development of convective instability using equation (3.18), (3.19) and (5.7) with only the first term on R.H.S. In dimensionless units, we chose the radiative conductivity as  $1.0 \times 10^{-3}$  which is representative of a layer  $\approx 200$  km below the photosphere. Figure 5.1 shows the time variation of the longitudinal velocity at  $z = 0.48$  for  $\beta_0 = 6.0$  and for 4 values of the tube radius. The boundary conditions imposed were "open" boundary conditions as described in section 4.3. We see an oscillatory behaviour with a tendency for increasing amplitude at later times. The oscillations have a period of  $\approx 12$  dimensionless time units. The amplitudes of these oscillations increase with decreasing value of the tube radius for the range of value  $\tau_0 = 4.2$  to  $\tau_0 = 0.5$ . It is interesting to compare these results with those for the adiabatic case (vide figure 4.12). There too, we had noticed the oscillatory behaviour with a similar period. In the adiabatic case, however, the computations could not be continued for  $t > 22$  units because there the pressure boundary condition led to a numerical runaway process which resulted in spurious negative pressures.

In the present set of calculations we introduced a condition in the computer programme which would halve

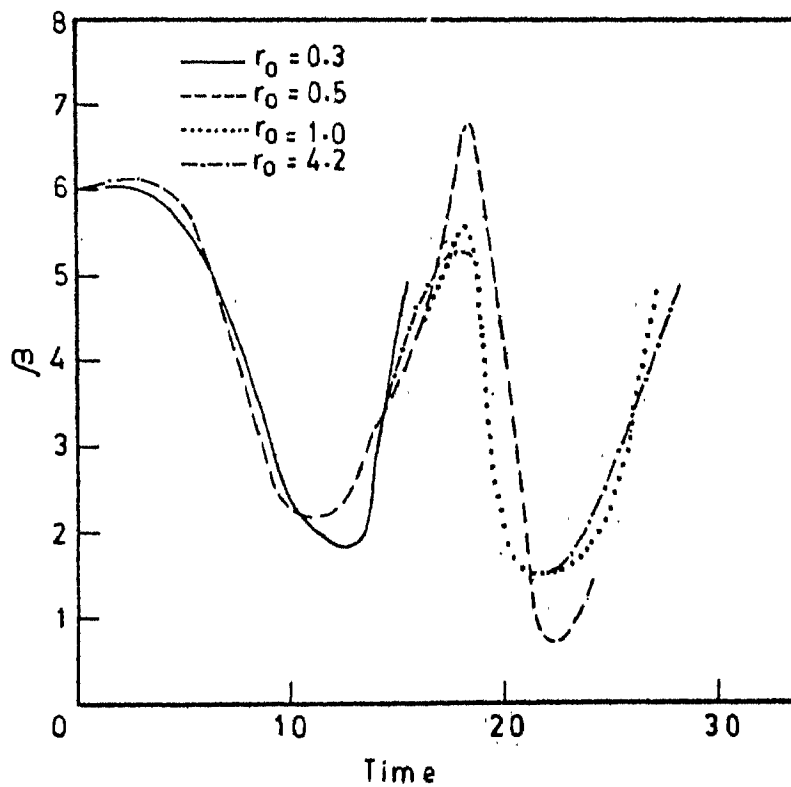
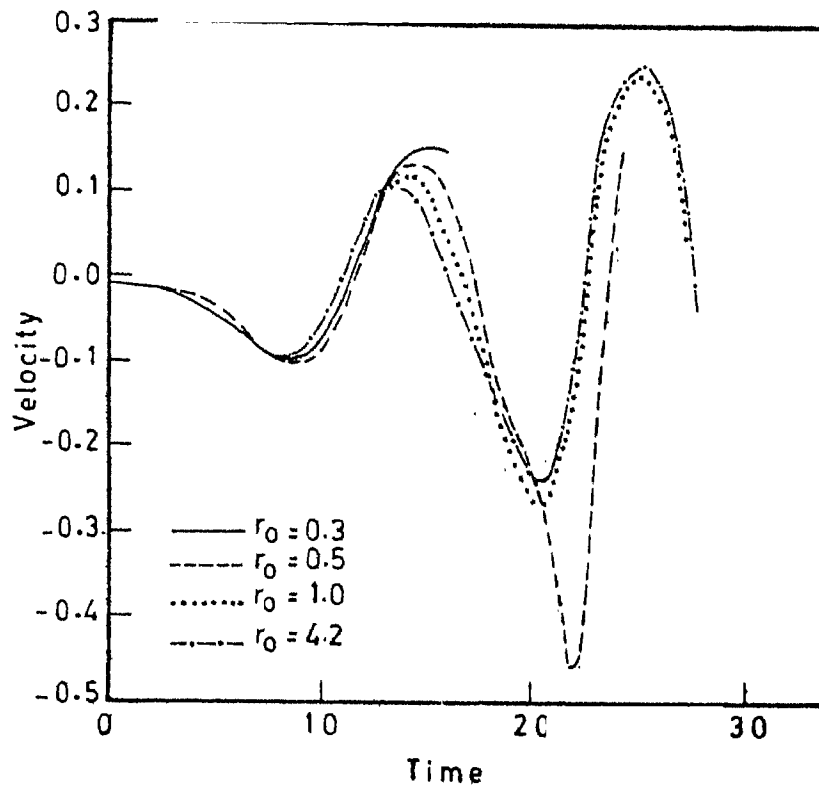


Fig.5.1 (top): Time dependence of velocity at  $z = 0.48$  in an "open" tube, for  $\beta_0 = 6.0$  and different values of radius  $r_0$ , laterally exchanging heat with its surroundings.

Fig.5.2 (bottom): Variation of  $\beta$  with time in the tube described in figure 5.1.



the time step if such a negative pressures were to occur. This was expected to halt the runaway process. Moreover, we changed the boundary condition of constant density at the base to one of extrapolated density from two preceding interior values. This density boundary condition becomes necessary whenever  $V$  is negative, since the third characteristic from the boundary no longer communicates with the interior solution (vide section 2.3). The spurious negative pressures were not encountered in the nonadiabatic cases which are being discussed in this chapter. Since, we did not repeat the adiabatic calculations with the new boundary conditions, we cannot say whether it was the presence of heat dissipation or the new density boundary condition that prevented this numerical breakdown. However, there occurs another difficulty in continuation of computations for small value of  $\tau_0$ . When the radius was changed from 0.5 to 0.46 (in dimensionless units) the computations had to be stopped at a stage when large pressure enhancements made the magnetic field locally imaginary. In this case, the halving of time step was of no use in halting the pressure build up. We, therefore, believe that this difficulty is not a numerical artifact. In a realistic situation the pressure build up would be contained by the tension

created in the curved field lines of the dilated flux tube. In this situation the slender tube approximation becomes a poor approximation and further progress can be made only by means of two dimensional calculations.

Figure 5.2 shows the behaviour of  $\beta$ , the ratio of gas pressure to magnetic pressure inside the tube at  $z = 0.48$  as a function of time for different values of  $\gamma_0$ , the initial tube radius. The behaviour of  $\beta$  is similar to that of velocity except for the phase. We can notice transient intensification of the field to values of  $\beta$  as low as 1.00.

Figure 5.3 demonstrates the stabilizing influence of the initial magnetic field. Here the velocity at  $z = 0.48$  in a tube of radius  $\gamma_0 = 0.5$  is plotted as a function of time for different values of  $\beta_0$ . There is no significant change in the period of the oscillations but the amplitudes are drastically reduced for  $\beta_0 = 4.0$  as compared to those in the case of larger  $\beta_0$ .

Figures 5.4 and 5.5 depict the spatial profiles of velocity and  $\beta$  respectively at different instants of time. We see that the spatial profiles of velocity oscillate between states of upflow and downflow with mixed flow at certain instants of time (not drawn in

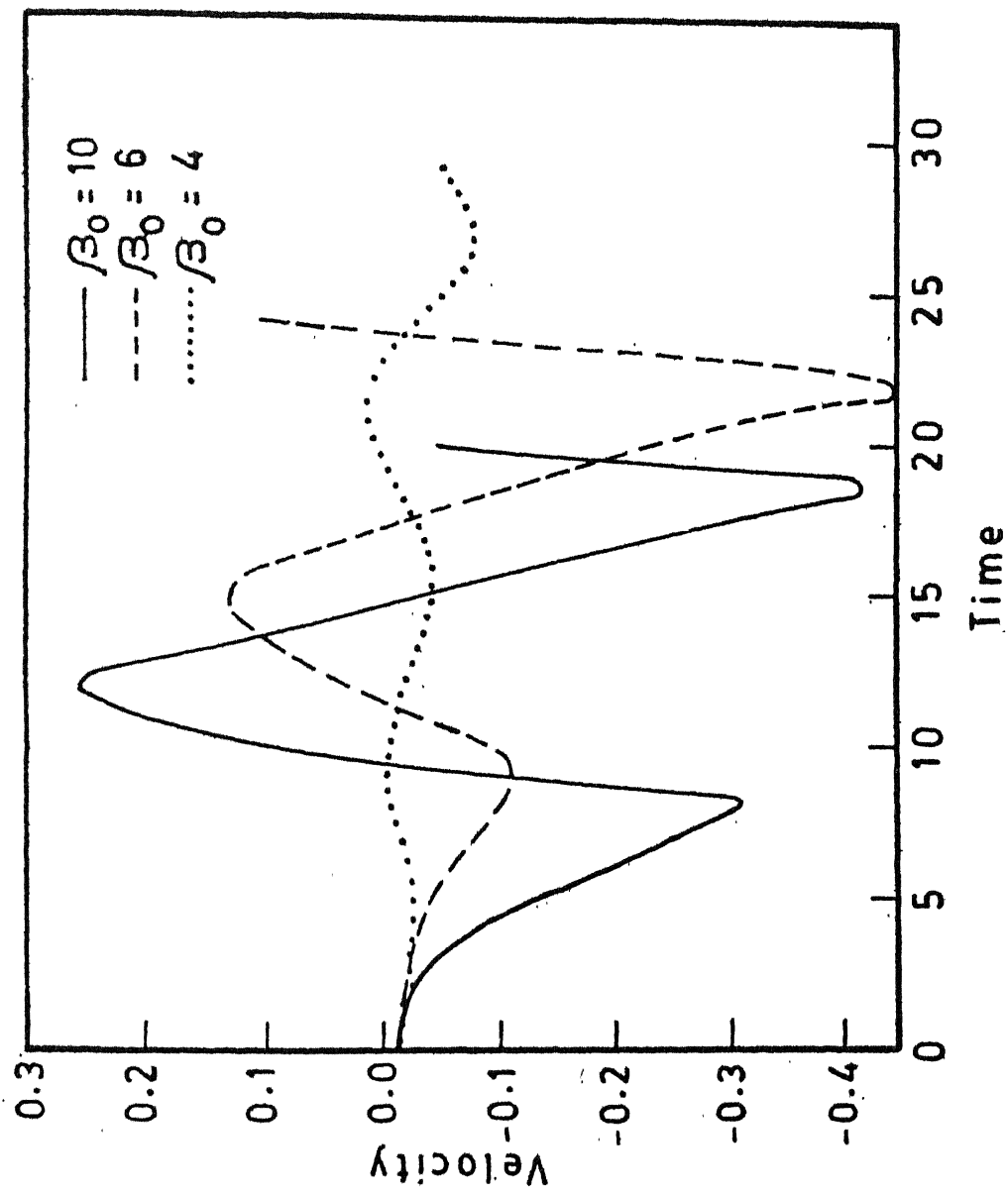


Fig.5.3 : Dependence on  $\beta_0$ , of the time development of velocity in a tube of radius  $r_0 = 0.5$ .

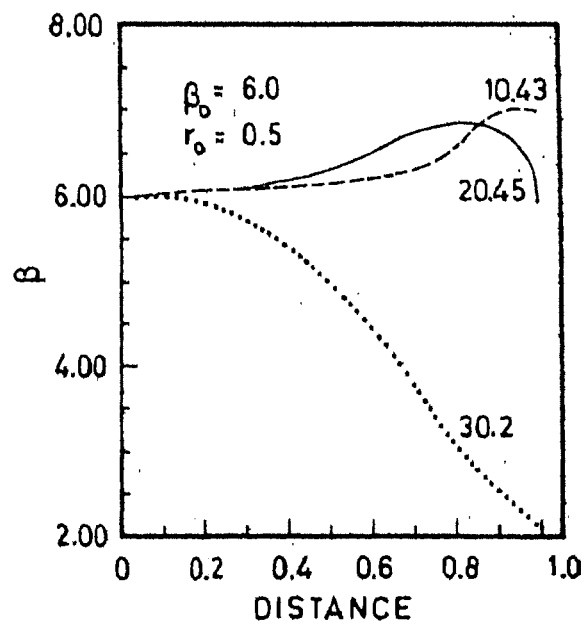
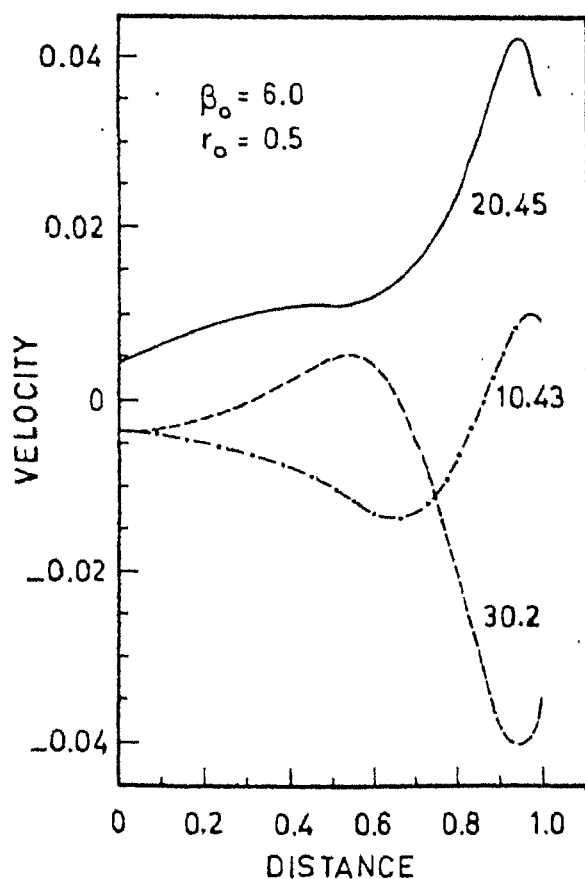
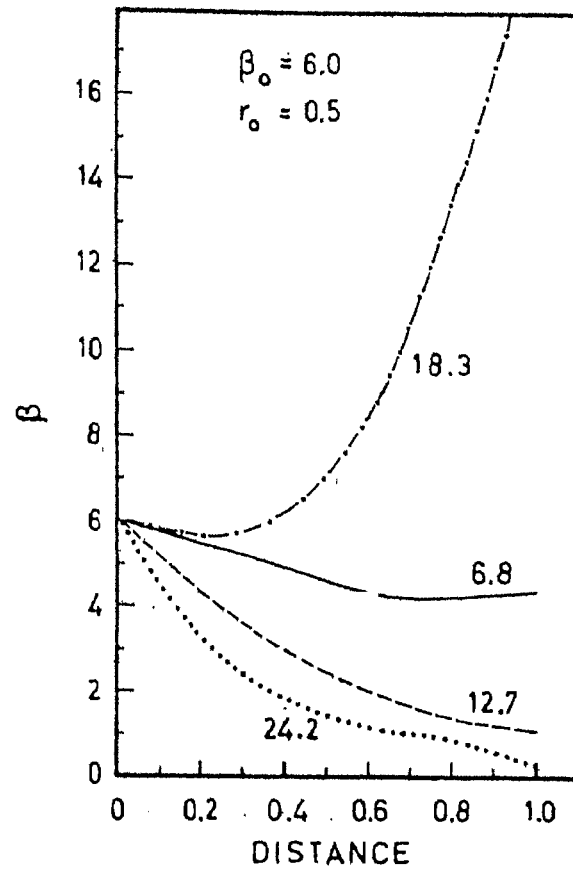
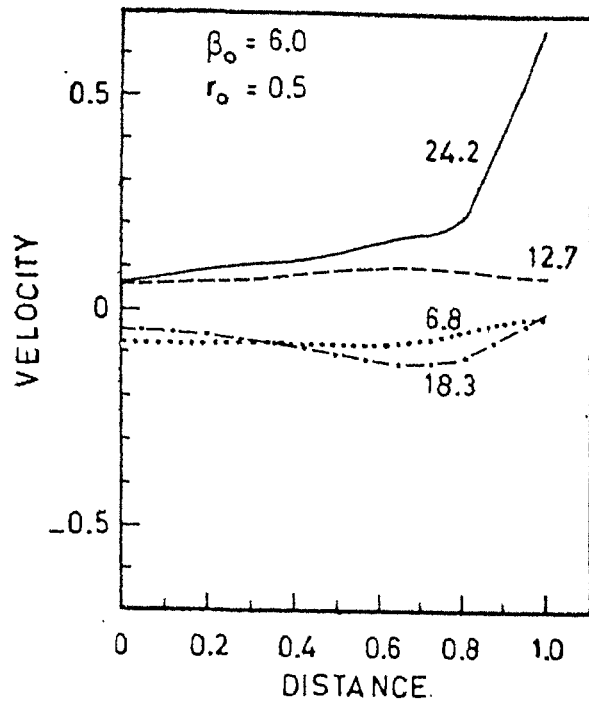


Fig.5.4(top left): Velocity profiles at different epochs in a tube exchanging heat laterally.

Fig.5.5 (top right): The spatial profiles of  $\beta$  corresponding to the velocity profiles of figure 5.4.

Fig.5.6 (bottom left): Velocity profiles with inclusion of longitudinal heat transport.

Fig.5.7 (bottom right): Spatial profiles of  $\beta$  corresponding to the velocity profiles in figure 5.6.

the figure). At later times we see the development of large gradients near the top boundary. Profiles of  $\beta$  also show similar behaviour. The effect of longitudinal heat transport on this behaviour will be discussed in the next subsection.

### 5.5.2 Longitudinal transfer of heat:

We now consider the effect of longitudinal heat transfer on the convective instability. We first considered the case of constant radiative conductivity and, therefore, retained only the first two terms on the R.H.S. of equation (5.7). In a rigorous sense the character of the system of differential equations changes here from hyperbolic to parabolic due to the appearance of the second derivative of temperature. However, we continued to use the method of characteristics to solve the time dependent initial value problem treating the second derivative as a 'source term'. At each instant, this 'source term' was calculated on the previous time line using a standard IBM subroutine for numerical differentiation. Such a procedure does not cause serious problems as long as the thermal conductivity is small. Figures 5.6 and 5.7 show the spatial profiles of velocity and the plasma- $\beta$  respectively at different instants of time in a tube with  $\beta_0 = 6.0$  and  $\tau_0 = 0.5$ . It is interesting to note that the  $\beta$

profiles show smoother behaviour at the top of the tube at later instants of time whereas the kinks in the velocity profiles at the top of the tube continue to persist. One cannot predict whether these would be smoothed out with the inclusion of viscosity. Figures 5.8 and 5.9 show the temporal behaviour of velocity and plasma- $\beta$  in a tube with  $\beta_0 = 6.0$  and  $4.0$  respectively and with the same value of  $\tau_0 = 0.5$ . One notices three striking facts viz., the presence of overstability, the smaller period of oscillation and the greatly diminished amplitude of oscillation as compared to the case with lateral heat exchange alone. Compared to this, the differences between the case of lateral heat exchange alone and the adiabatic case were rather small. This shows that the longitudinal heat transport has a greater effect on the convective instability of flux tubes with  $\tau_0 = 0.5$ . In the context of solar photospheric magnetic fields, it is also interesting to see that intensification of such tubes by this process would be transient and would be accompanied by only small and oscillatory flows. Here the calculations were not continued beyond  $t > 30$  and, therefore, we do not know the saturation amplitudes of the overstability. However,  $t = 30$  corresponds to  $\approx 1000$ s for tubes with base temperature  $T_b = 10^4$  K. Therefore, other processes such as granulation might interfere with the overstability within this time.

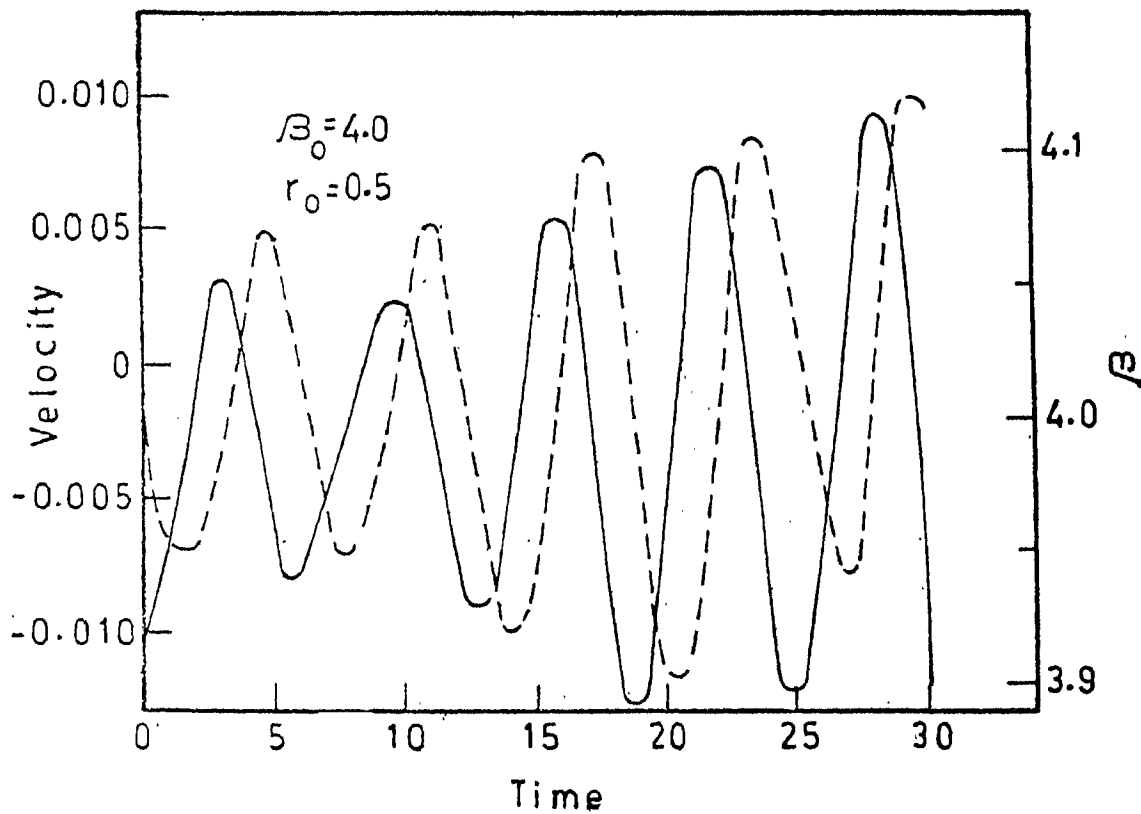
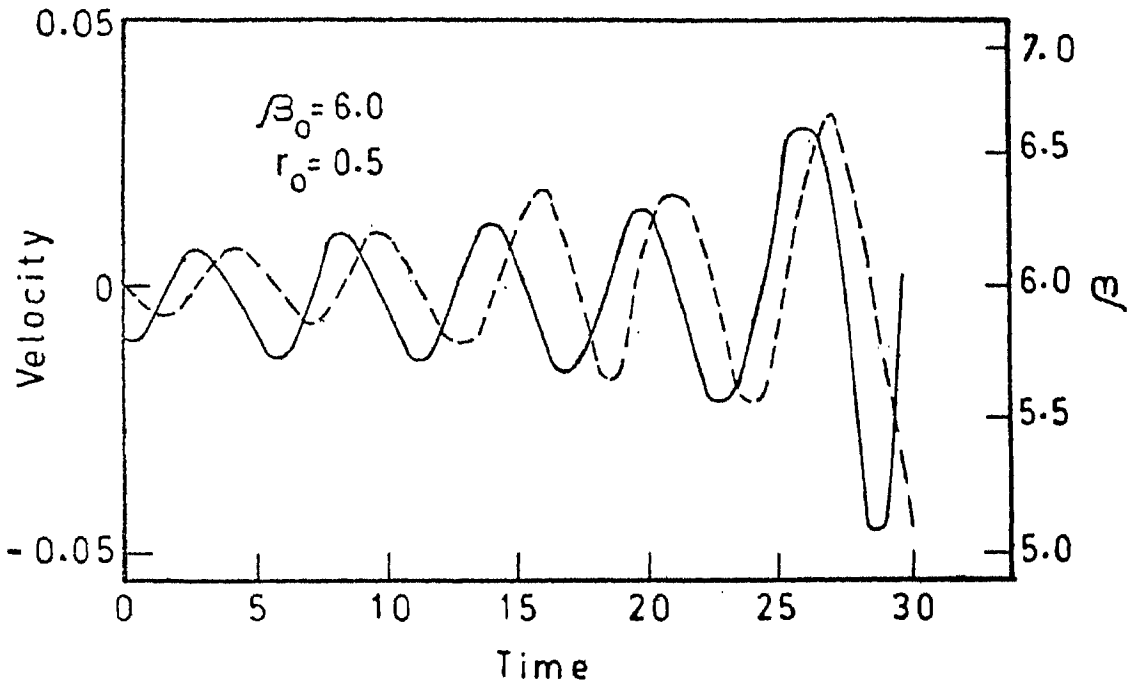


Fig.5.8 (top): Time dependence of velocity (dashes) and (solid lines) at  $z = 0.48$  in an open tube with heat transport and  $\beta_0 = 6.0$ .

Fig.5.9 (bottom): Similar to figure 5.8 but for  $\beta_0 = 4.0$ .

5.5.3 Heat conduction with a realistic form of conductivity:

As already remarked in the beginning of section 5.5, a variable conductivity is not compatible, in general, with a hydrostatic polytropic stratification. The solar plasma shows a wide range of variation in the radiative opacity and consequently in the heat diffusivity. A few hundred kilometers below the photosphere, it is the bound-free opacity of the hydrogen atom which dominates (Cox & Giuli, 1968). The large variation in the electron density as a function of depth creates a correspondingly large variation in the opacity and, therefore, in the radiative conductivity. In order to study such a situation we first calculated a static equilibrium model for the environment of the flux tube with such a variable heat diffusivity. For this we calculated a least squares fit for the relation

$$\kappa = \kappa_0 \left( \rho / \rho_0 \right)^\mu \cdot (T/T_0)^\nu, \quad (5.28)$$

using Spruit's (1977) values for  $\kappa$ ,  $\rho$  and  $T$ .

Here  $\rho_0 = 3.126 \times 10^5$  dynes  $\text{cm}^{-2}$ , and  $T_0 = 1.003 \times 10^4$  K corresponding to a depth of  $1.779 \times 10^2$  km in the model.

We obtained

$$\mu = -0.65 \quad \text{and} \quad \nu = 12.$$



This expression for the opacity was used in the heat conductivity given by

$$K = 16\sigma T^3 / 3\kappa\rho. \quad (5.29)$$

The static energy equation

$$K \frac{dT}{dz} = K_0 \left( \frac{dT}{dz} \right)_0 \quad (5.30)$$

and the hydrostatic pressure balance

$$\frac{d}{dz} p = -\rho g / \mathcal{R}T, \quad (5.31)$$

were solved simultaneously using an Adam's predictor-corrector algorithm. The resulting state is depicted in figure 5.10. It must be mentioned here that the thickness of the layer between temperatures  $10^4$  K and 6000 K in this model is smaller than the corresponding thickness in Spruit's model because we have entirely ignored the convective transport of heat.

The model of figure 5.10 was used as the environment of a tube with  $T_e = T_i$  and  $\beta_0 = 6.0$ . The initial state of the tube was then calculated as explained in section 3.2. This state was perturbed with a small initial velocity perturbation and the evolution of the flow was studied, taking the full energy equation (5.7).

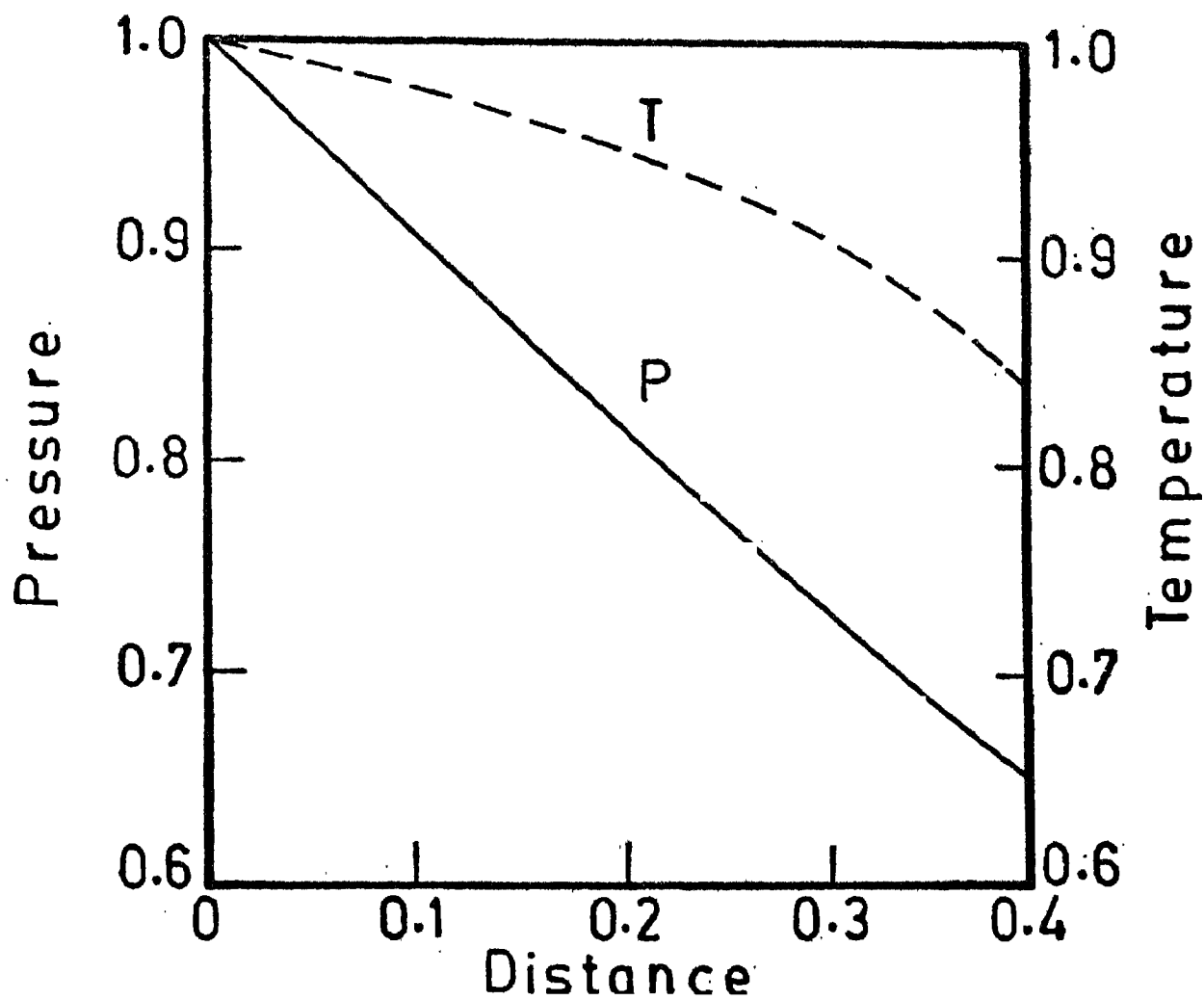


Fig.5.10: Initial hydrostatic state for a tube's environment  $(p_e, T_e)$  where heat transport is solely by radiation with opacity varying as  $\kappa = \kappa_0 (T/T_0)^{12} \cdot (p/p_0)^{-0.65}$ .

The development of the flow at two points is shown in figure 5.11. There is once again oscillatory behaviour with still larger frequency and smaller amplitude as compared to the cases described in section 5.5.2. This calculation may not have any direct relevance to the solar convection zone because of the neglect of convective transport in the environment of the tube. It is, however, interesting to note the competing influences of longitudinal and lateral heat transport in this case. The conductivity varies inversely as the 8th power of temperature. Therefore, the heat entry from outside is enhanced whenever the tube cools. This tends to compensate for the cooling due to the convective instability and thus the lateral heat flow has a stabilizing influence. On the other hand, the longitudinal heat transport is expected to enhance the instability by means of the famous " $\alpha$  - mechanism" or "Eddington valve" mechanism. Furthermore, since the lateral heat exchange increases inversely as the square of the radius of the tube, one can conclude that the lateral heat exchange would stabilize sufficiently thin flux tubes.

Finally, figure 5.12) shows the spatial variation of the temperature gradient at different values of time. It is clearly seen that there is a gradual flattening

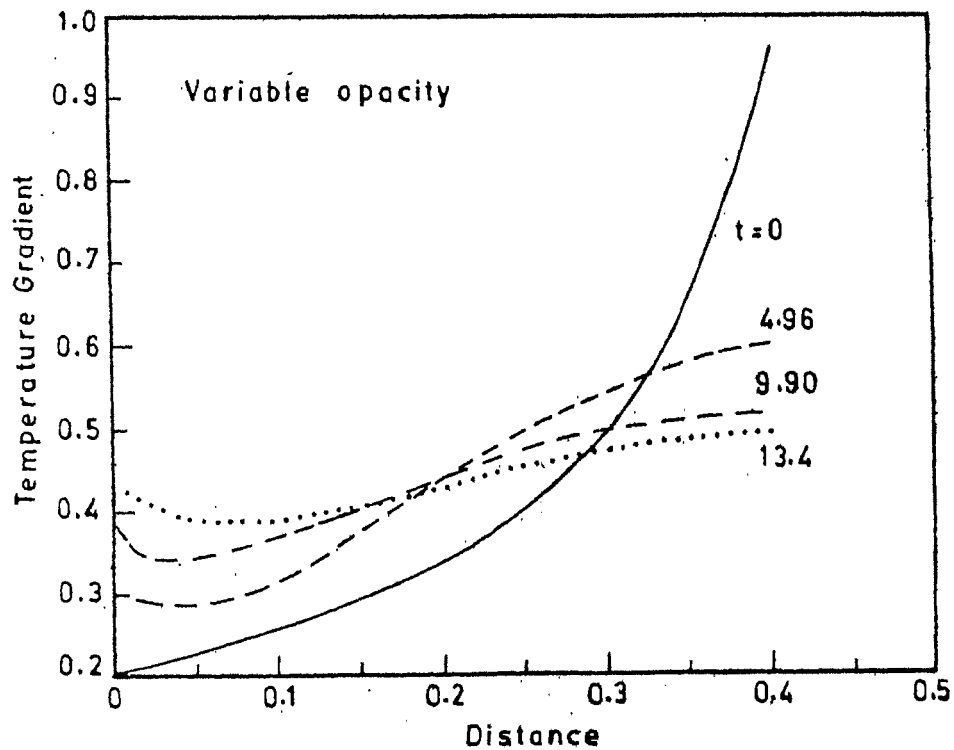
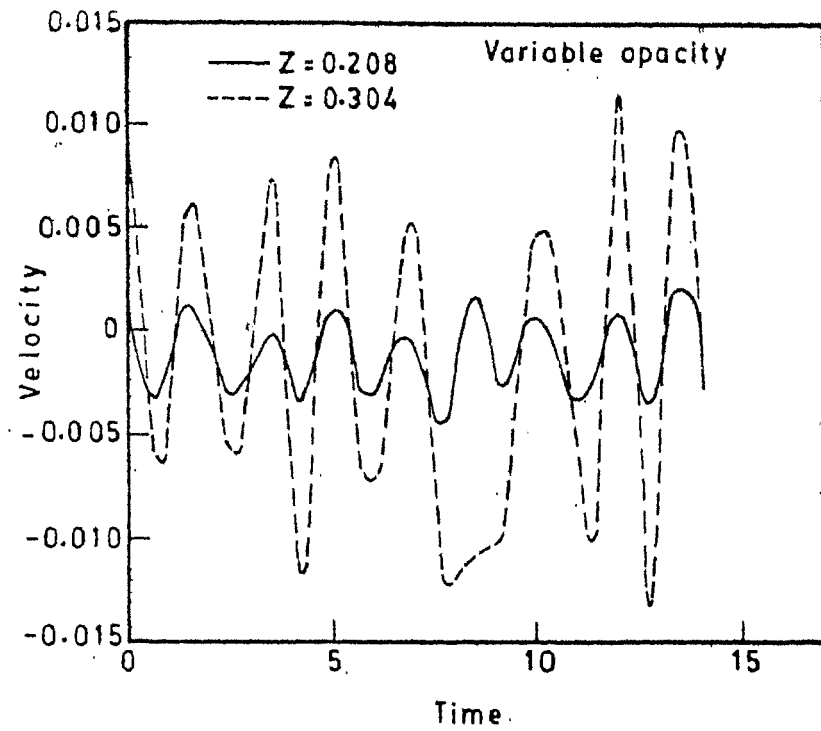


Fig.5.11 (top): Variation of velocity in a tube embedded in an atmosphere given by figure 5.10 and with  $\beta_0 = 6.0$ .

Fig.5.12 (bottom): Evolution of the spatial profiles of the temperature gradient in the tube described in figure 5.11.

of the profile, which means a tendency to acquire a polytropic state. One does not know, however, whether this could be the general tendency of any non-polytropic stratification with heat transport.

### 5.6 Discussion:

As remarked earlier a noteworthy feature of these calculations is the period of the oscillatory behaviour. In the case of radial heat transport, the period seems to be similar to the adiabatic case. When longitudinal heat transport is included, the period is seen to be nearly half of the previous one. This indicates that the dominant modes of oscillation in these two cases are different. In both cases the amplitudes are seen to decrease with increasing magnetic field. In the case of longitudinal heat transport, this is reminiscent of the decrease of the growth rate of the slow mode with increasing magnetic field (Antia, 1979). In the variable opacity case of section 5.5.3, the smaller period might be, most probably, the result of the shorter length of the tube considered. However, these explanations for the increase of frequency of oscillations are only tentative and one must await the results of more extensive calculations.

In summary we see that heat conduction does exert considerable influence on the convective instability of flux tubes. The most important results in relation to solar magnetic fields are the possibility of time dependent field intensification and absence of large unidirectional flows. A detailed discussion follows in the next i.e. final chapter of this thesis.

## 6. SUMMARY OF CONCLUSIONS AND DISCUSSION

### 6.1 Summary of the main results of earlier chapters:

We saw that when a magnetic field line is made to move normal to itself, with a velocity varying with distance along the field line, the motion exerts a centrifugal force on the gas if the latter is "frozen" with the field. This force generates an upflow if the magnitude of the lateral velocity increases with height. Similarly a downflow is produced if the lateral velocity decreases with height. We then assumed a model for the lateral motion of field lines simulating the jostling of solar magnetic flux tubes by the solar photospheric granulation. In this model we assumed that the magnitude and spatial variation of the lateral motion of field lines are similar to the observed variation of the rms vertical velocity of the granulation. With this assumption we saw that significant downflows could be generated along the magnetic field.

Next we studied the response of magnetic flux tubes to external pressure fluctuations in the slender flux tube approximation. We concentrated our attention on two forms for the pressure fluctuation. In the first

form, the fluctuations decreased monotonically with height and had an oscillatory behaviour in time simulating evanescent waves. In the case of a uniform tube we saw that for small times, the velocity response to such a perturbation contains a term which is unidirectional and growing in time. However, in the case of a polytropic tube, the velocity response was oscillatory when the travel time of the tube waves over one scale height of the pressure perturbation was large compared to the period of the perturbation. When the travel time was small compared to this period the response developed into a unidirectional downflow. We also saw that for the typical parameters corresponding to granulation, the response would be oscillatory rather than unidirectional. The second form of pressure was assumed to be oscillatory in space as well as in time simulating standing waves. In this case we confirmed the existence of the resonance predicted by Roberts (1979) from a linear analysis. This resonance occurs when the period of the pressure fluctuation equals the tube travel time over the wavelength of the perturbation.

We then investigated the nonlinear development of convective instability within slender flux tubes. An initial polytropic tube was chosen and the effects of initial superadiabaticity  $\delta$ , initial ratio of gas



pressure to magnetic pressure  $\beta_0$  and of two sets of boundary conditions were studied in the limit of adiabatic variations. We could see a wide variety in the time development of the instability. There is overstability for low  $\beta_0$ , an evolution to steady flow for some intermediate  $\beta_0$  and large amplitude unsteady behaviour for larger values of  $\beta_0$ . The motions were less violent when the boundary condition permitted lateral expansion of the tube at the top. We explained this due to the diversion of a fraction of flow energy into kinetic energy of lateral motions.

The effect of heat transport by radiation was next considered. The energy equation in this case was formulated in the slender flux tube approximation. A linear analysis revealed the presence of four modes. In the limit of small dissipation and moderate superadiabaticity, we saw that two of the modes resembled the convective slow modes, while the other two could be identified as a thermal mode and a "thermal convective" mode respectively. When the convective time scale approaches the thermal relaxation time scale, such a simple classification of the modes is not possible.

From nonlinear calculations we found that lateral heat exchange leads to oscillations. The mean amplitude of these oscillations is larger for smaller radii of the

flux tube. For  $\beta_0 = 6.0$ , the periods of the oscillations were found to be similar to the period for the adiabatic case. When heat transport along the tube axis was also included, we saw that the amplitude of oscillations was considerably reduced. Further, this amplitude is smaller for larger values of the magnetic field. The period of oscillation became half of what it was when lateral heat exchange alone was considered. For  $\beta_0 = 6.0$  the intensification of magnetic field proceeded in an oscillatory manner. However, for  $\beta_0 = 4.0$ , no intensification was seen. When we considered the case of a realistic form of opacity, the amplitude of the oscillations became still smaller.

## 6.2 Limitations on the applicability of the results to the solar magnetic flux tubes:

The physical conditions in the solar magnetic flux tubes and their environment are very complex. The various complexities include (i) the stratification due to gravity, (ii) the compressibility and the partial ionization of matter, (iii) energy losses and gains by radiation, convection and waves, and (iv) the curvature

of field lines. To study all these features simultaneously is a formidable task. There is also the danger of swamping essential information about the physics of the problem in a deluge of details. It is, therefore, profitable to progress in small steps. This was the philosophy behind our calculations of the idealised cases reported in the earlier chapters. This approach does put limitations on the applicability to realistic situations. In this section, we discuss these limitations.

The most severe limitation regarding the results of chapter 2 is the neglect of the lateral equation of motion. This neglect would not be a serious limitation if we had some independent means of knowing the lateral displacement of the field lines as a function of height. In the absence of such data, the validity of the results hinges on the validity for the assumed form for the displacements. Our assumption of a form similar to that for granulation is valid only for the Alfvén travel time. If 500 km of the tube is bent locally, then "straightening" by propagation of Alfvén waves with a speed  $\approx 8 \text{ km s}^{-1}$  would occur after nearly one Alfvén travel time  $T_A$ , which is  $\approx 60\text{s}$ . Thereafter, the field line may no longer possess the assumed curvature and the attendant centrifugal acceleration may be

considerably reduced after such a time duration. On the other hand, the axial flow will not cease immediately, but will decay on the sound travel timescale  $T_s$ , which again is  $\approx 60s$ . If one approximates the entire time profile of the velocity along the field as a linear increase till  $T_A$  and thereafter an exponential decay with a time constant  $T_s$ , then the mean velocity of flow over the life time  $T_G$  of the granule can be estimated as  $\approx a T_A (\tau_A/2 + T_s) / T_G$  when  $T_s \ll T_G$ . In this expression,  $a$  is the mean acceleration during the linear increase of the axial velocity. In the calculation of section 2.8, the lateral velocity at the base of the tube was assigned a value  $= 0.5 \text{ km s}^{-1}$ . The mean acceleration corresponding to this velocity can be approximately taken as  $V_* / T_A$  where  $V_*$  is the axial velocity attained after a time  $T_A$ . For the base of the tube  $a$  turns out to be  $\approx 800 \text{ cm s}^{-2}$  (figure 2.14). The observations of Dunn & Zirker (1973) show horizontal motions of  $\approx 1.5 \text{ kms}^{-1}$  for the filigree. Since the centrifugal acceleration depends on the square of the lateral velocity (section 2.7), the acceleration  $a$  corresponding to  $\approx 1.5 \text{ kms}^{-1}$  is  $\approx 800 \times (1.5/.5)^2 = 7200 \text{ cm s}^{-2}$ . Substituting this value of  $a$  in the expression for mean velocity, we have for  $T_s \approx T_A \approx 60s \ll T_G \approx 600s$ , the mean velocity

$\langle v \rangle \approx 700 \text{ ms}^{-1}$ . Thus one could reasonably expect mean downflows  $\approx 700 \text{ ms}^{-1}$  to be generated as a result of the buffeting of magnetic flux tubes even after taking the back reaction of the field into account.

In the case of the response of a slender flux tube to external pressure fluctuations, the "fudge" factor, viz., the efficiency of conversion from velocity fluctuations to pressure fluctuations was already discussed in chapter 3. In any case we saw that this process is unlikely to drive systematic downflows. However, the resonant response of the tube to standing waves will have important implications for the heating of the solar magnetic tubes in higher layers of the solar atmosphere.

The convective collapse of magnetic flux tubes was studied (chapter 4) for a tube of length equal to only one pressure scale height. This short length may appear as a limitation especially in view of the hyperbolic nature of the system of differential equations, which amplifies the effect of boundary conditions at large times. However, as discussed in section 4.5, a realistic flux tube cannot be unkinked for lengths larger than one pressure scale height. Thus if one is to remain within the frame work of the slender flux tube approximation, then it would be inconsistent to consider longer tubes. In this sense, therefore, it is the slender flux tube

approximation which limits the range of applicability of our results. It also hinders continuation of the calculations for specific cases whenever at some point the gas pressure inside the tube exceeds the gas pressure outside. This limitation of the slender flux tube approximation must be borne in mind while generalising the results to a tube with an arbitrarily varying cross-section.

One encounters a related problem while formulating the energy equation for slender tubes (chapter 5). The expression for the heat source term for lateral heat exchange is  $4K(T_e - T_i)/\tau_0^2$ , where  $K$  is the radiative conductivity,  $\tau_0$  is the radius of the tube while  $T_e$  and  $T_i$  are the temperatures outside and inside the tube respectively. In deriving this expression one tacitly assumes that  $(T_e - T_i)/T_i \propto (\tau_0/\Lambda)^2$ , where  $\Lambda$  is the scale length of variation of  $\tau_0$ . This means that  $T_e$  and  $T_i$  must not differ by more than a few per cent at any epoch. This condition was found to be satisfied during the development of the instability. In this way the formulation of the energy equation (5.7) is justified a posteriori.

The initial state for the case of variable opacity (section 5.5.3) has a steeper temperature gradient than the gradient of a realistic convection zone model. The

convective instability of such an initial state can hardly be used to make predictions for solar magnetic flux tubes. However, the purpose of the calculation was merely to see the physical effects arising from a variable opacity.

### 6.3 Application to the problem of downflows within solar magnetic flux tubes:

According to Beckers (1981), the velocity of the downflow within magnetic tubes is equal to or slightly less than that in the intergranular lane which are the most preferred sites for these tubes. Owing to the high electrical conductivity of the plasma, the presence of systematic downflows within tubes raises the question of the gas supply. The observations of Harvey & Hall (1975) and Harvey (1977) indicate velocities  $\approx 2.2$   $\text{kms}^{-1}$  at deeper layers of the photosphere. This requires a larger drain of gas than what can be supplied by the mechanism suggested by Giovanelli (1977) viz. the diffusion of neutral atoms across the magnetic field near the temperature minimum. It remains to be seen if interchange instability, as suggested by Parker (1979) could supply enough gas to maintain such large downflows.

We have seen that granular buffeting can drive mean downflows  $\approx 700$   $\text{ms}^{-1}$  even after making allowance for the back reaction of the field (Section 6.2).

The other processes such as the application of external pressure perturbations (chapter 3) or convective instability (chapter 4 & 5) produce either oscillatory flows or downflows of very small magnitude. The values of downflow velocity as reported by Giovanelli & Ramsey (1971), Giovanelli & Brown (1977) and Giovanelli & Slaughter (1978) for higher regions of the photosphere compare favourably with the value predicted by our calculations of the granular buffeting. This value is also compatible with the supply of the gas by the diffusion process.

#### 6.4 Application to the problem of kilogauss fields of the solar magnetic flux tubes:

Webb & Roberts (1978) as well as Spruit & Zweibel (1979) show that under adiabatic conditions, tubes with field strengths smaller than a critical value  $\approx 1400$  G would be convectively unstable. They further conclude that such an unstable tube would collapse to a more intense convectively stable state. Our nonlinear calculations of evolution from an initial unstable state show that the presence of heat transport would introduce the following two modifications.

First, the state of marginal stability would be shifted to a higher values of  $\beta_0$ . This can be inferred



from the following facts. Our adiabatic calculations showed overstability for  $\beta_0 = 2.0$  with  $\Gamma - \tau = 1.05$ . When heat transport is included, however, the tube is seen to be almost stable even with  $\beta_0 = 4.0$  and a larger value of  $\Gamma - \tau = 1.5$ .

Secondly, with the inclusion of heat transport the resulting flows and magnetic fields are not steady but oscillatory. This result is perhaps not very startling in the light of Antia's (1979) linear calculations. There he demonstrated the existence of overstable modes, both for convectively stable and unstable stratifications with uniform vertical magnetic field and thermal dissipation. In our nonlinear calculations we find that the oscillations in the field strength have substantial amplitudes, e.g.,  $\approx 30\%$  for  $\beta_0 = 6.0$ . The observations of Giovanelli et al (1978) do not show oscillations in the magnetic flux down to the limit of detectability ( $\approx 2\%$ ). One would like to know whether observations with higher spatial resolution would show up any oscillations in the field intensity.

If it turns out that the field strengths are indeed non-oscillatory, then one would require a mechanism different from convective collapse to maintain steady intense fields. The superadiabatic effect suggested by Parker (1978a) appears satisfactory, for this purpose.

Parker estimates that a downflow of  $10 \text{ ms}^{-1}$  would suffice to maintain kilogauss fields. From our calculations, we see that downflows of considerably larger magnitude can be driven by granular buffeting. It is thus very tempting to link the flow and field within the tube in a consistent manner. The same superadiabatic gradient which generates convective turbulence outside the tube, could be responsible for driving downflows via granular buffeting, as well as maintaining kilogauss fields via Parker's (1978a) mechanism.

There is, however, a possibility that this mechanism would become less effective when thinner tubes are considered. This is because heat leak from outside the tube could decrease the cooling produced by the downflow. One can estimate approximately the radius below which the mechanism would fail by equating the timescale of adiabatic cooling ( $\Lambda/v$ ) to the time scale of heat leak from the surroundings ( $\tau_c^2/\chi$ ). This yields the critical radius  $\tau_c$  as  $(\chi \Lambda/v)^{\frac{1}{2}}$ , where  $\chi$  is the thermal diffusivity,  $\Lambda$  is the temperature scale height and  $v$  is the velocity of the downflow. For  $\chi \approx 10^{11} \text{ cm}^2 \text{ s}^{-1}$ ,  $\Lambda \approx 100 \text{ km}$  and  $v \approx 1 \text{ km s}^{-1}$ , one estimates  $\tau_c \approx 30 \text{ km}$ . It is interesting to note that Unno & Ribes (1979) arrive at similar conclusions for facular points in the context of their hydrodynamic model of a flux tube.

Finally, one cannot rule out the possibility of alternative mechanisms for producing intense magnetic fields, either by turbulent processes (Kraichnan, 1976) deep in the convection zone or by some magnetogas-dynamical processes at the base of the convection zone (Gokhale, 1977a,b).

#### 6.5 Future developments:

Several of the results presented in this thesis need theoretical refinement as well as observational verification. For the case of granular buffeting one has to take into account the back reaction of the magnetic field in a more rigorous way. Observationally one would like to know the degree of jostling of the filigree as a function of height. The calculation of the resonant response of flux tubes to external perturbations must be extended to larger times with the inclusion of radiative dissipation. Such a calculation would aid the understanding of the dynamics and heating of magnetic flux tubes.

The convective instability must be studied with 2-D or 3-D magnetohydrodynamical equations, starting from a realistic stratification and including the effects of radiative heat transfer in the Eddington approximation. We intend to pursue such calculations if and when access to sufficiently fast computers becomes available.

Such calculations would certainly improve upon the present knowledge of convective collapse of flux tubes. This in turn would be important for understanding similar phenomena on other stars as well. Thus, theoretical calculations with more realistic physical conditions as well as observations of higher spatial and temporal resolutions will be needed for a better understanding of the interaction of solar magnetic flux tubes with convection.

REFERENCES

- Abramowitz, M. & Stegun, I.A. (1965) Handbook of Mathematical Functions, Dover, New York, p. 875.
- Antia, H.M. (1979) Ph.D. Thesis, Univ. of Bombay.
- Antia, H.M. & Chitre, S.M. (1979) Solar Phys. 63, 67.
- Bappu, M.K.V. & Sivaraman, K.R. (1971) Solar Phys. 17, 316.
- Beckers, J.M. (1981) in The Sun as a Star (ed: S.Jordan), NASA-SP 450, p. 11.
- Beckers, J.M. & Schröter, E.H. (1968) Solar Phys. 4, 142.
- Busse, F.H. (1975) J. Fluid Mech. 71, 193.
- Chandrasekhar, S. (1952) Phil. Mag. (7) 43, 501.
- Chandrasekhar, S. (1961) Hydrodynamic and Hydromagnetic Stability, Clarendon Press, Oxford.
- Cowling, T.G. (1976a) Magnetohydrodynamics, Adam Hilger, Bristol, p. 70.
- Cowling, T.G. (1976b) M.N.R.A.S. 177, 409.
- Cox, J.P. & Giuli, R.N. (1968) Principles of Stellar Structure, Vol.1, Gordon & Breach, New York, p. 381.
- Cram, L.E. & Wilson, P.R. (1975) Solar Phys. 41, 313.
- Danielson, R.E. (1961) Astrophys. J. 134, 289.
- Daras-Papamargaritis, H. & Koutchmy, S. (1983) Astron. Astrophys. 125, 280.
- Defouw, R.J. (1970) Solar Phys. 14, 42.
- Deinzer, W., Hensler, G., Schmitt, D., Schussler, M. & Weisshaar, E. (1982) IAU Symp. No.102 (Abstract)
- Deubner, F-L. (1976) Astron. Astrophys. 51, 189.

- Dunn, R.B. & Zirker, J.B. (1973) Solar Phys. 33, 281.
- Durrant, C.J., Mattig, W., Nesis, A., Reiss, G. & Schmidt, W. (1979) Solar Phys. 61, 251.
- Frazier, E.N. (1970) Solar Phys. 14, 89.
- Galloway, D.J. & Weiss, N.O. (1981) Astrophys. J. 243, 945.
- Gibson, R.D. (1966) Proc. Camb. Phil. Soc. 62, 287.
- Gilman, P.A. (1981) in The Sun as a Star (ed: S. Jordan) NASA-SP 450, p. 231.
- Gingerich, O., Noyes, R.W., Kalkofen, W. & Cuny, Y. (1971) Solar Phys. 18, 347.
- Giovanelli, R.G. (1977) Solar Phys. 52, 315.
- Giovanelli, R.G. & Brown, N. (1977) Solar Phys. 52, 27.
- Giovanelli, R.G. & Ramsey, J.V. (1971) in IAU Symp. No.43, 293.
- Giovanelli, R.G. & Slaughter, C. (1978) Solar Phys. 57, 255.
- Giovanelli, R.G., Livingston, W.C. & Harvey, J. (1978) Solar Phys. 59, 49.
- Gokhale, M.H. (1977a) Kodaikanal Obs. Bull. Ser. A 2, 10.
- Gokhale, M.H. (1977b) Kodaikanal Obs. Bull. Ser. A 2, 19.
- Gough, D.O. & Tayler, R.J. (1966) M.N.R.A.S. 133, 85.
- Harvey, J. (1977) Highlights of Astronomy 4(II), 223.
- Harvey, J. & Hall, D. (1975) Bull. A.A.S. 7, 459.
- Harvey, J., Livingston, W.C. & Slaughter, C. (1972) in Line Formation in a Magnetic Field, NCAR, Boulder, p. 227.
- Hasan, S.S. (1982) IAU Symp. No.102 (abstract).
- Hasan, S.S. & Venkatakrisnan, P. (1980) Kodaikanal Obs. Bull. Ser. A, 3, 6.

- Hasan, S.S. & Venkatakrisnan, P. (1981) *Solar Phys.* 73, 45.
- Howard, R. (1971) *Solar Phys.* 16, 21.
- Howard, R. (1972) *Solar Phys.* 24, 123.
- Kato, S. (1966) *Publ. Astron. Soc. Japan*, 18, 201.
- Knobloch, E., Weiss, N.O. & Da Costa, L. (1981) *J. Fluid Mech.* 113, 153.
- Kopp, R.A. & Pneuman, G. (1976) *Solar Phys.* 50, 85.
- Kraichnan, R.H. (1976) *J. Fluid Mech.* 77, 753.
- Ledoux, P. & Walraven, TH. (1958) *Handbuch der Physik*, Vol.51, p. 526.
- Leibacher, J. & Stein, R.F. (1981) in *The Sun as a Star* (ed: S. Jordan) NASA-SP 450, p. 263.
- Leighton, R.B., Noyes, R.W. & Simon, G.W. (1962) *Astrophys. J.* 135, 474.
- Livingston, W.C. & Harvey, J. (1971) *IAU Symp. No.43*, 51.
- Mehlretter, J.P. (1974) *Solar Phys.* 38, 43.
- Moore, D.W. & Spiegel, E.A. (1966) *Astrophys. J.* 143, 871.
- Nordlund, A. (1982) *IAU Symp. No.102* (abstract).
- Pai, Shih-I. (1962) *Magnetogasdynamics and Plasma dynamics*, Springer-Verlag, Wien, p. 108.
- Parker, E.N. (1955) *Astrophys. J.* 121, 491.
- Parker, E.N. (1963) *Astrophys. J.* 138, 552.
- Parker, E.N. (1974a) *Astrophys. J.* 189, 563.
- Parker, E.N. (1974b) *Astrophys. J.* 190, 429.
- Parker, E.N. (1978a) *Astrophys. J.* 221, 368.
- Parker, E.N. (1978b) *Astrophys. J.* 222, 357.
- Parker, E.N. (1979) *Cosmical Magnetic Fields*, Clarendon Press, Oxford, p. 268.

- Proctor, M.R.E. & Galloway, D.J. (1979) *J. Fluid Mech.* 90, 273.
- Proctor, M.R.E. & Weiss, N.O. (1982) *Reports on Prog. in Phys.* 45, 1317.
- Rae, I.C. & Roberts, B. (1982) *Astrophys. J.* 256, 761.
- Ramsey, H.E., Schoolman, S.A. & Title, A.M. (1977) *Astrophys. J.* 215, L41.
- Roberts, B. (1979) *Solar Phys.* 61, 23.
- Roberts, B. (1981a) *Solar Phys.* 69, 27.
- Roberts, B. (1981b) *Solar Phys.* 69, 39.
- Roberts, B. & Webb, A.R. (1978) *Solar Phys.* 56, 5.
- Sheeley, N.R. (1971) *IAU Symp. No.43*, 310.
- Simon, G.W. & Leighton, R.B. (1964) *Astrophys. J.* 140, 1120.
- Sivaraman, K.R. & Livingston, W.C. (1982) *Solar Phys.* 80, 227.
- Skumanich, A., Smythe, C. & Frazier, E.N. (1975) *Astrophys. J.* 200, 747.
- Sneddon, I.N. (1957) *Elements of Partial Differential Equations*, McGraw-Hill, Tokyo.
- Spruit, H.C. (1977) *Ph.D. Thesis, Univ. of Utrecht.*
- Spruit, H.C. (1979) *Solar Phys.* 61, 363.
- Spruit, H.C. (1981a) in *The Sun as a Star* (ed: S. Jordan) NASA-SP 450, p. 385.
- Spruit, H.C. (1981b) *Astron. Astrophys.* 98, 155.
- Spruit, H.C. (1982) *Solar Phys.* 75, 3.
- Spruit, H.C. & Roberts, B. (1983) *Nature*, 304, 401.
- Spruit, H.C. & Zweibel, E.G. (1979) *Solar Phys.* 62, 15.
- Stein, R.F. (1981) *Astrophys. J.* 246, 966.
- Stenflo, J.O. (1976) *IAU Symp. No.71*, 69.



- Syrovatsky, S.I. & Zhugzhda, Y.D. (1968a) *Sov. Astron.* 11, 945.
- Syrovatsky, S.I. & Zhugzhda, Y.D. (1968b) *IAU Symp.* No.35.
- Tannenbaum, A.S., Wilcox, J.M., Frazier, E.N. & Howard, R. (1969) *Solar Phys.* 9, 328.
- Tayler, R.J. (1971) *quart. J. R.A.S.* 12, 352.
- Thompson, W.B. (1951) *Phil. Mag* (7) 42, 1417.
- Unno, W. & Ando, H. (1979) *Geophys. Astrophys. Fluid Dyn.* 12, 107.
- Unno, W. & Ribes, E. (1979) *Astron. Astrophys.* 73, 314.
- Venkatakrishnan, P. (1979) *Solar Phys.* 63, 135.
- Venkatakrishnan, P. (1981) *Bull. Astron. Soc. India*, 9, 214.
- Venkatakrishnan, P. (1983) *J. Astrophys. Astron.* 4, 135.
- Venkatakrishnan, P. & Hasan, S.S. (1981) *J. Astrophys. Astron.* 2, 133.
- Walen, C. (1949) *On The Vibratory Rotation of the Sun* (Henrik Lindstahls Bokhandel, Stockholm).
- Webb, A.R. & Roberts, B. (1978) *Solar Phys.* 59, 249.
- Webb, A.R. & Roberts, B. (1980) *Solar Phys.* 68, 71.
- Weiss, N.O. (1966) *Proc. Roy. Soc. London, Ser. A* 293, 310.
- Weiss, N.O. (1964) *Phil. Trans. A* 256, 99.
- Weiss, N.O. (1981a) *J. Fluid Mech.* 108, 247.
- Weiss, N.O. (1981b) *J. Fluid Mech.* 108, 273.
- Weiss, N.O. (1981c) *J. Geophys. Res.* 86b, 11689.
- Zucrow, M.J. & Hoffman, H.D. (1976) *Gas Dynamics*, Vol.I, John Wiley, New York, p. 622.

Papers published during the course of this work  
which are utilised in this thesis:

1. "Flow of gas along a magnetic field of time dependent geometry" - by S.S. Hasan and P. Venkatakrishnan, 1980. Kodaikanal Observatory Bulletin Series A, Vol. 3, 6.
2. "Time-dependent interaction of granules with magnetic flux tubes" - P. Venkatakrishnan and S.S. Hasan, 1981. Journal of Astrophysics and Astronomy, 2, 133.
3. "Non-linear development of convective instability with slender flux tubes" - by P. Venkatakrishnan, 1983, Journal of Astrophysics and Astronomy 4, 135.

Paper 1 and 2 formed the basis for chapter 2, while paper 3 formed the basis for chapter 4. The results of Chapters 3 and 5 have not yet been sent for publication.

VITA

Name: P. Venkatakrishnan

Date and place of birth: 3 July 1953, TRIVANDRUM

Education:

H.S.C.	March 1969	Kendriya Vidyalaya, Trivandrum
B.Sc.	March 1972	University College, Trivandrum
M.Sc.	March 1974	University College, Trivandrum

Appointments:

Research Assistant, Indian Institute of Astrophysics, Kodaikanal	March 1974 - August 1975
Research Associate, Indian Institute of Astrophysics, Bangalore	September 1975 - September 1980
Fellow Indian Institute of Astrophysics, Bangalore	October 1980 onwards